Proceedings of International Conference
Applications of Structural Fire Engineering
Prague, 29 April 2011

Session 3

Composite Structures and Connections

ANALYSIS OF STEEL–CONCRETE COMPOSITE BEAM WITH INTERLAYER SLIP IN FIRE CONDITIONS

Tomaž Hozjan[a], Jerneja Kolšek[b], Igor Planinc[a], Miran Saje[a] and Stanislav Srpčič[a]

[a] University of Ljubljana, Faculty of Civil and Geodetic Engineering, Ljubljana, Slovenia
[b] Kraški Zidar d.d., Sežana, Slovenia

INTRODUCTION

Steel–concrete composite beams are often employed in office and industrial buildings for fast and economic erection. Most usually they comprise a steel girder and a reinforced concrete slab interconnected by shear connectors. The number of shear connectors largely determines whether the composite cross-section behaves as compact or partially connected. In any cases, the deformation of the beam causes some relative tangential displacement (slip) between the steel girder and the concrete slab. While usually being very small, slip can have a substantial effect on the overall ductility of the beam, which indicates that it should be taken into account in the analysis (Ranzi et al, 2007). This seems to be particularly true when analysing behaviour of composite beams subject to extreme conditions including fire.

Mathematical modelling of behaviour of a steel-concrete composite beam during fire is a demanding problem. It appears, however, that the problem can be solved with a sufficient accuracy, if it is divided in two independent uncoupled processes, each to be solved separately. The first process consists of determining the spatial and time distributions of temperature and pore pressure in the steel–concrete composite beam. The second process describes the mechanical response; there the temperature and pore pressure distributions serve as a loading to result in the mechanical response of the slab subjected to the simultaneous action of mechanical and fire loads (Hozjan, 2009).

There is a number of mathematical models available to determine the temperature field in the composite concrete–trapezoidal steel plate slab. The growth of temperature in concrete triggers an increase of pore pressure and induces the moisture transport through the heated concrete such that moisture travels from the moist section to a dry one or condenses. The model by Tenchev et al. (2001) is implemented in the present work. It represents a substantially modified model previously proposed by Bažant et al. (1997) and is now considered to be rather complete for the analysis of concrete structures in fire. It is represented by a system of coupled transient differential equations, describing heat and mass transfer and pore pressure development. We note that the Thenchev model is only one among a few recent mathematical models of moisture and heat transfer in concrete at elevated temperatures proposed in literature.

There are various models for describing a mechanical response of a steel–concrete composite beam subject to simultaneous action of mechanical and fire loads. Most of them employ the finite element methods. Their precision largely depends on a proper modelling of the interaction between the reinforced concrete slab and the trapezoidal steel plate, the applied material models of concrete, reinforcement and steel plate at elevated temperatures, and the corresponding models of temperature and viscous strains of steel, creep of concrete and transient strains of concrete. The problems are often computationally so demanding that the analysis must be limited to 2D.

In this paper we present a new numerical model for the analysis of steel–concrete composite beams exposed to fire. The model consists of two successive steps. For the description of slow transient phenomena involving heat and mass transport and the pore pressure increase in concrete, a somewhat modified thermo-hydro-chemical model of Tenchev is employed (Tenchev et al, 2001). For the determination of mechanical response of the steel-concrete composite slab during fire numerical model with the following assumptions is used: (i) the layers of a steel–concrete composite slab are described with Reissner's kinematically exact model of the beam, (ii) the slip can occur at the interface between the layers but no transverse separation between them is possible,

(iii) an additive split of strains, where thermal, mechanical and viscous strains of steel at elevated temperatures, along with creep of concrete and transient strains of concrete are considered, (iv) strain-based finite elements are employed. In the numerical example that follows, we test the accuracy of the present numerical model by comparing the results of our model with the data of experimental data (Wainman et al, 1988) and the numerical results of Huang et al. (1999).

1 FIRE ANALYSIS OF STEEL–CONCRETE COMPOSITE BEAM

1.1 First step of the fire analysis

Development of gas temperature in the fire compartment depends on many parameters and is therefore both a complex task to do and unreliable. For this reason engineers use simplified parametric temperature–time curves instead, which provide relationships between gas temperature in a compartment and time for a number of standardized situations (Ma et al, 2000). Once the variation of the surrounding gas temperature in the compartment has been defined, heat and mass transfer in the composite beam can be performed.

1.1.1 Heat and mass transport in composite beam

A coupled heat and moisture transfer in concrete exposed to fire can be mathematically described with a system of differential equations consisting of mass conservation equations for each phase of concrete and the energy conservation equation (Thenchev et al, 2001) as follows:
Water conservation:

$$\frac{\partial \overline{\rho}_L}{\partial t} = -\nabla \mathbf{J}_L - \dot{E}_L + \frac{\partial \overline{\rho}_D}{\partial t} \tag{1}$$

Water vapour conservation:

$$\frac{\partial \left(\varepsilon_G \rho_V \right)}{\partial t} = -\nabla \mathbf{J}_V + \dot{E}_L \tag{2}$$

Air conservation:

$$\frac{\partial \left(\varepsilon_G \rho_A \right)}{\partial t} = -\nabla \mathbf{J}_A \tag{3}$$

Energy conservation:

$$\left(\underline{\rho C} \right) \frac{\partial T}{\partial t} = -\nabla \cdot \left(-k \nabla T \right) - \left(\underline{\rho C \mathbf{v}} \right) \cdot \nabla T - \lambda_E \dot{E}_L - \lambda_D \frac{\partial \overline{\rho}_D}{\partial t} \tag{4}$$

In Eqs. (1)–(4) ρ_i is the density of a phase i, $\mathbf{J}_i$ is the mass flux of each phase i (L is free water, V is water vapour and A is dry air) per unit volume of gaseous material, $\varepsilon_G \rho_V$ and $\varepsilon_G \rho_A$ are mass concentrations of air and water vapour per unit volume concrete, $\dot{E}_L$ is the rate of evaporation of free water (including desorption), t is time. In Eq. (4) $\underline{\rho C}$ is heat capacity of concrete, k is thermal conductivity of concrete, $\underline{\rho C \mathbf{v}}$ relates to the energy transferred by fluid flow, λ_E is the specific heat of evaporation, λ_D is specific heat of dehydration and T is the absolute temperature. As in the model proposed by Tenchev et al. (2001), we here assume that the liquid pressure is equal to the gas pressure, $P_G = P_L$. This causes the capillary pressure, P_C, to be equal to zero, which is physically true only at a full saturation of pores with liquid water. It is also assumed that air and water vapour behave as an ideal gas and $\overline{\rho}_L$ of free water is determined with the help of sorption curves defined by Bažant et al. (2001).
By summing Eqs. (1) and (2) we end up with three partial differential equations. The solution is obtained numerically with the finite element method, where the primary unknowns of the problem

are temperature T, pore pressure P_G and water vapour content ρ_V . For a detailed description of the problem and its numerical formulation, see Tenchev et al. (2001).

1.2 Second step of the fire analysis

Once the temperature variation in time and space has been obtained, we may start the second step of the fire analysis where we determine the stress-strain state of steel–concrete composite slab. We find the solution in an incremental way.

We divide the time of the duration of fire into time intervals $[t^{i-1}, t^i]$, and determine iteratively the stress and strain state at each time t^i. The layers of the steel–concrete slab are modelled by Reissner's geometrically exact beam theory (Reissner, 1972), but with the effect of shear deformations being neglected.

We consider an initially straight, planar, two-layer steel–concrete slab of undeformed length L. The steel–concrete slab is subjected to a conservative, time independent load, and a time-dependent growth of temperature; for further details a reader is referred to Hozjan (2009).

The related governing equations are:

Kinematic equations:

$$1+u^{j\prime}-\left(1+\varepsilon^{j}\right)\cos\varphi=0,\quad j=a,b \tag{5}$$

$$w'+\left(1+\varepsilon^{a}\right)\sin\varphi=0 \tag{6}$$

$$\varphi-\kappa=0 \tag{7}$$

Equilibrium equations:

$$\mathrm{R}_X^{j\prime}+q_X^j+p_X=0,\quad j=a,b \tag{8}$$

$$\mathrm{R}_Z'+q_Z=0 \tag{9}$$

$$\mathrm{M}'-\mathrm{M}_c'=0 \tag{10}$$

$$Q^{a}\left(1+\varepsilon^{a}\right)-M_c^{a}-m_Y=0 \tag{11}$$

$$M^{b}=M-M^{a} \tag{12}$$

$$R_Z^{b}=R_Z-R_Z^{a} \tag{13}$$

$$\mathrm{N}^{j}=\mathrm{R}_X^{j}\cos\varphi-\mathrm{R}_Z^{j}\sin\varphi,\quad j=a,b \tag{14}$$

$$\mathrm{Q}^{j}=\mathrm{R}_X^{j}\sin\varphi+\mathrm{R}_Z^{j}\cos\varphi,\quad j=a,b \tag{15}$$

Constitutive equations:

$$\mathrm{N}^{j}-\mathrm{N}_c^{j}=0,\quad j=a,b \tag{16}$$

$$\mathrm{M}^{a}-\mathrm{M}_c^{a}=0 \tag{17}$$

Constraining equations:

$$\Delta'=\varepsilon^{a}-\varepsilon^{b} \tag{18}$$

$$p_X^a-p_X^b=0 \tag{19}$$

$$p_Z^a-p_Z^b=0 \tag{20}$$

$$\left[\frac{\mathrm{M}_c^{a\prime}+m_Y^a}{\left(1+\varepsilon^{a}\right)}\right]'=\mathrm{R}_X^{a\prime}\sin\varphi^{a}+\mathrm{R}_Z^{a\prime}\sin\varphi^{a}+\mathrm{N}^{a}\kappa^{a} \tag{21}$$

$$p_t=\mathrm{G}\left(x,\Delta,T,\sigma,\ldots\right) \tag{22}$$

$$x^{*}=x+\Delta \tag{23}$$

where $(\square)'$ denotes the derivatives with respect to x and index j denotes the particular layer of the composite beam (a and b). Variable u^j is the component of a displacement vector and φ^j is the rotation angle at the reference axis. w is the lateral displacement and φ is the rotation at the

reference axis of the composite beam. Variables ε^a and ε^b are extensional strains (membrane deformations), κ^a and κ^b pseudocurvatures (flexural deformations) of layer *a* and *b*, respectively. Variable κ is related to the reference axis of the composite slab. N^j, Q^j and M^j represent equilibrium generalized internal forces of layers *a* and *b*. N_c^j, and M_c^j denote constitutive generalized internal forces of layers *a* and *b*. q_X^j, q_Z and m_Y are external distributed loads. p_X^a, p_X^b, p_Z^a, p_Z^b and p_t are the components of the contact traction vector that acts in the contact plane. The slip in the contact between the two points that coincide in the undeformed shape is denoted by Δ. x^* represents a material, undeformed coordinate of that particular material point of layer *b* which, in the deformed state, gets in contact with the material point of layer *a* having coordinate x. Based on the given stress and strain state in the time interval *i-1* and temperature at time interval *i*, we can determine the strains in time interval *i* of any point of the steel-concrete slab by the equations:

$$D^{j,i} = D^{j,i-1} + \Delta D^{j,i} \tag{24}$$

where $D^{a,i}$ and $D^{b,i}$ are the increments of the total strains (also termed the 'geometrical deformations') in the time interval i. Considering the principle of additivity of strains and the material models of concrete and steel at elevated temperatures, gives the strain increment, ΔD^i, as the sum of the strain increments due to temperature, ΔD_{th}^i, stress, ΔD_{σ}^i, creep, ΔD_{cr}^i, and transient strains of concrete, ΔD_{tr}^i:

$$\Delta D^{a,i} = \Delta D_{th}^{a,i} + \Delta D_{\sigma}^{a,i} + \Delta D_{cr}^{a,i} \tag{25}$$

$$\Delta D^{b,i} = \Delta D_{th}^{b,i} + \Delta D_{\sigma}^{b,i} + \Delta D_{cr}^{b,i} + \Delta D_{tr}^{b,i} \tag{26}$$

For a detailed description of an each strain increment, see Hozjan (2009).

2 NUMERICAL EXAMPLE

We consider the steel–concrete composite beam exposed to standard fire ISO 834 (Wainmann et al, 1988) as shown in Fig. 1.

2.1 Thermal and moisture analysis of composite beam exposed to fire ISO 834

In Fig. 1 the relevant data of the steel-concrete simply supported beam is presented: geometry, loading, reinforcement and the finite element mesh over the cross-section employed in the calculations of heat and moisture fields. In performing the diffusion analysis, the connection between the steel and concrete surface has been considered perfect during fire.

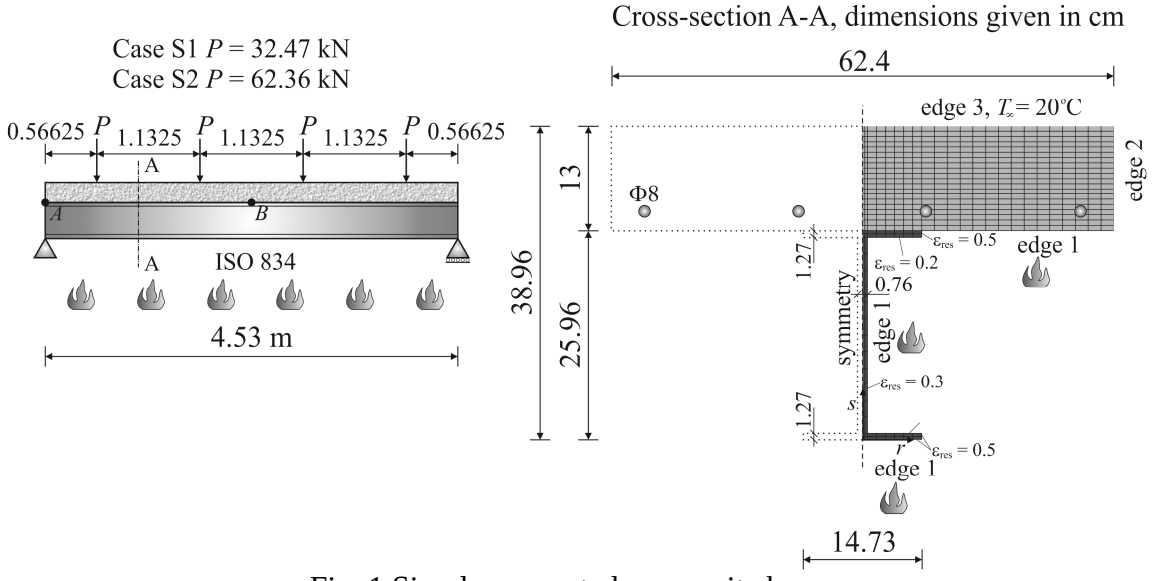

Fig. 1 Simply supported composite beam.

At the contact between steel and concrete, the heat flux is taken to be permitted but the moisture flux is prevented due to the impervious steel surface and the perfect contact, resulting in the zero gradient of pore pressure and vapour content. Consequently, vapour cannot escape through the boundary between steel and concrete. The remaining data are: density of concrete 2400 kg/m³, density of cement 300 kg/m³, initial temperature 20℃, initial pore pressure 0.1MPa, initial water vapour content 0.013 kg/m³, water vapour content on boundary 0104 kg/m³, initial porosity of concrete 0.15, initial permeability of concrete $1 \cdot 10^{-16}$ and initial free water amount 10 kg/m³.
The distribution of temperature over the cross-section of the composite beam at 10, 30 and 60 min is presented in Fig. 2a. As expected the results show that the rate of increase in temperature of the steel beam is much higher than that of the concrete slab. This is due to a higher thermal conductivity and lower specific heat of steel. We may also notice that the temperature in the top flange and in the upper part of the web of the steel profile is lower compared to the bottom part. This is due to the heat flow from the steel beam to the less hot concrete slab.

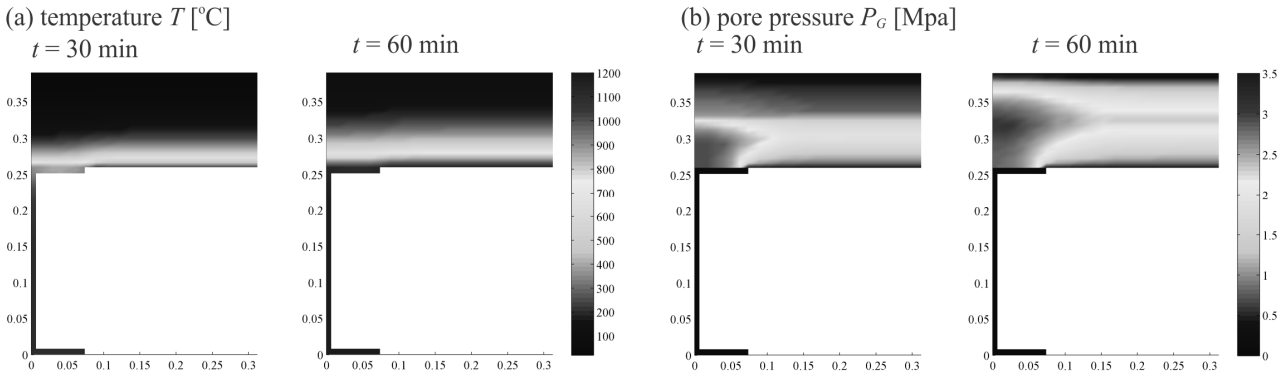

Fig. 2 (a) Distribution of temperature over the cross-section at 30 and 60 min. (b) Distribution of pore pressure over the cross-section at 30 and 60 min.

Fig. 2b shows the distributions of pore pressure over the cross-section at significant instants. As observed from the figures, the increase of pore pressure is largest at the contact between the steel beam and the concrete slab. After 60 min of fire have passed, the increased pore pressure zone spreads between the steel-concrete contact and the increased free water front. The zone of the high pore pressures extends with the increase of temperature and tends to spread over the whole concrete section. We can notice that the high pore pressure in concrete is also due to the impervious steel-concrete contact. Since the pore pressure on the area near the bottom of concrete deck, which is not in contact with the flange of the steel beam, is substantially smaller than the pore pressure over the area where the steel flange and the concrete deck are in contact.

2.2 Mechanical analysis of composite beam exposed to fire ISO 834

Fig. 3 shows the increase of the midspan deflection with temperature of the bottom flange for cases S1 and S2. The present numerical results are compared with the experimental data (Wainmann et al, 1988) and with the numerical results (Huang et al, 1999). It is clear that the agreement with both the experimental and the numerical data is good. In both cases, S1 and S2, failure of the composite beam as predicted by the present formulation takes place due to failure of the composite cross-section. Prior to failure, a material instability was observed in the concrete part of the cross-section, yielding shortly after to the material instability of the composite cross-section. As observed from Fig. 3, the rapid increase of the midspan deflection starts at about 700°C (case S1) and 650°C (case S2), leading to the failure of the critical cross-section. As already mentioned, failure temperatures agree well with those in experiment which are roughly 780°C and 670°C in cases S1 and S2, respectively. The computed critical deflections also agree well with the measured ones.

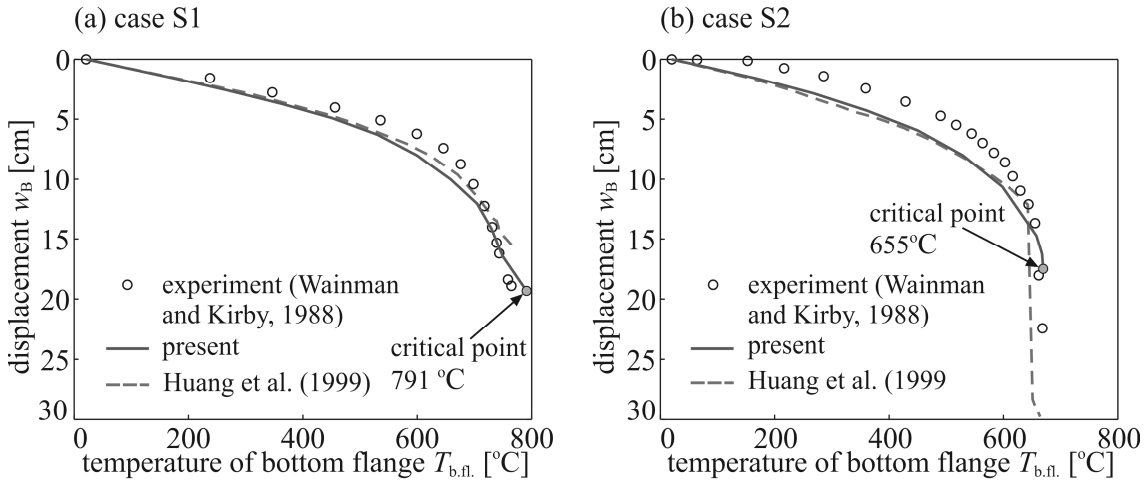

Fig 3. The variation of the midspan deflection with temperature. (a) case S1; (b) case S2.

3 ACKNOWLEDGMENT

The work of J. Kolšek was partly financially supported by the European Union, European Social Fund. The support is gratefully acknowledged.

4 SUMMARY

We presented the numerical model for the fire analysis of planar composite beam structures. The temperature field in concrete was determined with a coupled model of slow transient phenomena involving heat and mass transport and pore pressure increase in concrete. For the mechanical analysis, the strain-based non-linear beam finite element was used. The model considers both the kinematical and material non-linearity. The slip between the concrete slab and the steel sheet is allowed, while the delamination is neglected. The numerical example shows that the present beam formulation is appropriate for the thermo-mechanical analysis of frame-like structures structures, as it is accurate and robust.

REFERENCES

Bažant Z.P., Kaplan M.F., Concrete at high temperatures: material properties and mathematical models, Longman, Harlow, 1996.

Hozjan T., Nonlinear analysis of composite planar structures exposed to fire, University of Ljubljana, Faculty of Civil and Geodetic Engineering, Doctoral thesis (in Slovene), 2009.

Huang Z., Burgess I.W., Plank R.J., The influence of shear connectors on the behaviour of composite steel-framed buildings in fire, J. Const. Steel Res, 51(3):219–237, 1999.

Ma, Z.C., Makelainen P., Parametric temperature-time curves of medium compartment fires for structural design. Fire Saf. J., 34(4):361–375, 2001.

Reissner E., On one-dimensional finite-strain beam theory: The plane problem, Journal of Applied Mathematics and Physics (ZAMP), 23, 795–804, 1972.

Ranzi G., Bradford M.A., Direct stiffness analysis of a composite beam-column element with partial interaction, Comp. Struct., 85(15–16):1206–1214, 2007.

Tenchev R.T., Li L.Y., Purkiss J.A., Finite element analysis of coupled heat and moisture transfer in concrete, subjected to fire, Num. Heat Transfer Part A, 39(7):685–710, 2001.

Wainman D.E., Kirby B.R., Compendium of UK standard fire test data, unprotected structural steel–1., Ref. No. RS/RSC/S10328/1/87/B, Rotherham (UK): Swinden Laboratories, British Steel Corporation, 1988.

FIRE SAFETY ENGINEERING APPLIED TO COMPOSITE STEEL-CONCRETE BUILDINGS: FIRE SCENARIOS AND STRUCTURAL BEHAVIOUR

Emidio Nigro[a], Anna Ferraro [a], Giuseppe Cefarelli [a],

[a] University of Naples FedericoII, Department of Structural Engineering (D.I.ST.), Naples, Italy

INTRODUCTION

The structural analysis carried out in non-linear field (mechanical and geometrical) and full scale tests (BRE, 2004) show that the behaviour of structures subjected to fire is influenced not only by thermal degradation of materials, but also by further multiplicity of factors, such as the constraint conditions, structural redundancy, stiffness and ductility of the members of the structure, and loading paths. No less important are the fire scenarios and their severity, the spread of flames, the growth rate and the ventilation factor of the compartment (which influences the types of fire).
The Fire Safety Engineering (performance-based approach) allows, through the definition of specific fire scenarios and the application of advanced computational models, to take into account in an accurate way the temperature distribution within the elements and the mechanical and geometric nonlinear structural response in the fire situation. Therefore, the current Italian (D.M.16-02-2007; D.M.09-03-2007; D.M.09-05-2007; D.M.14-01-2008) and European (EN 1991-1-2; EN 1994-1-2) codes for fire structural design allow both prescriptive and performance-based approaches (Fig 1).
In this section we describe the global fire analysis of composite steel-concrete frames belonging to an office building. The considered frame presents a 24 meters overall length consisting of three equal spans and a 14 meters height consisting of four levels. The frame belongs to a three-dimensional structure with a square plant and bracing in the direction perpendicular to the frame studied: Fig. 2 shows a carpentry type and geometric characteristics of the considered frame.

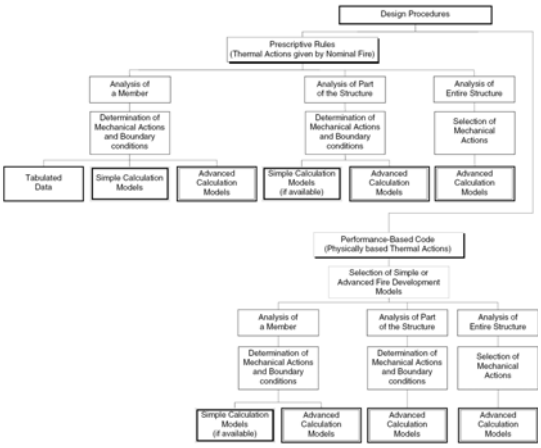

Fig. 1 Fire design methods according to the Eurocodes.

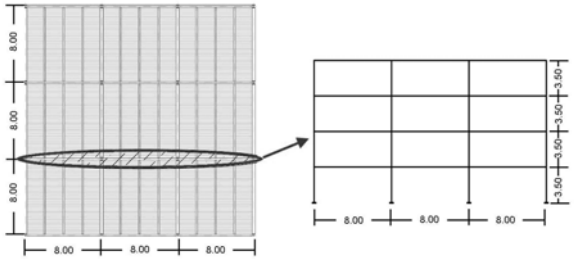

Fig. 2 Carpentry type and geometric characteristics.

The columns are arranged with the axis of maximum inertia within to the plane of the frame. Beam-to-column connections ensure the rigidity of the nodes and they are assumed to be able to withstand the forces for a time at least equal to the time of fire resistance of elements transmitting the forces. The building was designed and checked under normal conditions for all load combinations required by the Italian Technical Standards for Construction (D.M.14-01-2008). After the analysis in normal situation, it was performed a design in fire situation by the tabular method proposed by EN 1994-1-2. It is useful to underline that the new Italian Technical Code is largely inspired to Eurocodes.

The seismic design of the frame was done in low ductility class and according to the capacity design criteria required by the Italian Code (D.M.14-01-2008).
The composite steel-concrete floor consists of a profiled steel sheeting Siscofloor 5/75/720 bond with concrete slab thickness of 75 mm, for a total height of the slab of 150 mm. Moreover, there is a longitudinal reinforcement ϕ10/25cm in the concrete slab for the limitation of crack width. The secondary beam is composite with steel beam HE140B connected to the slab with headed stud connectors. The design of structures for earthquake resistance was conducted with reference to seismic zones 2 according to the Italian Code. The columns of the frame designed are partially encased with HE500B steel profile. The beams are composed by a HE260B steel profile and a composite slab 15 cm thick. The seismic design of the columns is mainly regulated by the damage limitation state, therefore they result oversized with respect to the ultimate limit state. In particular, for the ultimate limit state, the beams have a load level in hogging bending moment close to unity, in each case. In order to have a standard fire resistance of 45 minutes (R45), based on the tabular data suggested in EN1994-1-2, the composite beam was also designed as partially encased with 16 cm^2 of reinforcement in the concrete between the flange. Moreover, the partially encased composite columns have a standard fire resistance of 45 minutes.
The design vertical loads on the structure were determined according to the Italian Code (D.M.14-01-2008), which classifies the fire as an exceptional action. Therefore, the mechanical actions to be considered for fire design situation were defined by the exceptional load combination *Eq. (1)*:

$$F_d = A_d + G_{k1} + G_{k2} + \sum_{i=1}^{n} \psi_{2i} \cdot Q_{ki} \tag{1}$$

The characteristic value of variable load, Q_{k1}, was defined for the specific use of the office areas.
Each floor can be considered as a compartment. The compartment is open space and it has a plant area of 576m^2, 12 windows width 5.0m and height 1.50m. The enclosure is made by material with density 2000 kg/m^3, specific heat 1113 J/kgK and thermal conductivity 1.04 W/mK.
The specific fire load (D.M.09-03-2007) is defined as the total heat potential of all combustible materials that are placed in the fire compartment with reference to the gross area of the compartment, adjusted by parameters corresponding to the participation in the combustion of the several materials. The fire load is an index of fire hazard: the more is the fire load, the more is the severity of an fire. In the case study the fire load density is assumed equal to q_f = 655MJ/m^2. It's corresponding to the 95% fractile of the fire load Gumbel statistical distribution (see Nigro et al, 2009). The design fire load density is calculated using the following equation *Eq. (2)*:

$$q_{f,d} = \delta_{q1} \cdot \delta_{q2} \cdot \delta_n \cdot q_f = 600 \ MJ/m^2 \tag{2}$$

where δ_{q1}*=1.0* factor taking into account the fire activation risk due to the size of the compartment;
δ_{q2}*=1.0* factor taking into account the fire activation risk due to the type of occupancy;
δ_n*=0.765* factor taking into account the different active fire fighting measures i.
These factors are defined according to Italian code (D.M.09-03-2007).
The fire analysis were carried out exposing the structure both to standard time-temperature fire curve (see Nigro et all, 2008; 2009; 2010b) and to natural time-temperature fire curves (see Nigro et all, 2011), i.e. localised fire (pre-flashover fire simulated by Hasemi's method) or generalised fire (post-flashover fire simulated by parametric curve). The structural fire analyses were performed with an advanced structural model, which allows taking into account the nonlinear behaviour of materials and structure, and the effects of constrained thermal deformation.
The structural analysis was conducted by analyzing a representative plane frame. Both thermal and mechanical analyses were conducted using the nonlinear program SAFIR2007, developed at the University of Liege (see Franssen, 2008).

1 FIRE ANALYSES

The possible types of natural fire are both localised fires and generalised fires. The first can be dangerous for some structural members, the second can be dangerous for all structural elements

present in the compartment. The generalised fire can be represented by the parametric temperature-time curve (Fig. 3): it can be evaluated on the basis of the design fire load density and the characteristics of the compartment (previously described), as proposed in Annex A of EN 1991-1-2. While, the thermal action of a localized fire can be assessed, as described in Annex C of EN 1991-1-2 from the rate of heat release (RHR) curve of Fig. 4.

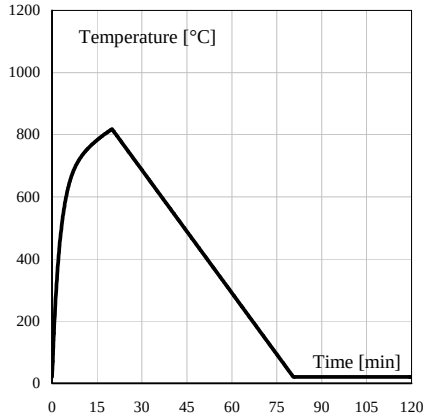

Fig. 3 Parametric Temperature-time curve.

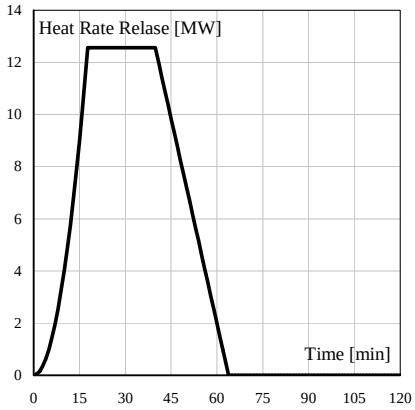

Fig. 4 Heat Release Rate curve.

Five different fire scenarios are chosen in order to evaluate the structural behaviour through the analysis of a representative plane frame, which is highlighted by blue line in Fig. 5. In Fig. 5 is reported the localized fire position and the diameter D of the fire. In Fig. 6 and in Fig. 7 are reported the analysis results (temperatures, bending moments and axial loads) for all analyzed fire scenarios. In particular, Fig. 6 shows the results for the columns, while Fig. 7 the results relating to the beams.

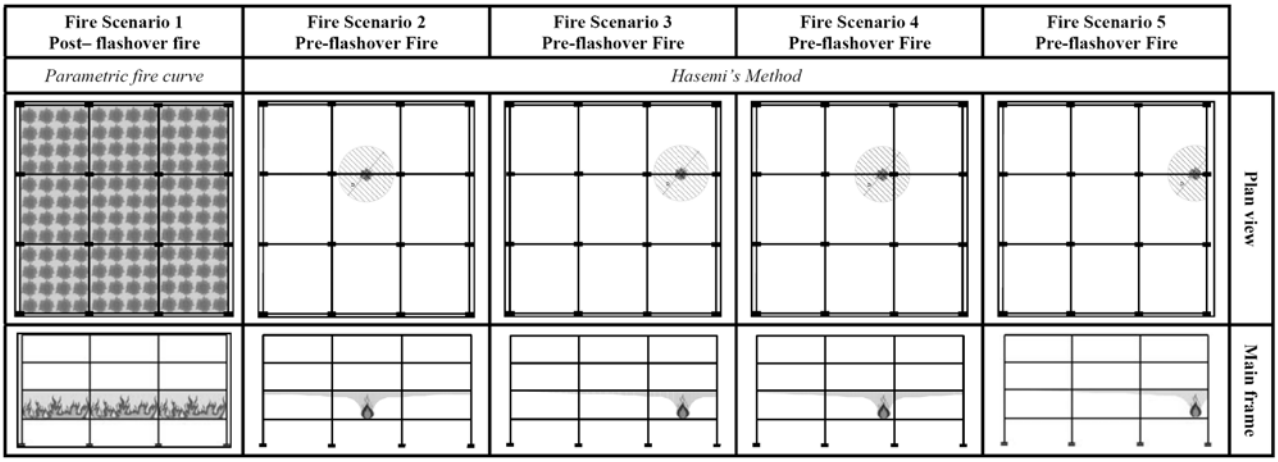

Fig. 5 Fire scenarios.

As a consequence of the heating the structural members begin to expand. The thermal elongation of the beam is constrained by the lateral stiffness of the columns and therefore the heated beam is subjected to compressive axial forces. Moreover, an increment of the hogging bending moment is produced by the thermal curvature. The axial force of the internal columns, heated on all sides, increases; in fact the columns thermal elongation is constrained by the shear stiffness of the beams. Instead, the lateral columns, heated on a single side, show an increase of the bending moment due to both the beam thermal curvature and the P-Δ effects. In the lateral cross-sections the bending moment increases during the fire exposure time due to interstorey drift caused by the thermal expansion of the heated beams. The collapse may occur not only due to material thermal degradation of the column top section, which is heated from only one side, but mainly due to the stress increase induced by hyperstatic effects due to heating.

1.1 Fire Scenario 1.

In order to understand the structural behaviour, it is analyzed the generalized fire scenario 1 (black curves in Fig. 6 and in Fig. 7). As a consequence of the heating the structural members begin to expand. The thermal elongation of the beam is constrained by the lateral stiffness of the columns and therefore the heated beams are subjected to compressive axial forces (Fig. 7). Moreover, an increment of the hogging bending moments is produced by the thermal bowing.

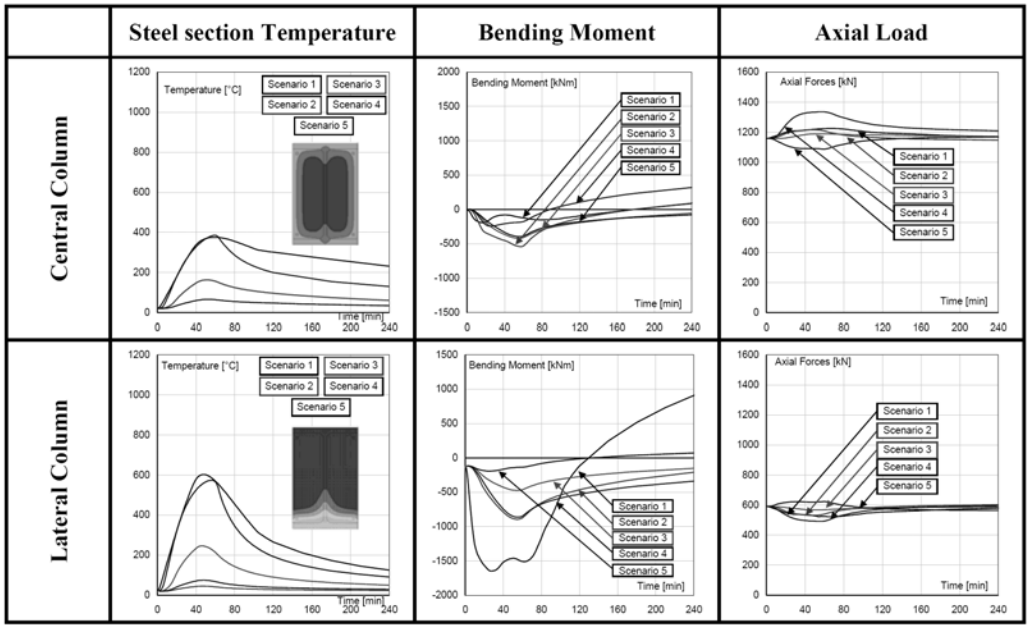

Fig. 6 Evolution of temperatures and stresses in the columns.

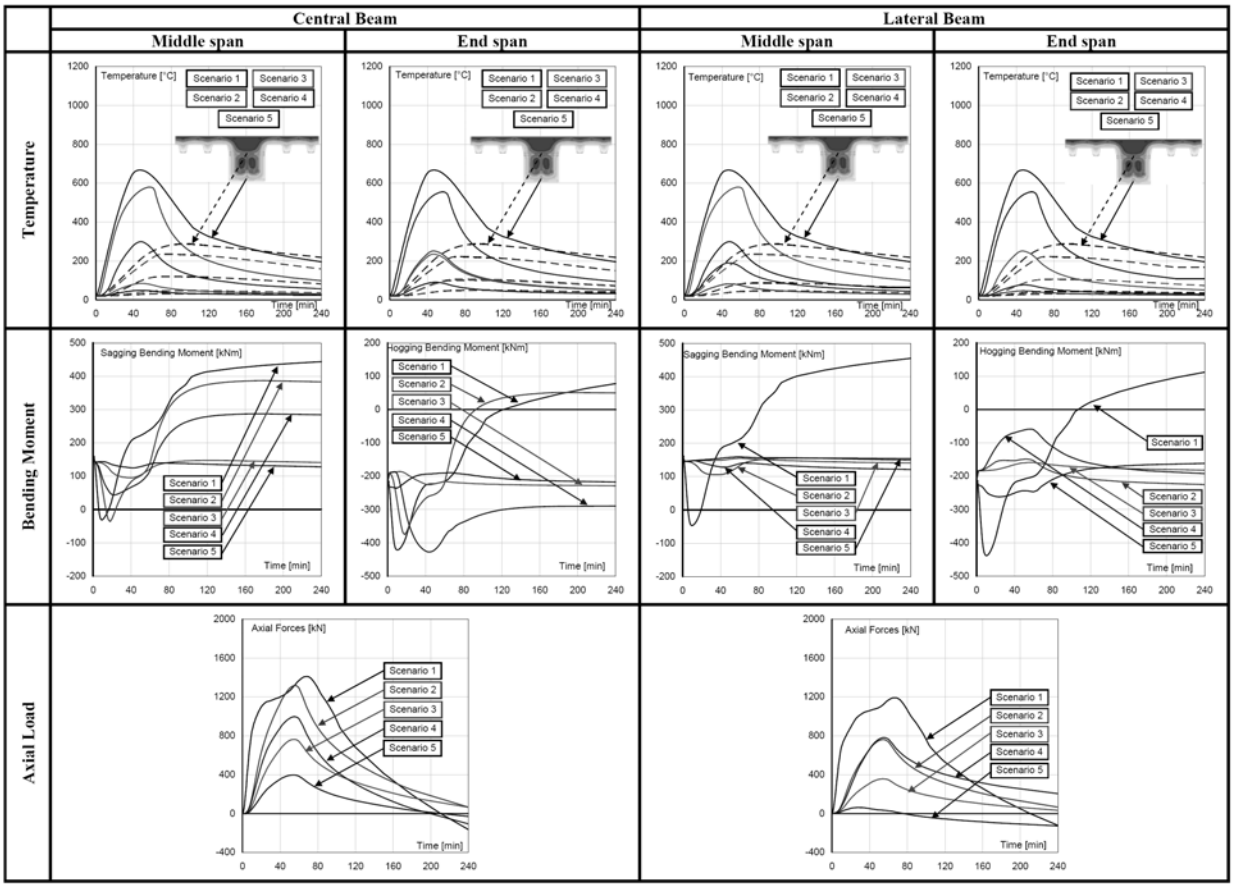

Fig. 7 Evolution of temperatures and stresses in beams.

The bending moment diagram and the corresponding deformed shape at different fire exposure time are reported in Fig. 8. The lateral columns, heated on a single side, show an increase of the bending moment due to both the beam thermal bowing and the P-Δ effects. The lateral columns, heated on a single side, show an increase of the bending moment due to both the beam thermal bowing and the P-Δ effects. The axial force of the internal columns, heated on all sides, increases; in fact, the columns thermal elongation is constrained by the shear stiffness of the beams. After about 50 minutes of fire exposure the cooling of the structural members begins (Fig. 6 and in Fig. 7), with consequent thermal bowing opposite to that of the heating phase; such curvature is able to reverse the trend both of the bending moment and the displacement of the beams (Fig. 7). The structure does not return to the same initial conditions after the fire exposure; in fact, during the heating and cooling phase plastic deformations occur at the ends of the structural members, as shown by the diagrams of bending moments during the fire exposure time (Fig. 7) and the residual strains at the end of the cooling phase (Fig. 8).

1.2 Fire Scenario 2.

The previous remarks can be done for each other scenarios. The deformed shape and the corresponding bending moment diagram at different time of exposure to fire scenario 2 are reported in Fig. 9. This case is interesting because, as can be seen from Fig. 6 and in Fig. 7 (red curves), after the fire exposure the beam is stressed by sagging bending moments over the entire central span and it has plastic hinges at its ends. However, the residual strains after fire exposure of the members not directly exposed to fire are smaller than the ones of fire scenario 1; even the bending moment diagrams of these members are slightly different from the ones at the beginning of fire.

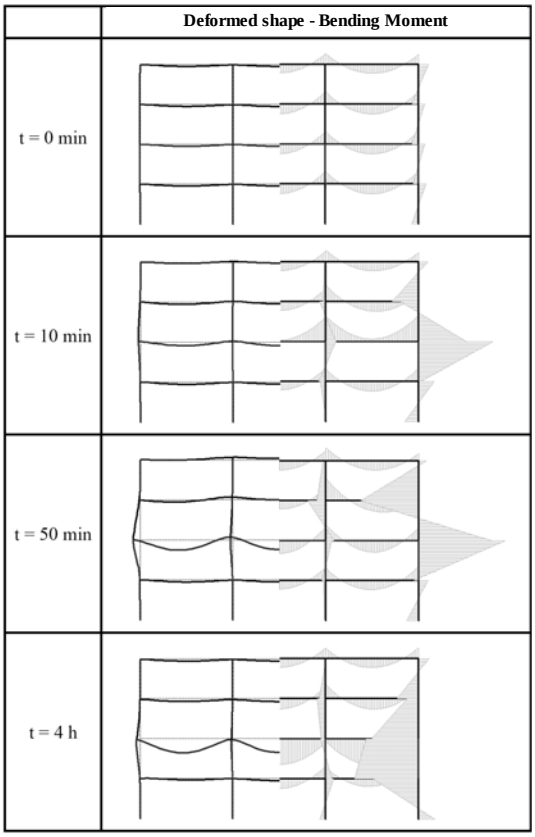

Fig. 8 Deformed shape and bending moment (Fire Scenario 1).

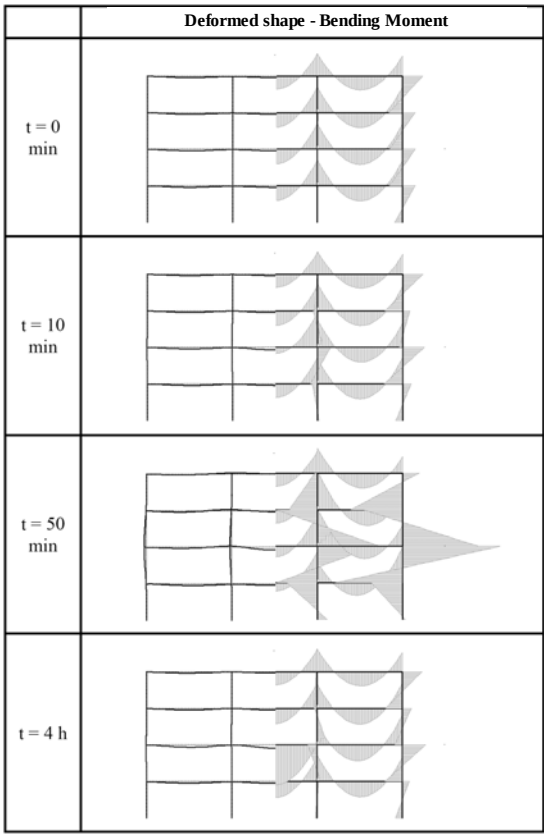

Fig. 9 Deformed shape and bending moment (Fire Scenario 2).

2 CONCLUSIONS

The Fire Safety Engineering (performance approach) allows, through the definition of specific fire scenarios and the application of advanced computational models, to estimate the structural response in the fire situation. In Italy, the fire safety building regulations are basically prescriptive; however, the performance based design and advanced calculation methods may be applied either in the lack of prescriptive rules or in the case of "derogation" with respect to prescriptive rules.
The central stage in Fire Safety Engineering process is the correct identification of fire scenarios. In this paper many different fire scenarios have been considered. In particular the structural behaviour for natural fires has been evaluated considering generalised and localised fire conditions.
For the case study, the obtained results show first of all that the level of indirect actions caused by constrained thermal expansions is more significant for generalised fire scenarios (i.e. fires involving large compartments) which can lead to possible failure of columns.
Moreover, a natural fire, differently from a standard fire, is characterized by a heating phase and a cooling phase. During the heating fire exposure the structural behaviour is non-linear and plastic strains can be achieved in the structural members; for this reason, the structure during the cooling phase is different from the initial structure. Therefore, after the cooling phase the stresses and the forces in the structural element can be different from the ones before the fire exposure. The stresses and forces induced by constrained thermal deformations may cause structural collapse; however, they cannot fully controlled by the prescriptive approach, as this approach is based on the assumption of a standard fire curve which increases unrealistically

REFERENCES

BRE, Results and Observations from full-scale fire test at BRE. Cardington 2004.

Ministry of Interior (Italian Government) 16 February 2007. Classificazione di resistenza al fuoco di prodotti ed elementi costruttivi di opere da costruzione, GU n. 74 del 29 marzo 2007

Ministry of Interior (Italian Government) 9 March 2007. Prestazioni di resistenza al fuoco delle costruzioni nelle attività soggette al controllo del Corpo nazionale dei vigili del fuoco, GU n. 74 del 29 marzo 2007.

Ministry of Interior (Italian Government) 9 May 2007. Direttive per l'attuazione dell'approccio ingegneristico alla sicurezza antincendio, GU n. 117 del 22 maggio 2007.

Ministry of Infrastructure and Transport (Italian Government) 2008. Technical Code for the Constructions. G.U. n. 29 of 14 Jenuary 2008.

EN 1991-1-2. Eurocode 1. Actions on structures - Part 1-2: General actions - actions on structures exposed to fire, November 2002.

EN 1994-1-2. Eurocode 4. Design of Composite Steel and Concrete Structures - Part 1-2: General rules - Structural fire design, August 2005.

Franssen J.M., (2008) - User Manual for SAFIR2007a: A Computer Program for Analysis of Structures Submitted to the Fire, University of Liege, Belgium, January.

Nigro E., Ferraro A., Cefarelli G., Structural fire analysis of composite steel-concrete frames (in Italian). Costruzioni Metalliche n. 6: 49-62, 2008.

Nigro E., Pustorino S., Cefarelli G., Princi P., Progettazione di strutture in acciaio e composte acciaio-calcestruzzo in caso di incendio (in italian), Ed. Hoepli, Milano, 2009.

Nigro E., Ferraro A., Cefarelli G., Member, substructure and global structural fire analyses of steel-concrete composite frames. International Conference on Urban Habitat Constructions under Catastrophic Events. Naples, September 16-18, 2010a.

Nigro E. Ferraro A., Cefarelli G., Application of FSE approach to the structural fire safety assessment of steel-concrete composite structures. International Conference on Urban Habitat Constructions under Catastrophic Events. Naples, September 16-18, 2010b.

Nigro E., Ferraro A., Cefarelli G., Fire Safety Engineering Approach Applied to Structures. (in Italian). In press on Costruzioni Metalliche n. 1, 2011.

MUNICH FIRE TESTS ON MEMBRANE ACTION OF COMPOSITE SLABS IN FIRE – TEST RESULTS AND RECENT FINDINGS

Martin Stadler [a], Martin Mensinger [b], Peter Schaumann [c], Jörg Sothmann [c]

[a] Technische Universität München, Chair for Metal Structures, Munich, Germany, Member of TUM Graduate School
[b] Technische Universität München, Chair for Metal Structures, Munich, Germany
[c] Leibniz Universität Hannover, Institute for Steel Construction, Hannover, Germany

INTRODUCTION

Composite beam slab systems show a very good behaviour in case of fire. Due to large deformations membrane forces are activated inside the slab and wider spans can be bridged. Secondary beams are not necessary at elevated temperatures and can be left unprotected. In several European countries research projects were carried out to analyse this phenomenon. In Great Britain and Switzerland membrane action is already used to design slab systems in fire. To enable such design rules in Germany further investigations are required. Available design methods need to be adapted to German design rules and some remaining issues have to be clarified. For this reason the research project "Nutzung der Membranwirkung von Verbundträger-Decken-Systemen im Brandfall" (Utilisation of membrane action for design of composite beam-slab-systems in fire) was initiated by the authors.
Main objective of the project is to understand the behaviour of intermediate beams between two slab panels. Large rotations lead to huge cracks in the concrete chord above the edge beams. That may reduce the load bearing capacity of these beams. Two large scale fire tests have been performed in Munich (Fig. 1 and Fig. 2) to analyse this issue, to calibrate numerical models and to validate analytical assumptions. Test results and latest findings of the project are presented in this paper.

Fig. 1 First Munich fire test

Fig. 2 Second Munich fire test

1 TEST ARRANGEMENT

The test arrangements should represent office buildings and similar multi storey structures. The specimens both consisted of two slab panels with overall dimensions of 5.0 m by 12.5 m (Fig. 3 and Fig. 4). They were supported by hot rolled I-beams and six reinforced concrete columns. The columns were not part of the investigation. All edge beams were protected with intumescent coating for a fire resistance of 60 minutes. The secondary beams were left unprotected. Two tests with slightly different arrangements have been performed. Only the orientation of the secondary beams, the flooring system and the intumescent coating system has been varied. The first specimen was built with a lattice girder precast slab and the second one with a profiled steel sheeting composite slab. The cross sections and reinforcement amount have been designed for an office building at

ambient temperature according to EN 1994-1-1. The utilization factors S_d/R_d were chosen very close to 100% to avoid structural integrity based on oversizing.

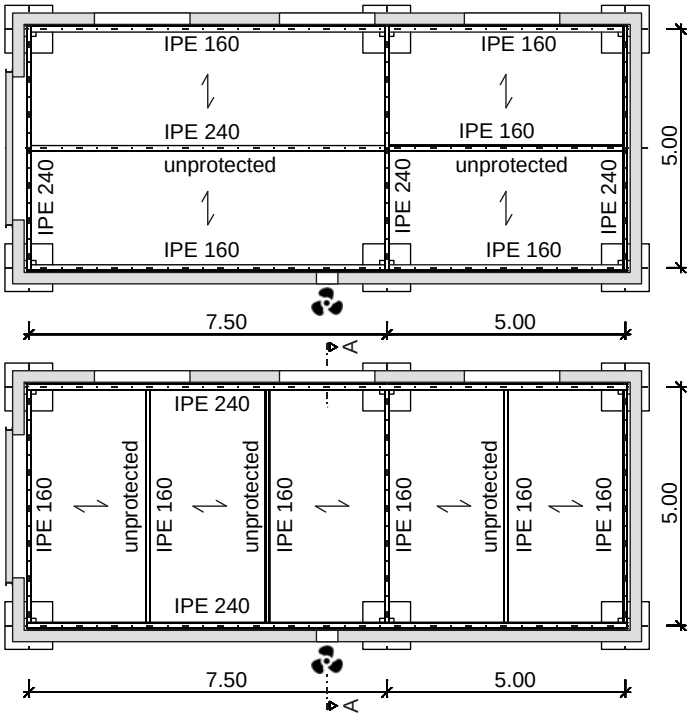

Fig. 3 Plan view of test 1 (above) and 2 (below)

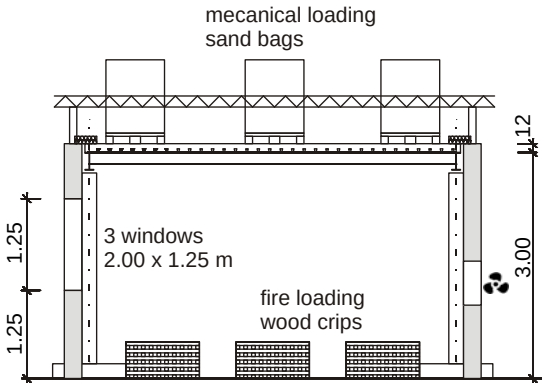

Fig. 4 Section A-A

The fire exposure of the slabs was intended to follow as close as possible the ISO 834 fire curve. The edge beams also have been inside the furnace to be able to deform freely and to investigate the influence of the edge beams on membrane action. The loading should be representative for office buildings. To ensure these boundary conditions a 3.0 m high temporary furnace was built by aerated concrete bricks. Sandbags were placed on top of the slab to simulate a uniform distributed load of 2.1 kN/m². Wood cribs consisting of 4.9 m³ spruce timber constituted the fire load. Three windows in one wall provided natural ventilation and a fan was installed in the opposite wall to readjust the ventilation.

2 TEST RESULTS

2.1 Test 1

At the first test with the lattice girder precast slab the gas temperatures exceeded 1000°C. Due to slightly non-uniform temperature distribution the maximum average gas temperature was about 900°C after 40 minutes (Fig. 5). The longer secondary beam heated up to 900°C the shorter beam even up to 950°C. The temperature in the edge beams remained below 500°C. Partially the intumescent coating detached from the lower flange. Therefore the lower flange of the intermediate beam reached almost gas temperature. The upper flange and the web stayed cooler than 500°C. The larger panel reached a maximum deformation of 260 mm after 60 minutes and the shorter panel about 200 mm. After 19 minutes a huge crack appeared in the smaller panel close to the intermediate beam (Fig. 6). The upper reinforcement layer ruptured completely in this crack and smoke passed through the gap. The slab did not collapse during the whole test but it lost its integrity (criterion “E”).

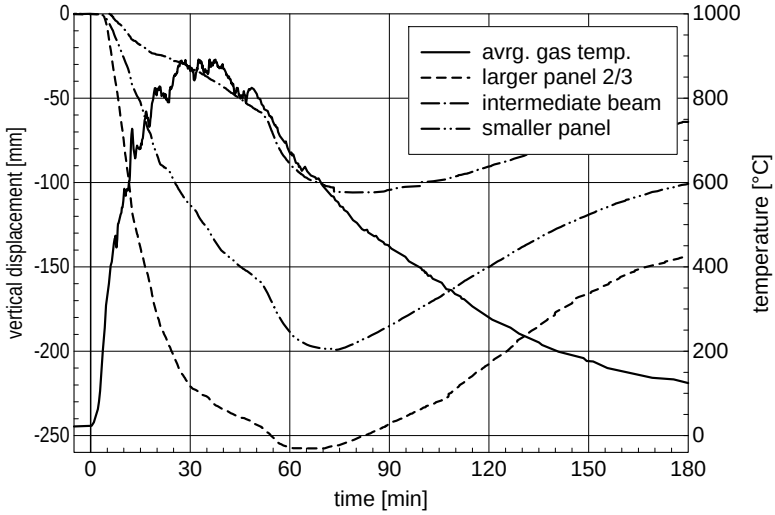

Fig. 5 Gas temperature and displacements first test

Fig. 6 Crack above intermediate beam first test

2.2 Test 2

The second test showed a very good behaviour of the composite slab during the whole experiment. The gas temperatures reached their maximum of more than 900°C after 40 minutes. The unprotected secondary beams reached over 800°C and the protected edge beams remained below 350°C. A maximum temperature of about 500°C was measured in the intermediate beam. The larger panel deformed vertically more than 250 mm and the smaller panel about 190 mm after 60 minutes (Fig. 7). The intermediate beam achieved the same deformation as the smaller panel after three hours. A large crack appeared above the intermediate beam (Fig. 8). However, all three criterions (REI) for fire resistance were kept during the whole test.

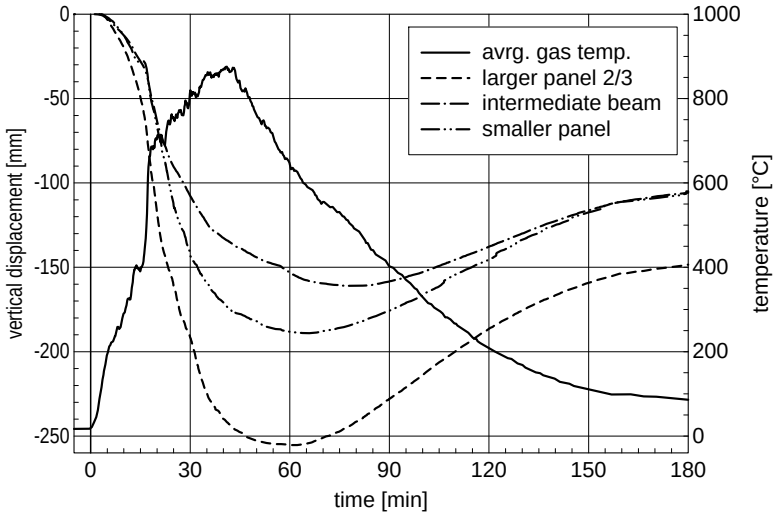

Fig. 7 Gas temperature and displacements second test

Fig. 8 Crack above intermediate beam second test

3 FIRE SIMULATION

In order to dimension the ventilation conditions the zone-model based software OZone developed by the University of Liege was used. The predicted temperature-time-curve matches the test data closely (Fig. 9). However, some differences occurred between measured and predicted temperature-

time-curve mainly caused by the humidity of the wood. The humidity considerably influences the combustion heat of fuel (c.h.o.f.) of the wood. The predicted curve was computed with the OZone default value for a c.h.o.f. of 17.5 MJ/kg. At the first test the wood had a measured humidity of 11.2%. This humidity leads to a reduced c.h.o.f. of 16.3 MJ/kg. With this reduction the simulated curve is very close to the measured curve in the heating phase. Only the cooling phase differs from the test data (Fig. 9).

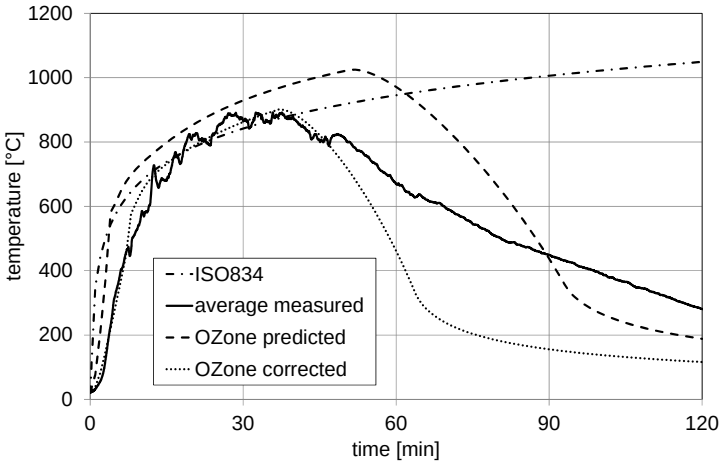

Fig. 9 Comparison of simulated and measured gas temperatures

4 EDGE BEAM BEHAVIOUR

The load bearing mechanism of the slab-beam-system is very complex. It will be discussed in the context of the first test. Assuming the slab has rigid vertical support and no edge beams the typical membrane force distribution occurs (Fig. 10). In each panel tensile membrane forces appear in the centre of the panel and a compression ring around the perimeter. This force distribution was described in former works and simplified design methods are based on it (e.g. Newman et al, 2000). But the forces change considerably when taking the edge beams into account (Fig. 11). A compression ring does not exist anymore. The edge beams elongate due to thermal expansion. This elongation is restrained by the slab and leads to compression in the beams and tension in the slab. In the model with rigid support the highest compression stresses in the concrete arise in the middle of the longer edge and the highest tensile forces occur in the middle of the slab in longitudinal direction. Whereas by including the edge beams the highest concrete compression emerges diagonal at the corners and considerable tensile forces occur above the intermediate beam.

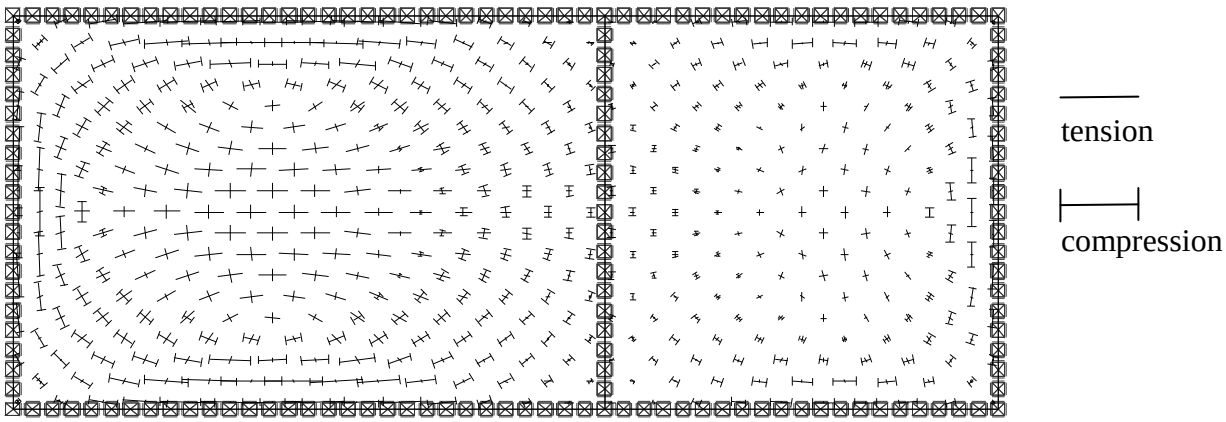

Fig. 10 Membrane forces, slab with rigid support

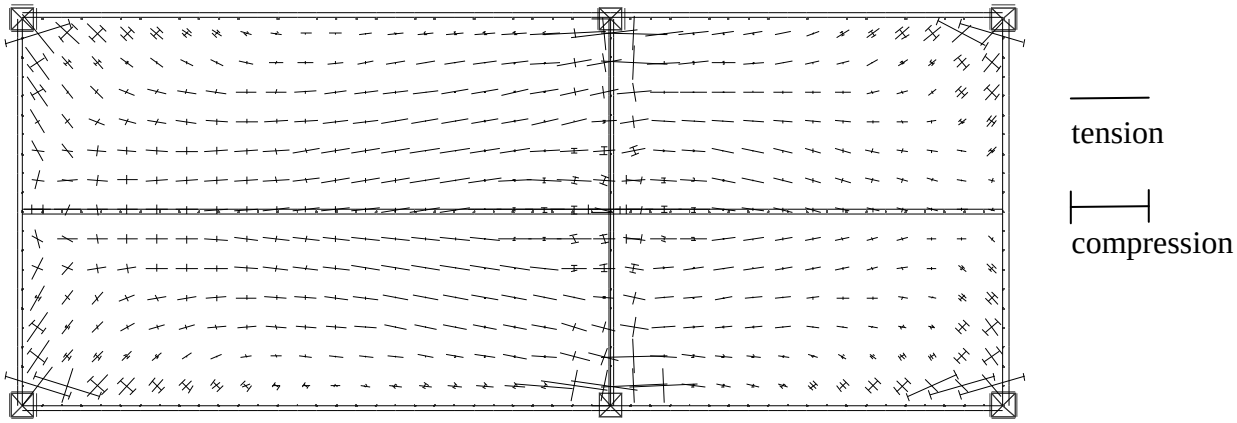

Fig. 11 Membrane forces, slab supported by edge beams

The tensile forces in the reinforcement above the intermediate beam are mainly caused by the hogging moment. This can be shown by considering the stresses in the top layer of the slab (Fig. 12a). Material nonlinearities reduce these stresses but even a bending hinge above the intermediate beam is not sufficient. The tensile forces are reduced but do not disappear (Fig. 12b). A possible explanation is that the slab acts like a three times supported cable in longitudinal direction. During the test all this led to cracking of the concrete above the intermediate beam, yielding and finally even to rupture of the reinforcement in the crack. With the ruptured reinforcement in the tension-zone the slab was not able to bear shear forces anymore and a huge shear crack was formed close to the intermediate beam. After that all the constraint forces have been removed and the slab again got into equilibrium with a different force distribution (Fig. 12c). To prevent this kind of failure further research is necessary.

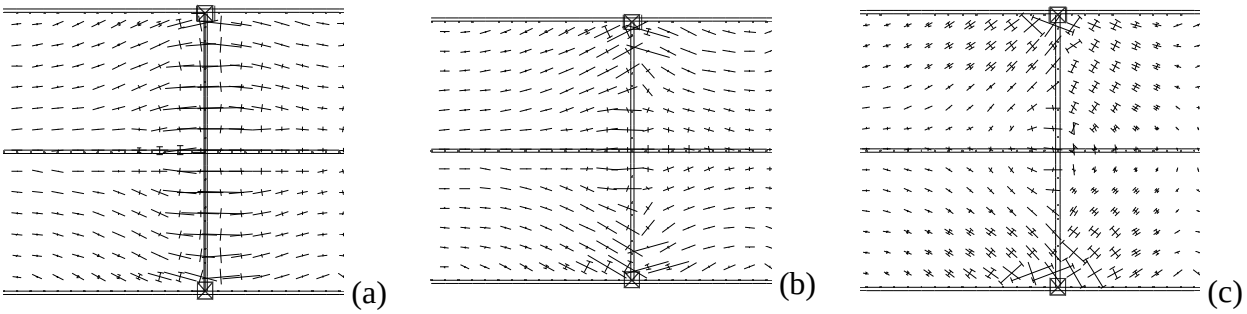

Fig. 12 Principal stresses top layer of slab, continuous (a) hinge (b) ruptured reinforcement (c)

5 SUMMARY

An on-going research project shall enable the use of membrane action for fire design of composite slabs in Germany. Within this project two large scale fire tests have been performed in Munich in 2010. The tests confirmed that membrane forces enhance the load bearing capacity considerably. In the test with the lattice girder precast slab a huge crack occurred above the intermediate beam. The slab lost its integrity and smoke streamed out of the crack. The provided explanation of the authors is that the reinforcement above the intermediate beam yielded due to the hogging moment and tensile membrane forces. No reinforcement was available anymore to transfer shear forces, a huge crack opened close to the intermediate beam and the reinforcement ruptured in the crack. Further research work is necessary to identify the parameters that induce this kind of failure and to develop design rules to avoid it in future.

6 ACKNOWLEDGEMENT

The authors would like to thank the sponsors of the project. Special thanks go to the German steel construction association DASt, the German ministry of economy and technology represented by the AiF and the construction company Max Bögl that enabled with big effort the assembly of the tests. Further supporters of the projects are: ArcelorMittal, Montana Bausysteme, Rütgers Organics, Sika, Xella, Hilti, stahl + verbundbau, Köco and HBM.
Das IGF-Vorhaben 16142 N der Forschungsvereinigung Deutscher Ausschuß für Stahlbau e.V. – DASt, Sohnstraße 65, 40237 Düsseldorf wurde über die AiF im Rahmen des Programms zur Förderung der industriellen Gemeinschaftsforschung und –entwicklung (IGF) vom Bundesministerium für Wirtschaft und Technologie aufgrund eines Beschlusses des Deutschen Bundestages gefördert.
(The IGF-research project 16142 N of the research association "Deutscher Ausschuß für Stahlbau e.V. – DASt, Sohnstr. 65, 40237 Düsseldorf" was supported via the AiF within the framework of the programme to support the cooperative industrial research and development (IGF) from the federal ministry of economy and technology due to a resolution of the German Bundestag.)

REFERENCES

Abu A. K., Burgess I. W., Plank R. J.: Slab panel vertical support and tensile membrane action in fire. In: Steel and Composite Structures 8 (2008), pp. 217–230

Abu A. K.: Behaviour of Composite Floor Systems in Fire. University of Sheffield, Department of Civil & Structural Engineering, Diss. 2009

Bailey C. G.: Membrane action of slab / beam composite floor systems in fire. In: Engineering Structures 26 (2004), pp. 1691-1703

Mensinger M., Schaumann P., Stadler M., Sothmann J.: Membranwirkung von Verbunddecken bei Brand – Stand der Technik. In: Stahlbau 79 (2010), Nr. 4, pp. 298–305

Newman G. M., Robinson J. T., Bailey C. G.: Fire safe design: A new approach to multi-storey steel-framed buildings, Steel Construction Institute, Ascot 2000 (SCI publication 288)

Tesar C. N.: Zum Tragverhalten von Verbunddeckensystemen im Brandfall, Diss. Zürich: vdf Hochsch.-Verl. an der ETH (IBK-Bericht, 309) (2008)

INFLUENCE OF SEMI-RIGID JOINT MOMENT-ROTATION CHARACTERISTICS ON THE BEHAVIOUR OF COMPOSITE STEEL-FRAMED STRUCTURES UNDER FIRE CONDITIONS

Zhen Yuan[a], Kang Hai Tan[a]

[a] Nanyang Technological University., School of Civil and Environmental Engineering, Singapore

ABSTRACT

This paper presents the results of a numerical study to illustrate the advantages of incorporating the actual behaviour of semi-rigid joints in the analyses of composite steel-framed structures under fire conditions using ABAQUS. To overcome the lack of a reliable and economical method to obtain the moment-rotation characteristics of composite joints under fire conditions, the authors have developed a new component-based mechanical model with inclusion of a new component model to represent the RC slab in tension. The predicted moment-rotation characteristics of joints were input as a 'spring' macro-element into the finite element analysis. Two representative sub-frames with and without axial restraint were analysed respectively to investigate qualitatively the influence of axial restraint on the sub-frame behaviour. In multi-span steel-framed structures with more than three spans, significant axial restraints to heated sub-structures often arise from adjacent unheated structures under fire conditions, due to structural continuity and redundancy. By comparing the beam behaviour within the two sub-frames, the significant influence of axial restraint can be illustrated. Parameters affecting the beam behaviour at elevated temperatures such as the beam-end boundary condition, load ratio and effect of axial restraint were also investigated. From the discussion of analytical results, it is shown that incorporating the semi-rigid joint characteristics in the analysis can greatly improve the beam performance at elevated temperatures.

1 INTRODUCTION

The main objective of this paper is to develop a more in-depth understanding of the behaviour of full-scale steel-framed structures incorporating composite beam-to-column joint characteristics under fire conditions, which can lead to a more rational analysis of composite steel-framed structures for the fire limit state. Current design of composite steel-framed structures in fire has been developed from the single member behaviour under standard fire conditions. This approach is widely considered to be too conservative since it generally leads to excessive fire protection to be applied to steel members. This is because a number of aspects of structural behaviour in fire, such as global and local failure of structures, restraint to thermal expansion imposed by surrounding structures, and force redistribution in highly redundant structures, cannot be replicated in isolated member tests.

Full-scale fire tests on a composite steel-framed structure such as Cardington tests (Moore and Lennon, 1997) provided first-hand observations of the frame behaviour under natural fire loads but it is very difficult to obtain detailed measurements, or to quantify various parameters that control the frame behaviour. Realistic scaled sub-frame fire tests are also few and usually simulate the transient-temperature conditions in fire tests. Hence, it is useful to develop numerical models to study the behaviour of steel-framed structures subjected to fire. Some researchers have developed 3-D numerical models of steel sub-frames under fire conditions (Liew et al., 1998; Tan et al., 2002; Liu, 2006; Santiago et al.,2008). However, the elevated-temperature moment-rotation behaviour of beam-to-column joints was often assumed to follow either a rigid-plastic or an elastic-plastic relationship, due to the lack of a reliable and economical method to obtain the moment-rotation (M-ϕ) characteristics of composite beam-to-column joints. To overcome this constraint, the authors have developed a new mechanical model with inclusion of a new component model to represent the

RC slab in tension. The new mechanical model can generate accurate *M-ϕ* characteristics of composite beam-to-column joints at elevated temperatures (Yuan, 2010).
In this paper the authors present the numerical results to illustrate the benefits and advantages of incorporating the actual behaviour of semi-rigid joints in the analysis of composite steel-framed structures under fire conditions using ABAQUS. Only the heating phase up to failure was analysed while the cooling phase was not included. This is due to a number of challenges, such as the lack of material constitutive data during the cooling phase and the much more computationally challenging problems of fracture and strain localisation in concrete slab.
A total of three parameters were investigated, which include beam-end boundary conditions (pinned, semi-rigid and rigid joints), the load ratio, and the axial restraint. Two representative sub-frames with and without axial restraint were analysed respectively to investigate *qualitatively* the influence of axial restraint on the sub-frame behaviour.

2 THE NEW MECHANICAL MODEL FOR COMPOSITE JOINTS

Based on the principles of the component method, the authors have developed a new component-based mechanical model for a composite steel top-and-seat-and-web (TSW) angle joint (Yuan, 2010) shown in Fig. 1. A major innovative feature of this model is the inclusion of a new joint component to represent an RC slab in tension. Each joint component is idealised as a 'spring' with certain stiffness and strength characteristics. The rotation centre of the joint under symmetric hogging moments is located at the point ***O*** in Fig. 1, which is the intersection of the centreline of the seat angle plate and the column flange.
The joint components include RC slab in tension (rcst), RC slab in longitudinal shear (rls), shear studs in shear (sts), column web in compression (cwc), column web in tension (cwt), column flange in bending (cfb), bolts in tension (bt), top angle in bending (tab), bolt in shear (bs), top angle in tension (tat), top angle in bearing (tabb), beam flange in bearing (bfbb), web angle in bending (wab), beam web in bearing (bwbb), web angle in bearing (wabb), beam web in tension (bwt), column web in shear (cws), seat angle in bearing (sabb), beam flange in compression (bfc) and seat angle in compression (sac). The general concept is to assemble the respective force-displacement relationship of each row of components to obtain the overall moment-rotation behaviour of the joint. The joint rotation for an applied moment is calculated based on the principle of equilibrium, compatibility and components force-displacement relationship at all rows of components. The complexities of the calculation process result from the interactions among different constitutive relationships and non-linearities of each row of components. However, the proposed joint model can be implemented through the Excel spreadsheet.

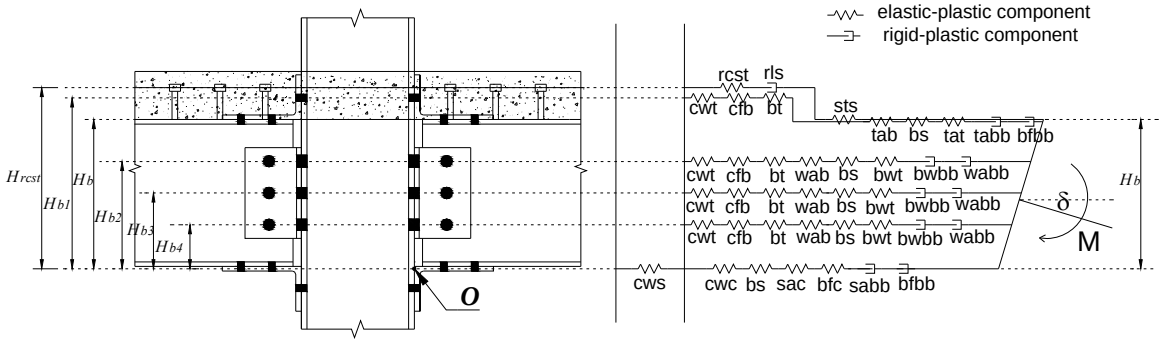

Fig. 1 New component-based mechanical model for a composite steel TSW angle joint

2.1 Initial rotational stiffness

Calculation of the initial rotational stiffness requires the input of initial stiffness of each component and the position of each component in the joint itself. The behaviour of each component is defined through either an elastic-plastic or a rigid-plastic spring. The former assumes that initial

deformations are reasonably linear with applied load until plastic deformation occurs, while the latter assumes that initial deformations are negligible until plasticity creeps in.
The component-based mechanical model can be simplified by the procedure shown in Fig. 2. Using the proposed spring model shown in Fig. 2 the force equilibrium conditions give rise to Eq. (1):

$$F_r = F_s;\ F_r + F_{b1} + F_{b2} + F_{b3} + F_{b4} = F_c \tag{1}$$

where F_r is the tension force in the RC slab and F_{bi} (i = 1,2,3,4) is the respective tension force in each row of springs, respectively. F_s is the shear force in shear studs and F_c represents the compressive force in the column web.

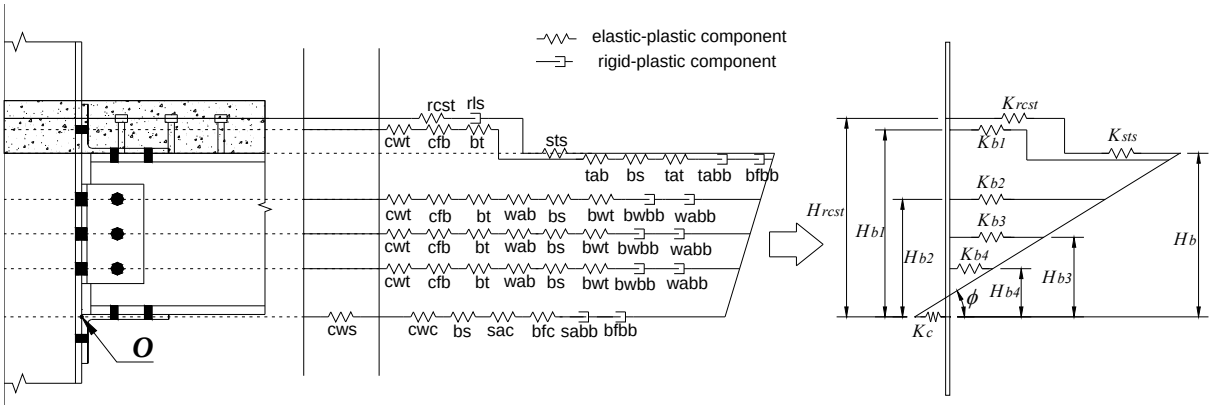

Fig. 2 Simplification process of the mechanical model into the spring model

From Hook's law the elongation of each row of spring is calculated as

$$F_r = K_r\Delta_r;\ F_{bi} = K_{bi}\Delta_{bi}, i = (1,2,3,4);\ F_s = K_s\Delta_s \tag{2}$$

where K and Δ are the stiffness and elongation of the respective row of springs.
The compatibility equilibrium gives rise to

$$\frac{\Delta_r + \Delta_s + \Delta_c}{H_b} = \frac{\Delta_{bi} + \Delta_c}{H_{bi}} = \phi \tag{3}$$

where H_b is the beam depth and H_{bi} (i =1,2,3,4) is the distance from each row of springs to the centreline of the seat angle plate in contact with the beam bottom flange.
After solving the algebraic equations, the forces in each row of springs can be obtained. Since at the initial stage of loading the internal tensile forces are low, all the components' behaviour is elastic. Therefore, the moment is calculated using forces in reinforcement and each row of springs in this case through Eq. (4).

$$M = F_r H_r + F_{b1} H_{b1} + F_{b2} H_{b2} + F_{b3} H_{b3} + F_{b4} H_{b4} \tag{4}$$

where M is the moment and H_r is the distance from rebar centre to the centre line of bottom seat angle plate in contact with the beam bottom flange. Hence, the initial rotational stiffness $K_{\phi,i}$ is equal to M/ϕ.

2.2 Moment Capacity

The joint moment capacity $M_{j.Rd}$ can be calculated from Eq. (5) by summing up the product of tension or compression capacity of each row of components and the distance between each row of components to the centreline of seat angle.

$$M_{j,Rd} = F_{r,Rd} H_r + F_{b1,Rd} H_{b1} + F_{b2,Rd} H_{b2} + F_{b3,Rd} H_{b3} + F_{b4,Rd} H_{b4} \tag{5}$$

where $F_{r,Rd}$ and $F_{bi,Rd}$ (i = 1,2,3,4) are the tension capacity of the RC slab and of each row of components, respectively. The tension/compression capacity of each row of springs is limited by the minimum strength of its constituent components, and individual row capacity when considering the failure mechanism involving a group of rows of springs. Moreover, it is obvious that the total capacity of any combination of rows of springs shall not exceed the aggregate sum of individual rows of components.

2.3 Influence of strain hardening

Strain-hardening behaviour of each component after reaching plastic capacity is important for correctly predicting the full-range moment-rotation curve of the joint and its ultimate moment capacity. To account for strain-hardening of steel, Faella et al. (2000) proposed a simple method without a significant increase in the computational effort. Fig. 3 shows a typical quadric-linear moment-rotation relation of a component, where f_y is the yield strength and f_u is the ultimate strength, E_h is the strain hardening modulus and k_ϕ is the initial rotational stiffness. This approach was adopted in the proposed mechanical model.

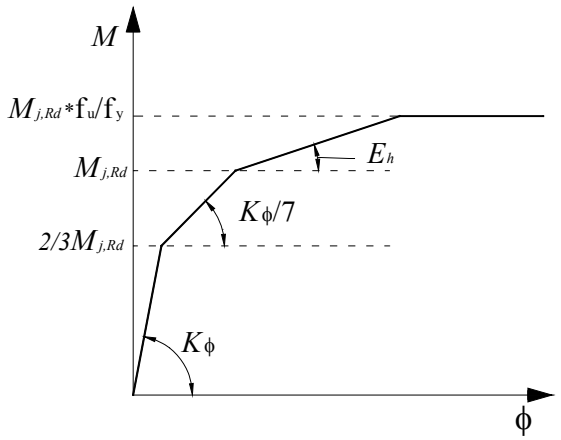

Fig. 3 A typical quadric-linear moment-rotation relationship of a row of components

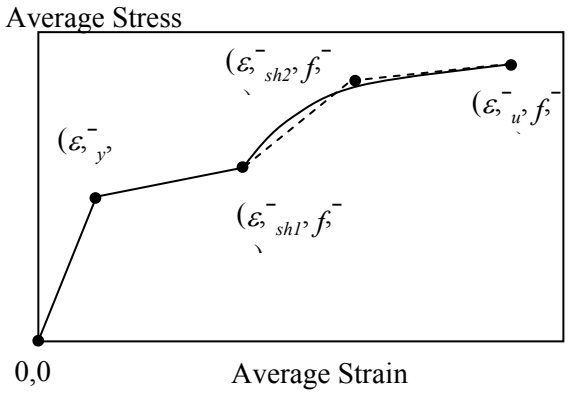

Fig. 4 The tri-segmental model and the multi-linear model of embedded reinforcing bars

2.4 The proposed new joint component of the RC slab in tension

The tension-elongation behaviour of the RC slab is highly non-linear due to tensile cracks and progressive bonding failures between embedded reinforcing bars and cracked concrete. To derive the tension-elongation relationship of the RC slab, two fundamental definitions need to be defined: (i) the space-averaged stress-strain relationship and (ii) the effective length of the RC slab in tension. This was achieved by utilising the individual constitutive models of cracked concrete and embedded rebar which were derived semi-theoretically and validated experimentally by Maekawa et al. (2003). Some minor modifications were applied to account for the important differences between the actual RC slab behaviour and the assumptions of Maekawa's model.

2.4.1 Space-averaged stress-strain relationship of an RC slab in tension

Although the localised stress and strain distribution within the cracked concrete and the steel bars are not uniform across the tensile cracks, this non-uniformity can be explicitly incorporated into structural analysis through averaging the stress and strain spatially along the full length of an RC element (Maekawa et al., 2003). Based on the micro-bond analysis, the space-averaged stress-strain response of an embedded rebar was found to fit well using a tri-segmental model proposed by Maekawa et al. (2003), as shown in Fig. 4. The first segment is linear up to the average yield point (e^-_y, f^-_y), which represents the elastic range of reinforcement. The second segment is still linear and is connected to the average strain-hardening point (e^-_{sh1}, f^-_{y1}), while the last segment is an

exponential curve, similar in form to the strain-hardening part of bare bars, up to the average ultimate stress and strain ($e,^{-}_{u}, f,^{-}_{u}$). The exponential part of the curve is simplified and replaced with a bi-linear curve with an additional strain-hardening point ($e,^{-}_{sh2}, f,^{-}_{y2}$) as shown in Fig. 4. The details of this stress-strain model can be found in Chapter 11 of Nonlinear Mechanics of Reinforced Concrete (Maekawa et al., 2003) and is not discussed here.

For modelling of concrete, the average tensile stress-strain relation proposed by Okamura and Maekawa (1991) can be expressed by Eq. (6), where f_t is the tensile strength of concrete, ε_{tu} is the tensile cracking strain equal to 0.02% and c is the coefficient equal to 0.4 for deformed bars.

$$\frac{\sigma_t}{f_t} = \left(\frac{\varepsilon_{tu}}{\varepsilon} \right)^c \tag{6}$$

Thus, the averaged tensile stress-strain relationship of an RC slab with a few major cracks can be obtained by superimposing the individual constitutive stress-strain model of the embedded steel bars and the cracked concrete slab together. If the average elongation of the RC slab is known and therefore the average strain is calculated, the total tensile force across the section of the RC slab can be computed.

2.4.2. Effective length of an RC slab in tension

To define the effective length, two distinct stages of behaviour are considered: before and after the occurrence of the first major tensile crack. The strain development along an embedded steel bar in a pull-out test before the occurrence of the first major crack is presented in Fig. 5(a) (Maekawa et al., 2003). It was observed that the strain at the stressed end increases proportionally with the applied load. On the other unstressed end, the strain is apparently always zero. From experimental measurements and numerical analysis (Maekawa et al., 2003), when the first major crack occurs, the rebar tensile strain generally lies between 0.0001 and 0.0003. At this strain, the length of the RC element that has developed significant strain is limited to a length of approximately twice the rebar diameter from the stressed end (Fig. 5(a)), while tensile strains at other locations are almost zero. To be conservative, the average strain of an RC slab is defined as 0.0001 at the occurrence of the first major crack. Hence, the effective length of the RC slab before the first major crack occurs is defined as two times the rebar diameter.

After the first major crack has occurred, the reinforcing bars over this major crack will experience an abrupt increase in localised strain because they will carry all the tensile forces. Consequentially, this will cause the strain development to progress quickly along the steel bars (Maekawa et al., 2003). Soon after that, the second and third major tensile cracks will occur. Tensile strain will develop to the full length of the RC element as illustrated in Fig. 5(b). The overall strain distribution is approximately a triangular shape (Fig. 5(a) and Fig. 5(b)). Assuming an RC slab has the same strain as the loaded end for the whole of its effective length, the effective length of the RC slab in tension is approximately equal to half of its full length (l_{full}). Therefore, the effective length (l_e) of an RC slab in tension is

$$l_e = 2 \times \textit{the diameter of rebar} \quad \text{before the first major crack occurs} \tag{7}$$

$$l_e = 0.5 \times l_{full} \quad \text{after the first major crack has occurred} \tag{8}$$

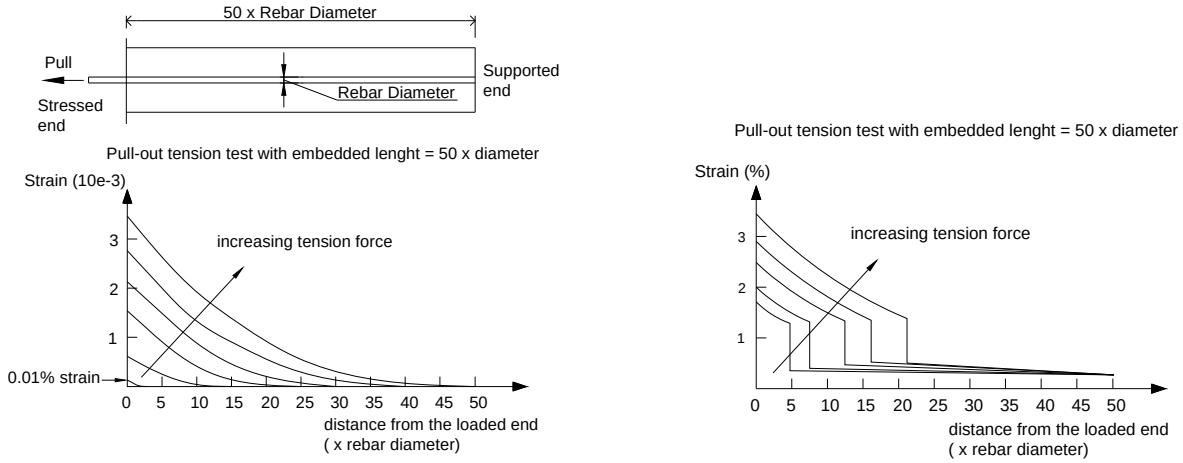

(a) (b)

Fig. 5 Strain distributions of embedded steel bars in a pull-out tension specimen before and after the occurrence of the first major tensile crack

After obtaining the space-averaged stress-strain relationship and the effective length of an RC element in tension, the tension-elongation relationship can be derived from Hook's law. Before the occurrence of the first major tensile crack, for an elongation, the average stress of the embedded rebar and the cracked concrete can be calculated from the average strain equal to the elongation/the effective length (twice the rebar diameter). The tension forces in the rebar and the cracked concrete can be calculated from the product of the average stress and the cross-sectional area of the rebar and the cracked concrete, respectively. The total tension force across the section of the RC element is the sum of the tension forces in the rebar and in the cracked concrete, respectively. Hence, the tension-elongation relationship of the RC element in tension can be derived. After the first major tensile crack has occurred, the effective length of the RC element will be changed to half of the full length under tension. The same approach before the occurrence of the first major tensile crack of is used to derive the tension-elongation relationship.

2.4.3. Modifications of the stress-strain models

It should be noted that the aforementioned stress-strain model for the embedded rebar and the cracked concrete was mainly verified against the pull-out tests of a single reinforcing bar from RC stubs. Hence, successful application assumes that tensile strain of all bars should be fairly uniform across the RC element section. However, for the RC slab subject to induced tension forces from a hogging moment, a variation of tensile strains and stress in the rebar across the section does exist (Gil and Bayo, 2008). The reinforcing bars near the column stub will develop higher tensile strains and hence fracture earlier than the reinforcing bars further away from the stub. Moreover, shear studs have an influence on the average stress-strain characteristic of the RC slab. Unfortunately, there is no test data on an RC slab in tension with embedded shear studs. Therefore, the actual behaviour of this element requires further test results.

In the absence of any experimental data for verification, it is recommended to adopt a conservative limit to define the ultimate tensile strength of an RC element. After a parametric study, it is found that the second strain-hardening stress (f_{y2}) (see Fig. 4(b)) is about 95% of the averaged ultimate stress (f_u), irrespective of the post-yield behaviour of bare bars, reinforcement ratios and concrete strengths. Hence, it is postulated that *the second strain-hardening stress (f_{y2}) is adopted as the characteristic ultimate strength for embedded reinforcement in the RC element in tension*.

2.5 Validation of the new mechanical model

As can been seen in Tab. 1, the new mechanical model yields accurate and consistent predictions of the M-ϕ behaviour of composite steel TSW angle joints at various elevated temperatures (Yuan, 2010).

Tab. 1 Summary of the test results and the analytical evaluations

Elevated Temperature Test									
Joint	BFC Temp.	$M_{u,test}$	$M_{u,pred}$	$M_{u,test}/$	Failure Mode		$K_{i,test}$	$K_{i,pred}$	$K_{i,test}/$
Specimen	(^{o}C)	(kNm)	(kNm)	$M_{u,pred}$	Test	Predicted	(kNm/rad)	(kNm/rad)	$K_{i,pred}$
C1-T1	434	201	202	0.995	A	A	141644	59606	2.376
C1-T2	569	138	133	1.038	B	B	25415	21073	1.206
C2-T1	633	165	150	1.100	B	B	21259	19632	1.083
C2-T2	646	150	139	1.079	B	B	17436	21098	0.826
C2-T3	491	211	208	1.014	B	B	85714	57163	1.499
C3-T1	651	207	214	0.967	C	C	43490	26866	1.619
C3-T2	551	278	263	1.057	C	C	53894	24039	2.242
C3-T3	424	338	326	1.037	D	D	86458	60262	1.435
Ambient Temperature Test									
C1-A1	26	215	225	0.956	D,A	D	37588	41690	0.902
C1-A2	26	154	133	1.155	B	B	40372	41708	0.968
C2-A1	26	269	256	1.051	B	B	104600	63591	1.645
C2-A2	26	279	253	1.103	B	B	61646	63591	0.969
C3-A1	26	286	273	1.048	B	B	81970	84025	0.976
C3-A2	26	278	275	1.011	B	B	65450	84154	0.778
			Mean	1.044				Mean	1.323
			SD	0.054				SD	0.508

Note: A = Local yielding/buckling of beam flange in compression; B =Longitudinal shear splitting of RC slab; C = Local buckling of column web in compression ; D = Yielding of main reinforcement bars; BFC = Beam flange in compression.

3 LOAD RATIO

For steel beams, the concept of load ratio R (BSI, 2003) is defined as the load or moment carried at the time of a fire to the moment capacity at 20°C (BS5950 Part 8). The load ratio R should be taken as the greater of:

$$R=\frac{M_f}{M_c} \quad or \quad R=\frac{mM_f}{M_b} \tag{6.1}$$

where M_f is the applied moment at the fire limit state, M_b is the buckling moment resistance (lateral torsional), M_c is bending moment resistance, and m is the equivalent uniform moment factor.
In all analyses the steel beams are uniformly loaded with a load ratio of 0.6 to represent typical full service loading, as recommended in BS5950 Part 8. In practice, the design of steel beams usually neglects the moment resistance of the beam-to-column joint, so the applied loads are the same for the pinned, semi-rigid and rigid joint cases.

4 FAILURE TEMPERATURE

The term ‘failure temperature’ is defined as the temperature at which the mid-span deflection of the middle beam reaches span/20, as recommended in BS 476: Part 21 (BSI, 1987). A limiting temperature of 1000°C was imposed due to excessive deflection of the central beam beyond this temperature. It should be recognised that the concept of ‘failure temperature’ is adopted only as a basis for comparing fire resistance performance. In actual fire conditions this criterion does not necessarily correspond to failure of structures.

5 A REPRESENTATIVE SUB-FRAME

A representative sub-frame is designed from a fire scenario in a braced steel-framed building, as illustrated in Fig. 6(a). The fire outbreak was confined to a middle compartment of a steel framed structure, where the middle beam is directly heated by the fire. Fig. 2(a) shows that the end-span beams do not provide any axial restraint to the middle beam. One the other hand, if the end-span beams provide significant axial restraint to the middle beam, then the axial restraint to the middle beam should be considered in the analysis.

The loading arrangement is shown in Fig. 6(a). Numerical studies conducted by El-Rimawi (1989) concluded that the results of sub-frame analysis are reasonably representative of the full-scale frame tests under fire conditions. Temperature distributions are shown in Fig. 6(b). The end-span beams, the upper columns and the beam-to-column joints outside the fire compartment were assumed to remain at 20°C. The middle beam temperature (1.0T) was assumed to be uniform across the beam section and along the entire beam length in the analysis. The lower columns were assumed to be thermally insulated and sustained only 0.5T. Temperature of the beam bottom flange within the joint zone was assumed to be 0.7T, as suggested by Lawson (1990). In addition, the temperature distributions within the joint were assumed to follow the observations in the isolated joint tests in Tab. 2 (Yuan, 2010).

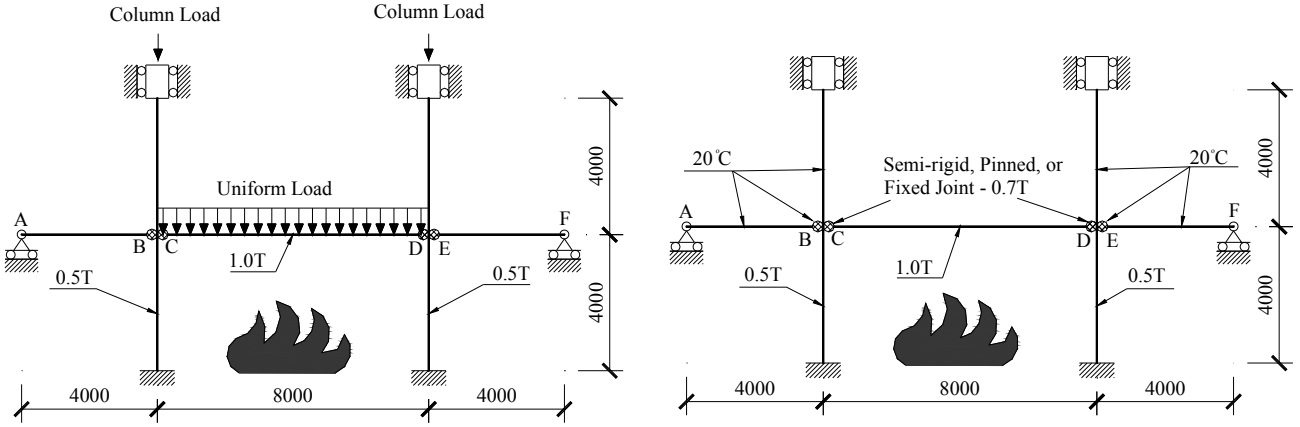

(a) (b)

Fig. 6 A representative sub-frame model and typical loading for a steel-framed structure without axial restraint

Tab. 2 Summary of the temperature profiles for eight joint specimens

Relative temperature to the beam bottom flange temperature	C1-T1	C1-T2	C2-T1	C2-T2	C2-T3	C3-T1	C3-T2	C3-T3	**Average**
Beam top flange	0.70	0.80	0.83	0.82	0.79	0.88	0.86	0.83	**0.82**
Beam mid-height web	0.97	0.99	0.99	0.99	0.99	0.98	0.99	1.00	**0.99**
Beam bottom flange	1.00	1.00	1.00	1.00	1.00	1.00	1.00	1.00	**1.00**
Central web angle	0.84	0.95	0.97	0.96	0.98	1.01	1.03	1.04	**0.97**
Seat angle	0.99	1.00	0.96	1.00	1.01	0.98	0.98	1.02	**0.99**
Top angle	0.70	0.81	0.79	0.78	0.71	0.77	0.76	0.70	**0.75**
Column Flange (near seat angle)	0.88	0.93	0.95	0.96	1.00	0.97	1.01	1.06	**0.97**
Column Flange (near top angle)	0.79	0.84	0.84	0.85	0.79	0.84	0.85	0.75	**0.82**
Column web in compression at seat angle	0.82	0.94	0.96	0.97	1.03	0.97	1.02	1.04	**0.97**
Reinforcement bar	0.27	0.21	0.27	0.24	0.25	0.23	0.25	0.26	**0.25**
Shear stud	0.41	0.57	0.52	0.50	0.48	0.44	0.48	0.43	**0.48**
Concrete slab at directly above top flange	0.47	0.51	0.49	0.50	0.47	0.49	0.44	0.42	**0.47**
Concrete slab at 50mm above top flange	0.34	0.33	0.31	0.33	0.30	0.29	0.24	0.29	**0.30**
Concrete slab at 100 mm above top flange	0.31	0.21	0.24	0.24	0.24	0.21	0.21	0.24	**0.24**
Furnace temperature	1.38	1.32	1.30	1.38	1.43	1.41	1.54	1.63	**1.42**

Nominal material properties were adopted for modelling steel beams, columns, reinforcement and the slab in the analysis. All beams and columns were assumed to be of Grade S355 steel. The RC slab thickness was assumed to be 130mm. The effective width of the RC slab was defined as one quarter of the interior longitudinal span (the effective width=2.0m), as specified in EC4 Part 1.1

(CEN, 2004). The same effective width was assumed for the end-span slabs for consistency. The slab reinforcement was 10T10 located at 100mm above the slab soffit. The nominal yield strength of reinforcement was 460N/mm^{2}with C40 (f_{cu} = 40 N/mm^2) as the concrete grade. Poisson's Ratio of 0.2 was adopted for concrete and 0.3 for structural steel and reinforcement. For the concrete slab in the hogging moment region, the maximum tensile strength of concrete was defined as 10% of its maximum compressive strength. Elevated-temperature material properties of concrete and steel were defined according to EC2 Part 1.2 (CEN, 2005) and EC3 Part 1.2 (CEN, 2005).

A half model of the representative sub-frame was analysed using ABAQUS (2008) to reduce the running time. In the finite element model, two-noded beam elements were used to model the beams and the columns. Four-noded thick shell elements were employed to model the slab. The beam elements were offset from the slab elements by using pre-set options in ABAQUS. Spring elements were used to simulate the moment-rotation curves of semi-rigid joints. Concrete damaged plasticity with tension stiffening material model was utilised to include concrete tension stiffening effect.

5.1 Influence of boundary conditions

The mid-span deflection of the middle beam was obtained for incorporating rigid, semi-rigid and pinned joint characteristics, respectively. This was achieved by idealising the beam-to-column joints at B, C, D and E in Fig. 6(a) with respective moment-rotation characteristics of rigid, semi-rigid and pinned joints. The 'rigid' joint assumed no relative rotation between the beam ends and the columns, while the 'pinned' joint assumed zero strength and stiffness. One the other hand, the beam-end joints at A and F were idealised as roller supports, allowing horizontal movements.

The semi-rigid joint characteristics were represented by utilising joint C1 configuration shown in Fig. 7**.** Based on the new mechanical model, the predicted ultimate moment resistance $M_{j,u}$ of joint C1 at ambient temperature is 227kNm. Meanwhile, the sagging moment capacity of the composite beam ($M_{b,Rd}$) is 345kNm according to EC4 Part 1.1. The joint moment-rotation characteristics at different temperatures were obtained from analytical predictions by the mechanical model, as shown in Fig. 8.

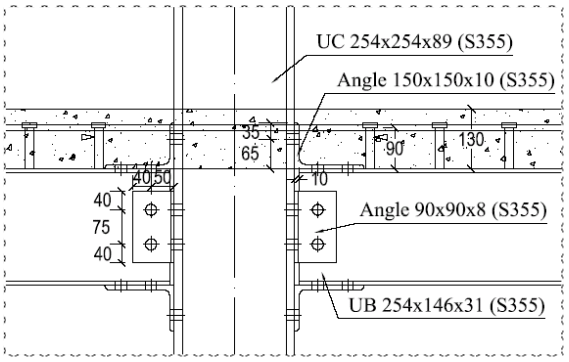

Fig. 7 Configuration details of joint C1

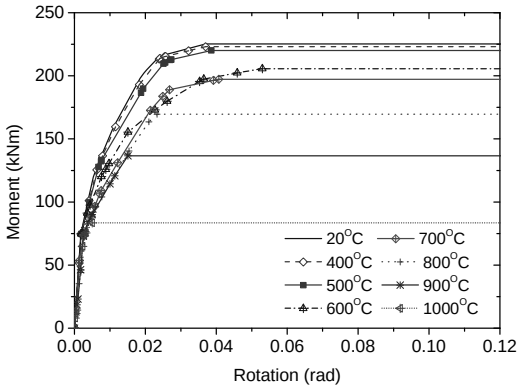

Fig. 8 Analytical moment-rotation relationships of joint C1

A load ratio of 0.6 is applied to the middle beam, which is equivalent to a uniform load of 25.9kN/m. The middle beam behaviour incorporating C1 joint characteristics is shown in Fig. 9, together with 'fully-rigid' and 'fully-pinned' joint characteristics. The middle beam deflection is very small for temperatures up to 400°C and 700°C for pinned and rigid joint cases, respectively. A further increase in temperature causes a progressive increase in middle beam deflection until it reaches 1/20 of beam span at the 'failure temperatures' of 670°C and 830°C for pinned and rigid joints, respectively. Thus, the failure temperature of the beam with rigid joints is nearly 160°C higher than those with pinned joints.

The middle beam response with semi-rigid joint C1 is close to that with rigid joints. The failure temperature is 810°C, which is 140°C higher than the beam with pinned ends. It is clear that incorporating semi-rigid joint characteristics greatly enhances the beam performance and increases

the failure temperature. Firstly, the stiffness of semi-rigid joints at the beam ends can significantly reduce the mid-span deflection. Secondly, the hogging moment resistance of the joint can help to redistribute excessive mid-span sagging moment to the two beam ends, compared with pinned-end case.

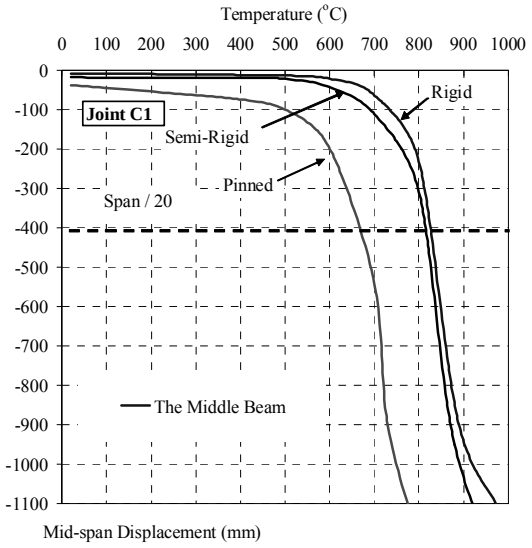

Fig. 9 Middle beam behaviour incorporating C1 joint characteristics

5.2 Influence of load ratio

In an actual multi-storey building, load levels may vary due to changes in building functions. Hence, the effect of the load ratio on the beam response under fire conditions was studied.

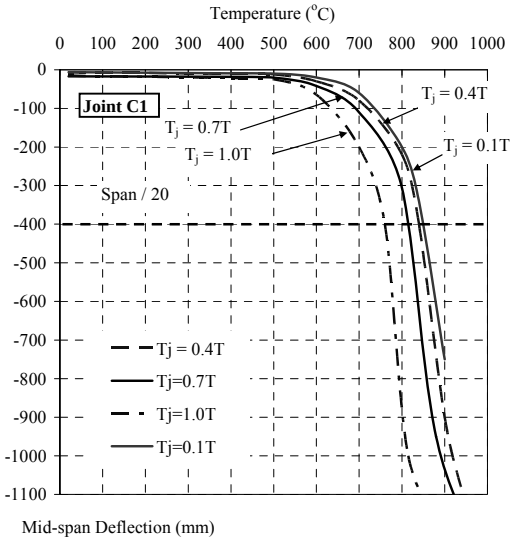

Fig. 10 Influence of joint temperature on the middle beam response

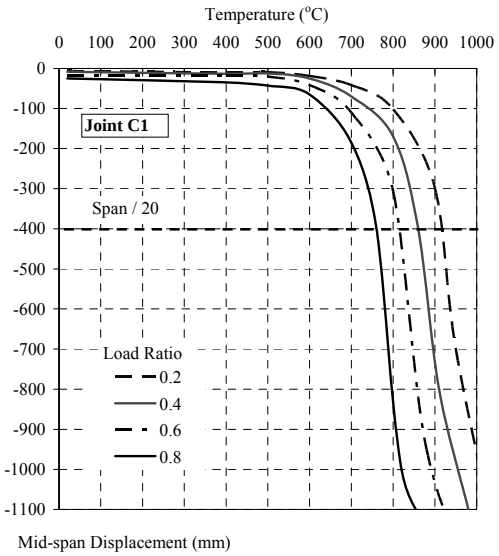

Fig. 11 Influence of the load ratio on the middle beam response

The middle beam behaviour incorporating joint C1 characteristics (semi-rigid joint) for nominal load ratios ranging from 0.2 to 0.8 are shown in Fig. 11. It is observed that the failure temperature decreases significantly in an almost linear manner when the load ratio increases. At a load ratio of 0.2, the failure temperature of the beam exceeds 920°C, but at a load ratio of 0.8, the beam failure temperature is reduced to 760°C. There is little change in the failure temperature of the beam up to a load ratio of 0.2.

5.3. Influence of axial restraint

The following study investigates *qualitatively* the influence of axial restraint on the middle beam response at elevated temperatures. If a multi-span steel structure has more than 3 spans and is subjected to a natural fire load, the fire design of the middle beam should consider the influence of structural restraint provided by unheated adjacent structures. At the heating stage, the middle beam will tend to elongate due to thermal expansion. Significant axial restraint induced at the heating stage will result in an increase in the mid-span deflection due to non-uniform heating and compression force induced in the beam at this stage. In the analyses, the beam-end joints at A and F in Fig. 6**(a)** were idealised as fixed supports, not allowing any movements or rotations.
To simplify the modelling process, it was assumed that the beam was uniformly heated across the section and along its axis so that there was no additional beam deflection due to thermal-bowing effect. The middle beam behaviour incorporating C1 joint characteristics analyses with and without axial restraint is compared in Fig. 12, together with three types of joint characteristics making six analyses.

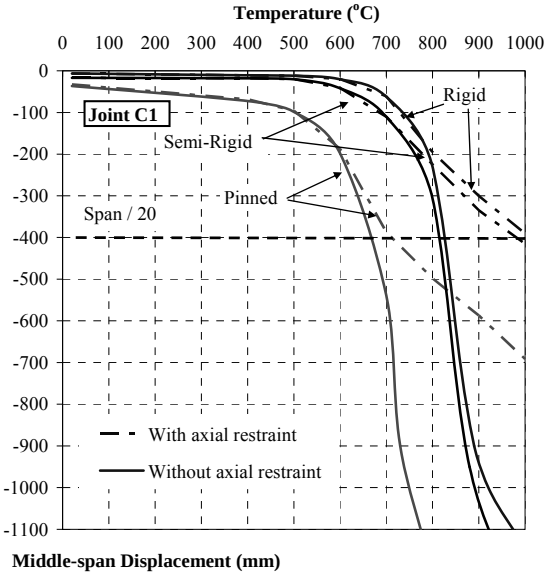

Fig. 12 Influence of axial restraint on the middle beam response incorporating joint C1 characteristics

It is observed that the influence of axial restraint on the maximum mid-span deflection is not very obvious when the middle beam deflection is less than 100mm at temperatures up to 700°C, beyond which the rate of mid-span deflection reduces quickly with increasing temperatures due to catenary action. At large beam deflections (approximately L/40), catenary action kicks in and helps the beam to resist applied load. Thereafter, the rate of beam deflection is reduced significantly at high temperatures (Fig. 12), compared with the beam without axial restraint. A further increase in temperature causes a progressive increase in the middle beam until it reaches 1/20 of beam span at 'failure temperatures' of 710°C and 1010°C for pinned and rigid joints, respectively (Fig. 12), which are higher than the respective 660°C and 830°C for the middle beam without axial restraint. It can be seen that the middle beam deflections with axial restraint are consistently less than those without axial restraint (Fig. 12).

6. CONCLUSIONS

A numerical study was carried out to illustrate the advantages of incorporating semi-rigid joint characteristics in the analysis of steel-framed structures under fire conditions using ABAQUS. A total of five parameters affecting the beam behaviour at elevated temperatures were investigated, including the beam-end boundary condition, the load ratio and the influence of axial restraint. The numerical results show that incorporating semi-rigid joint characteristics in sub-frame analyses

greatly enhance the beam behaviour under fire conditions. Besides, the inclusion of axial restraint in sub-frame analyses leads to significant improvements in the middle beam behaviour within multi-span steel-framed structures with more than three spans.

REFERENCES

ABAQUS Version 6.8. Analysis User's Manual. Simulia, U.S.A., 2008.

Al-Jabri, K. S. The Behaviour of steel and composite Beam-Column Connections in fire, Ph.D. Thesis, University of Sheffield, U.K., 1999.

British Standards Institution (BSI), "BS5950 Structural Use of Steelwork in Building - Part 8: Code of practice for fire Resistance Design", BS 5950 Part 8, U.K., 2003.

British Standards Institution (BSI), "Fire Tests on Building Materials and Structures: Methods for Determination of the Fire resistance of Load-bearing Elements of Construction", BS 476 Part 21, U.K., 1997.

El-Rimawi, J. A., "The Behaviour of Flexural Member under Fire Conditions", Ph.D. Thesis, University of Sheffield, U.K, 1989.

European Committee for Standardization (CEN), "Eurocode 4: Design of Composite Steel and Concrete Structures, Part 1.1: General rules and rules for buildings", EN 1994-1-1, Brussels, Belgium., 2004.

European Committee for Standardization (CEN), "Eurocode 2: Design of Concrete Structures, Part 1.2: General Rules – Structural Fire Design", EN 1992-1-2, Brussels, Belgium., 2005.

European Committee for Standardization (CEN), "Eurocode 3: Design of Steel Structures, Part 1.2: General Rules – Structural Fire Design", EN 1993-1-2, Brussels, Belgium., 2005.

Lawson, R. M. (1990), "Behaviour of Steel Beam-to-column Connections in Fire", The Structural Engineer, Vol. 68, No.14, pp. 263-271, 1990.

Liew, J. Y. R., Tang, L.K., Halmass Tore and Choo, Y. S. Advanced analysis for the assessment of steel frames in fire. Journal of constructional research steel, Vol. 47, pp. 19-45, 1998.

Liu, T. C. H. Fire resistance of unprotected steel beams with moment connections. Journal of constructional research steel, Vol. 62, pp. 1165-1170, 2006.

Moore, D. B. and Lennon, T. (1997), "Fire engineering design of steel structures", Progress in Structural Engineering and Materials, Vol. 1, No. 1, pp. 4-9., 1997.

Santiago, A., Simões da Silva, L., Vila Real, P. and Veljkovic, M. Numerical study of a steel sub-frame in fire. Computers and structures. Vol. 86, pp. 1619 – 1632, 2008.

Tan K. H., Ting S. K .and Huang Z. F. (2002), Visco-Elasto-Plastic Analysis of Steel Frames in Fire, Journal of Structural Engineering, Vol. 128, No. 1, pg. 105-114, 2002.

Yuan Z., "The Behaviour of Composite Top-and-Seat-and-Web Angle Joints at Elevated Temperatures", Ph.D. Thesis, Nanyang Technological University, Singapore, 2011.

COMPONENT-BASED ELEMENT FOR ENDPLATE CONNECTIONS IN FIRE

G. Dong, I. W. Burgess and J. B. Davison

Department of Civil and Structural Engineering, The University of Sheffield, Sheffield S1 3JD, UK

INTRODUCTION

This paper describes the development of a component-based finite element to model endplate joints between beams and columns in steel structures under fire conditions. Observations from the full scale fire tests at Cardington and collapse of buildings at the World Trade Centre in 2001 have raised concerns that joints are potentially the weakest parts of a structure (Burgess, 2007). When designing a steel building, the joints are always assumed to transfer shear reactions, and in some cases beam end-moments. In fact, due to the combination of thermal and mechanical effects caused by heating, the resultant forces on joints (in addition to shear) vary from pure moment, to moment and compression, and eventually to almost pure tension.

The Component Method is a practical approach initially proposed by Tschemmernegg *et al* (1987) for ambient-temperature conditions and now included in EC 3 Part 1-8 (CEN, 2005). This element is compatible with the EC3 Part 1-8 design method. A joint is divided into a collection of key components, whose behaviour is characterised as that of nonlinear springs. Its essential properties, including temperature variation, physical connection details and unloading characteristics, are taken into account in assigning properties to its components. Therefore, individual components are capable of dealing with loading-unloading-reloading cycles, and changing temperatures. Rigid links are used to connect the components in order to represent the whole joint, which enables the element to tackle the interaction of internal forces.

1 DEVELOPMENT OF THE COMPONENT-BASED ELEMENT

The development of the component-based element is divided into three basic steps:

Step1: identification of the active components.

Step2: specification of the component characteristics.

Step3: assembly of the active joint components.

1.1 Identification of the active components

Active components are those which either contribute to the deformation of a joint or limit its strength (Block, 2006). EC3 Part 1-8 (Table 6.1) lists the basic components for endplate connections. Figure 1 (Spyrou, 2002) shows the general zones of structural action within the connection for which components will be assembled to create this component-based element.

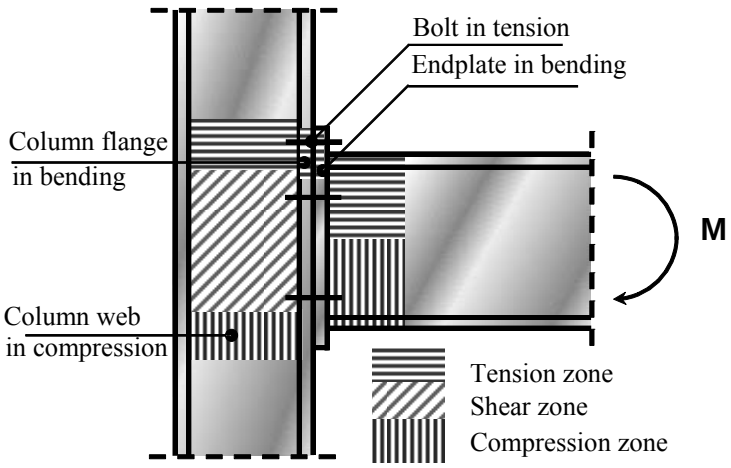

Fig. 1 Active component in COMPFIRE joints (Spyrou, 2002).

1.2 Specification of the component characteristics

In order cover the fire case, each component's behaviour must be analysed at elevated temperatures (using F.E. studies and/or experiments) and then described with a simplified analytical model. The component's performance in fire can then be modelled.

1.2.1 Typical tension/compression component Force/Displacement curve

In the present version of the connection element, the component behaviour (Figures 2 and 3) is based on a set of derivations from earlier studies (Hu *et al*., 2007 and Yu *et al*., 2009), and these will be characterised in the next version. Each component has an 'ultimate strength', at which its maximum resistance occurs. Beyond the ultimate strength, the component is considered as 'fractured', and stops working structurally. Practically, a compression component 'fracture' cannot occur, and the ultimate point is where the compression component buckles or its deformation is too large to be acceptable. In order to consider the component's behaviour at elevated temperature, reduction factors and ductility factors (Figures 4, 5 and 6) are temporarily introduced in the current version i.e. reducing the ambient temperature resistance and ductility for temperature effects. .

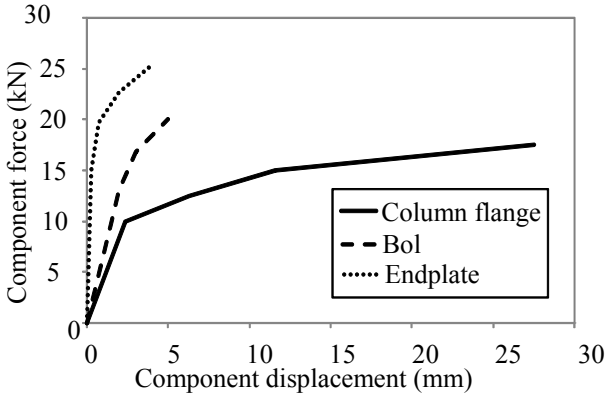

Fig 2 Tension component behavior at 20 °C

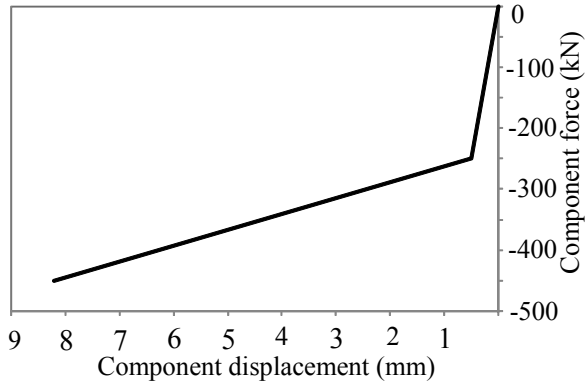

Fig 3 Compression Component behavior at 20°C

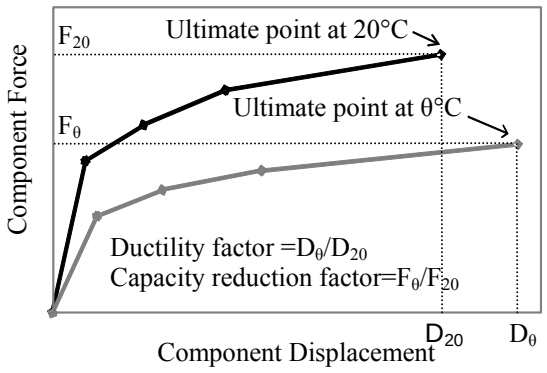

Fig 4 Definition of the ductility factor/reduction factor

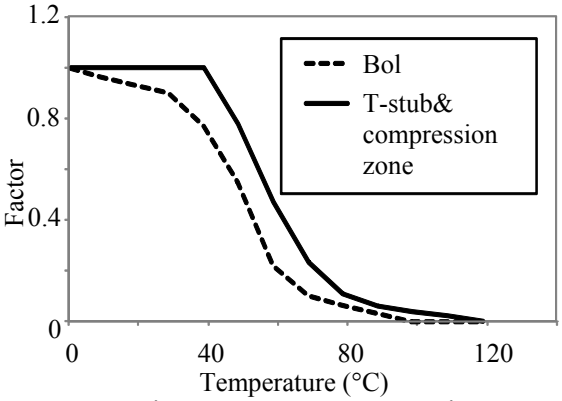

Fig 5 Component capacity reduction factor

1.2.2 Unloading of components

When a component carries a large enough force, the material maybe strained into the inelastic region, and the component will then have irreversible deformation ('residual deformation') when its force is removed . To date, the classic Massing rule has been employed to deal with this 'memory effect'. In the Massing rule, the unloading curve is the original loading curve doubled in scale and rotated by 180°. If the initial loading curve (Block, 2006) is represented by

$$D = f(F) \tag{1}$$

then the unloading curve can be described as

$$\frac{(D_A - D)}{2} = f\left(\frac{F_A - F}{2}\right) \tag{2}$$

Where intersection point (D_A, $F_{A)}$ in (Fig 7) are respectively the displacement and the force at which unloading occurred.

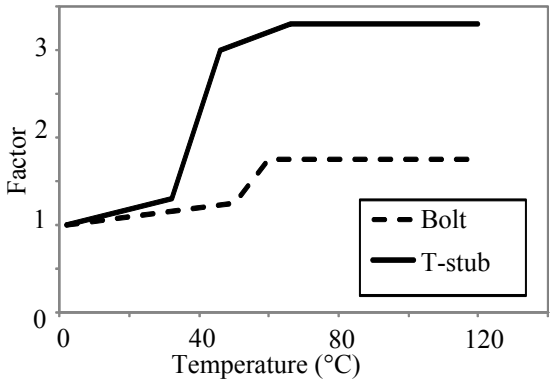

Fig 6 Ductility factor for tension component

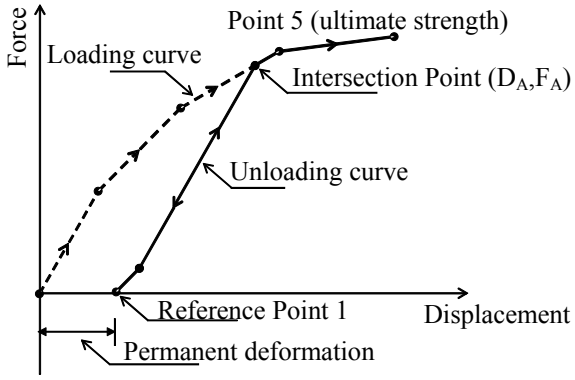

Fig 7 Typical loading/unloading curve

When a component is heated in a fire, its temperature changes continuously and the F/D curve is temperature-dependent. The component's permanent deformation is assumed not to change when only the temperature changes.

1.3 Assembly of active joint components.

Figure 8 shows a typical layout of the endplate connection component assembly. The connection element has 2 nodes, 1 and 2, to connect to the beam and column respectively and internally consists of 5 tension spring (bolt) rows and 2 compression spring rows. The components for vertical shear are not considered at present, but will be developed later.

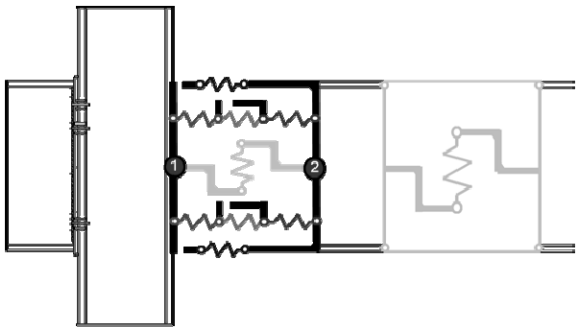

Fig 8 Component assembly for endplate connections

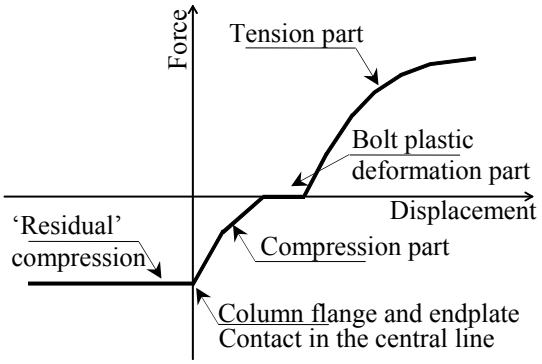

Fig 9 Typical tension bolt row F/D curve

A tension bolt row is characterised by an effective spring composed of a group of springs in series, representing the endplate in bending, a bolt in tension and the column flange in bending. Maximum resistance is defined by the weakest spring.

A typical Force/Displacement (F/D) curve for a tension bolt row consists of four parts (Figure 9): the 'tension part', 'bolt plastic deformation part', 'compression part' and 'residual compression part'. The 'tension part' shows the three components under tension. The 'compression part' represents the state in which the plastically deformed endplate and column flange are pushed back until their centres come into contact. The 'bolt plastic deformation part' represents the stage between the 'tension' and 'compression' parts, at which the applied tension reduces to zero, and the deformed endplate and column flange have not yet come into contact. As the bolt-in-tension component does not work under compression, its stiffness is zero during the 'bolt plastic

deformation' part. The 'residual compression' part is based on the assumption that the tension bolt row can transfer a certain amount of compression force. However, as the parts of the connection represented by the compression spring group are much stiffer than this, the compression spring group will transfer most of the compression force.

2 RESULTS

The current version of the component-based element has been successfully incorporated into a nonlinear global structural analysis program *Vulcan* (Huang, 2004). In order to test the element, an

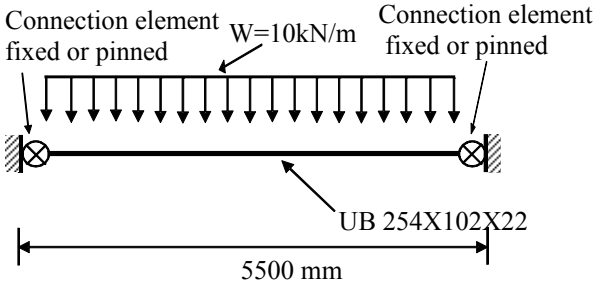

Fig 10 Isolated beam with connection elements

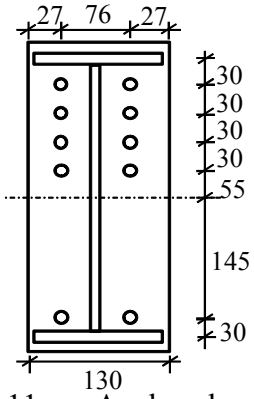

Fig 11 Analysed endplate connections

isolated beam, with connection elements at its ends, and with complete axial restraint beyond these, was designed (Figure 10). The beam section is 254x102UKB22. Endplate thickness is 12mm and the steel grade is S275. No out-of-plane deflection is allowed. The joint (Figure11) is designed to test the connection element's full capacity for 5 tension bolt rows. The joint data are hard-coded in the current version of the connection element.

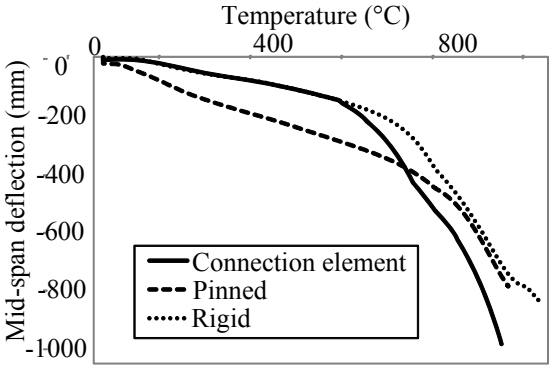

Fig 12 Beam mid-span deflections

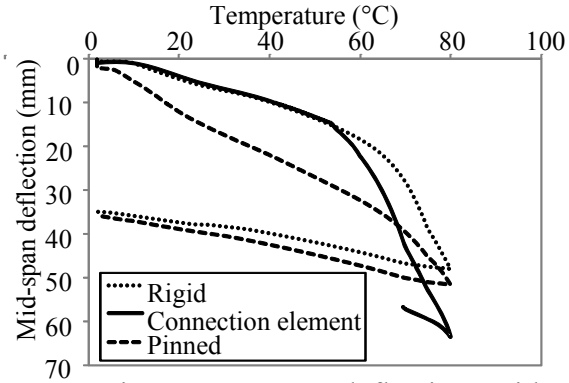

Fig 13 Beam deflection with cooling from 800°C

It can be seen from Figure 12 that at high temperatures (above 800°C) the deflections of the rigid and pinned connections become very close, when the beam is in its catenary stage and under nearly pure tension. It is also noticeable that the deflection of the beam with the connection elements lies initially between those of the beams with rigid and pinned connections. Above 685°C, the beam with the connection elements has a larger deflection than either of the rigid or pinned cases. This is because catenary action causes a net shortening of the distance between the beam ends which is greater than the thermal expansion, and the residue of this net shortening can be accommodated by extension of the bolt rows.

Figure 13 shows that the connection element is capable of modelling the cooling behaviour of

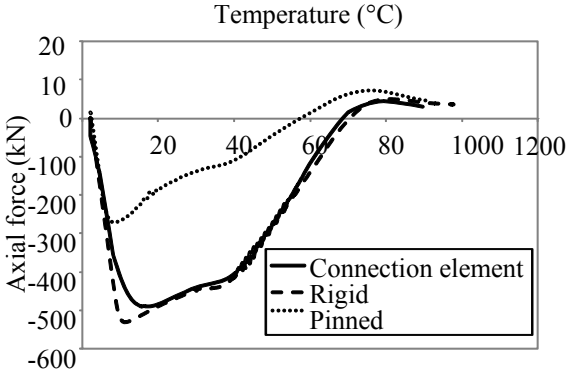

Fig 14 Axial force in connection

connections. The calculation has stopped due to fracture of the bolt in the first tension bolt row.

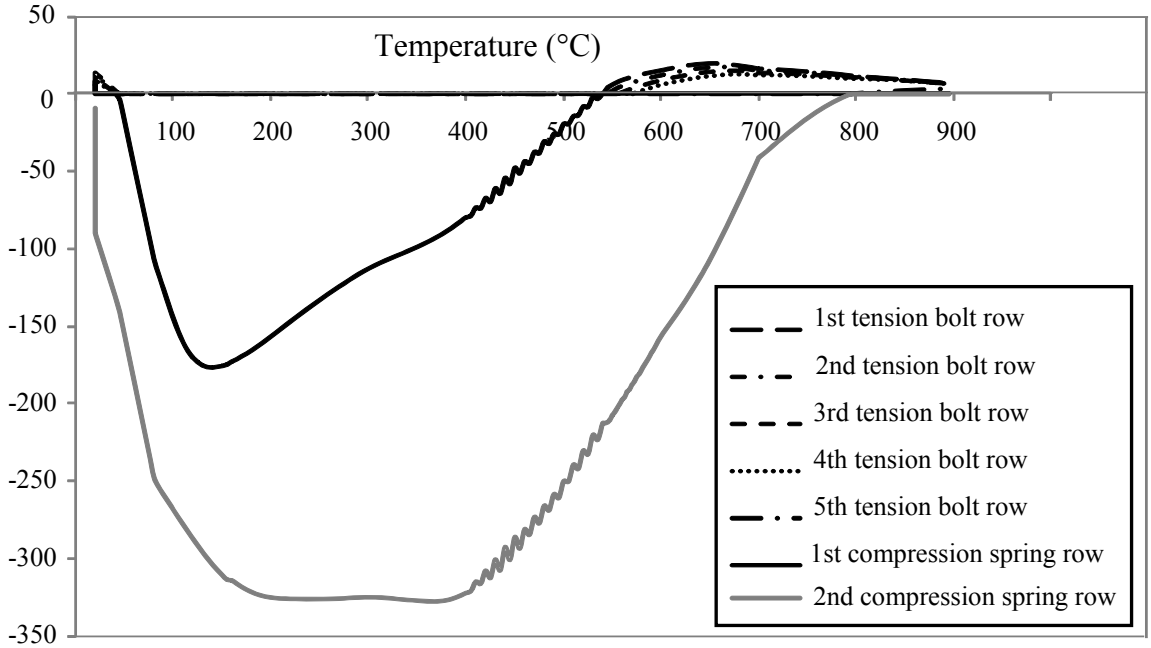

Fig 15 Component force

Figures 14 and 15 show how the connection element deals with the combination of forces in the joint when the beam is heated. In the initial stage, the top 4 tension bolt rows and the bottom (2^{nd}) compression spring row work to resist the beam end rotation due to the applied load. After the beam is heated it starts to expand, and the connection is subjected to a combination of compression and bending, at which stage all the top 4 tension bolt rows are gradually 'switched off' as the tension force in the top of the section is offset by the thermal expansion. Once all the tension bolt rows have temporarily stopped working, the top compression spring row starts to work together with the bottom compression spring row, and the whole section is under compression. With the temperature increasing further, the beam's deflection increases sharply, and the top 4 tension bolt rows progressively replace the top compression spring row in resisting the combination of compression force and moment. Above 600°C, the beam progressively develops catenary tension and reduces its bending action. Eventually all 5 tension bolt rows are working and both of the compression spring rows are 'switched off'.

3 CONCLUSION

This connection element can be used in modelling of the behaviour of steel structures in fire, and has now been very largely validated. It will contribute to the accurate prediction of the behaviour of buildings in fire scenarios, including the ductility and failure of connections, allowing progressive collapse sequences to be traced, and facilitating global performance-based design against fire.
Further component development and parametric studies are currently underway which will enable a more refined analysis tool to be used in structural modelling.

5 ACKNOWLEDGEMENT

The research leading to these results has received funding from the European Community's Research Fund for Coal and Steel (RFCS) under *grant agreement* n° RFSR-CT-2009-00021.

REFERENCES

Block F.M. (2006), “Development of a component-based finite element for steel beam-to-column connections at elevated temperatures”, PhD Thesis, University of Sheffield

Block, F.M., Davison, J.B., Burgess, I.W. and Plank, R.J. (2007), ‘The Development of a Component-Based Connection Element for Endplate Connections in Fire’, Fire Safety Journal, 42 (2007) pp 498–506.

Burgess I.W. (2007), 'Connection Modelling in Fire', Proc. COST C26 Workshop "Urban Habitat Constructions under Catastrophic Events", Prague, (2007) pp 25-34.

CEN (2005), “EC3: Design of steel structures, Part 1.8: Design of Joints”, European Committee for Standardization, Document BS EN1993-1-8:2005.

Hu, Y, Davison JB, Burgess IW and Plank RJ (2007), ‘Comparative study of the behaviour of BS 4190 and BS EN ISO 4014 bolts in fire’. The 3rd International Conference on Steel and Composite Structures (ICSC07). Manchester. July, pp 587-592. ISBN 978-0-415-45141-3.

Huang, Z., Burgess, I.W. and Plank, R.J. (2004), ‘3D Modelling of Beam-Columns with General Cross-Sections in Fire’, Paper S6-5, Third International Workshop on Structures in Fire, Ottawa, Canada, (May 2004) pp 323-334.

Spyrou S. (2006), “Development of a component-based model of steel beam-to-column joints at elevated temperatures”, PhD Thesis, University of Sheffield

Yu, H.X., Burgess, I.W., Davison, J.B. and Plank, R.J. (2009), 'Development of a Yield-Line Model for Endplate Connections in Fire’, J. Construct. Steel Research, 65 (6), (2009) pp1279-1289.

Tschemmernegg, F., Tautschnig, A., Klein, H., Braun, Ch. And Humer, Ch. (1987), “Zur Nachgiebigkeit von Rahmenknoten – Teil 1” (Semi-rigid joints of frame structures Vol. 1– in German), Stahlbau 56, Heft 10, pp299-306.

THE FRACTURAL BEHAVIOUR OF STEEL WELDS AT HIGH TEMPERATURE

Hongxia Yu [a]

[a] Dept. of Civil Engineering, Tsinghua University,Beijing, China

INTRODUCTION

The stiffness and strength of steel degrade with the increase of temperature quickly, which makes the behavior of steel constructions in fire hazards a major concern. To evaluate the stability of steel constructions in fire, the properties of structural steel at elevated temperatures have been extensively investigated (Kirby and Preston, 1988; Cooke, 1988). However, latest researches show that connections, rather than structural members such as beams or columns, are generally the weakest link in the structure. Fig. 1 shows a picture of connection failure in a full-scale structural fire test (Newman et al, 2004). Tearing of the endplate from the connected beam web can be clearly observed. Connections are the key elements to hold the structural members together and failure of which could quite possibly initiate the progressive collapse of the whole structure as demonstrated by the collapse of the WTC towers (NIST, 2008). Therefore, design connections with sufficient robustness have been internationally recognized to be important to prevent impropriate collapse of structures when subjected to accidental loads.

In a set of experiments designed to investigate the robustness of connections at high temperature, failure of welds have been widely observed to occur to the locations where flexible or flush endplate connections were welded to the beam web similar to that shown in Fig. 1 (Hu et al, 2008; Yu et al, 2011). Weld fracture at elevated temperatures are also observed for other structural members such as the concrete filled tubular column shown in Fig. 2. Contrary to the widely observed failure of welds in fire situation, little research has been performed on the behavior of structural welds at high temperature. Therefore, a set of experiments were designed to study the ultimate tensile resistance and fractural behavior of the two most common structural welds at various temperatures. The test results are reported in this paper.

Fig. 1 Fracture of a Partial depth endplate connection

Fig. 2 Fracture of the weld in a concrete filled steel tubular column fire test

1 TEST ARRANGEMENT

A total of 54 specimens were tested in two groups. The first group used Q235 steel with E43 electrode and the second group used Q345 steel with E50 electrode。For each group, 27 tests were performed for 9 temperatures including 20ºC and 100ºC-800ºC。For each temperature, three tests were performed to ensure the reliability of the results. The specimens were designed as two tapered steel bars welded together in the smaller ends as shown in Fig. 3a. The width at the smaller ends is 6mm and at the bigger ends is 20mm. The thickness of the specimen is 20mm uniform along the whole length. The finished specimen takes the shape as shown in Fig. 3b. By visual observation, the welding is clean and uniform with no obvious imperfections. The width of the weld is from 10-12mm and the thickness of the weld in the narrowest position is 7-8mm.

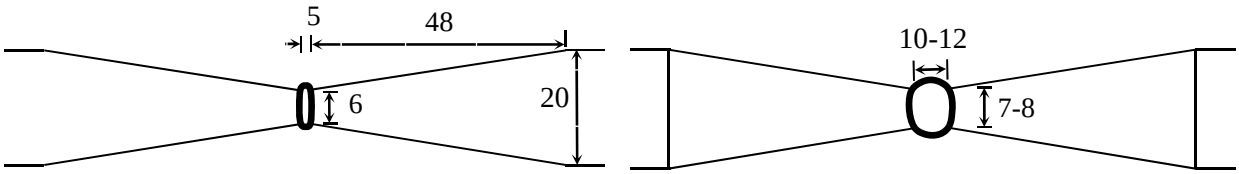

a. The designed specimen

b. The fabricated specimen

Fig. 3 Design and fabrication of the specimen

2 TEST RESULTS

2.1 Tensile Strength

The ultimate resistances of the two groups of tests are shown in Table 1. A graphical view of the results is shown in Fig. 4. It can be seen from the figure that the three results agree with each other very well for each temperature, especially when the temperatures are above 400ºC, which means the specimens were fabricated satisfactorily and the possibility of strong influence from the imperfections in the welds can be cleared.

Both groups show the rule that the tensile resistances reduce slightly at 100ºC, then start to increase until 300ºC. At 400ºC, the resistances are nearly the same with those at 20ºC. And from 400ºC upwards, the resistances reduces quickly. If all the resistances are divided by their average resistances at ambient temperature, the strength reduction factor can be obtained for these welds. Strength reduction factors for welds at elevated temperatures are also proposed by EC3: Part 1.2 (CEN, 2005). A comparison of the test results against the code proposal is shown in Fig. 5. It can be seen that the tested strength reduction factors follow that of the EC3 curve very well in the medium range of 500ºC to 600ºC. Below that, the test results show a slight increase of the resistance at around 300ºC and above that, the failure resistance is 50%-100%h higher than the code proposal.

Comparison of the weld strength reduction factor against the strength reduction factor for steel gives useful information regarding which of them will be more vulnerable to failure at high temperatures. Therefore, the strength reduction factor for hot-rolled steel according to a Chinese fire safety design code (CECS, 2006) is also shown in Fig. 5. It can be seen that the weld strength is slightly lower than the steel strength at 500ºC and 600ºC. At higher temperatures, they are very close to each other. In general, welds have similar strength reduction factors to that of hot-rolled steel. Since the strengths of weld and steel degrade at similar rates, weld failure in fire should not become a special concern.

Tab. 1 The ultimate resistances of the specimens

Temperature [ºC]	Q235 with E43 [kN]			Q345 with E50 [kN]		
	(1)	(2)	(3)	(1)	(2)	(3)
20	84	85.1	84.8	99.2	100	97.9
100	79.15	79.75	81.85	93.7	92.2	102.1
200	85.15	95.5	96.5	98.1	99.8	92.6
300	101.8	100.8	97	107.2	104	111.4
400	87.4	87.1	82.2	98.2	102.7	100
500	50.9	49.45	47.4	70.2	69.25	70.15
600	29	28.55	34.3	41.85	41.95	42.6
700	17.15	16.8	16.9	21.5	27	21.35
800	12.45	14.95	13.1	16.7	15.7	16.8

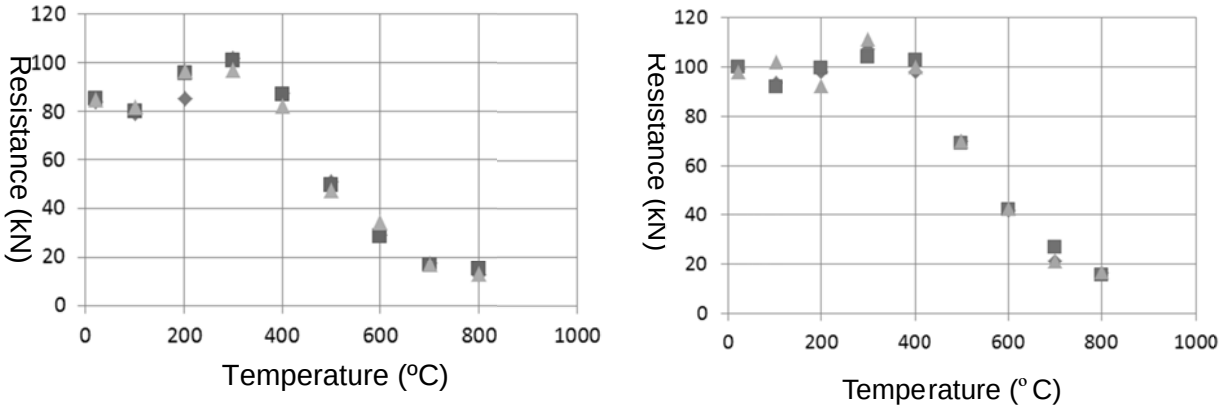

a. Q235 with E43

b. Q345 with E50

Fig. 4 Reduction of the weld resistances with temperature

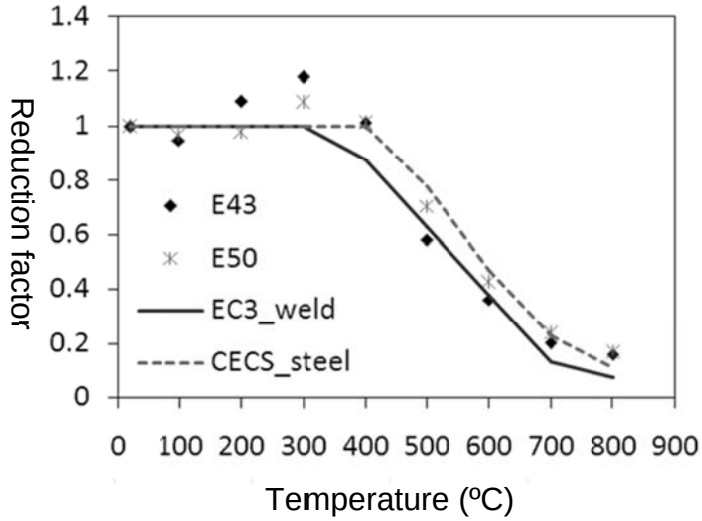

Fig. 5 Reduction of the weld strength in comparison with steel

2.2 Failure Mode

Several typical failure modes can be identified from the test results. They are shear fracture within the weld, irregular fracture within the weld, shear fracture at the interface and tensile failure at the interface as shown in Fig.6. When the temperature is from 20ºC to 400ºC, the failure mode could be any one among failure modes a, b and c and different failure modes do not seem to have a clear influence on the failure resistances. When the temperature is 500ºC and above, the failure mode is conformably mode d, i.e. the tensile failure at the interface between the weld and the steel with obvious necking of the failed section.

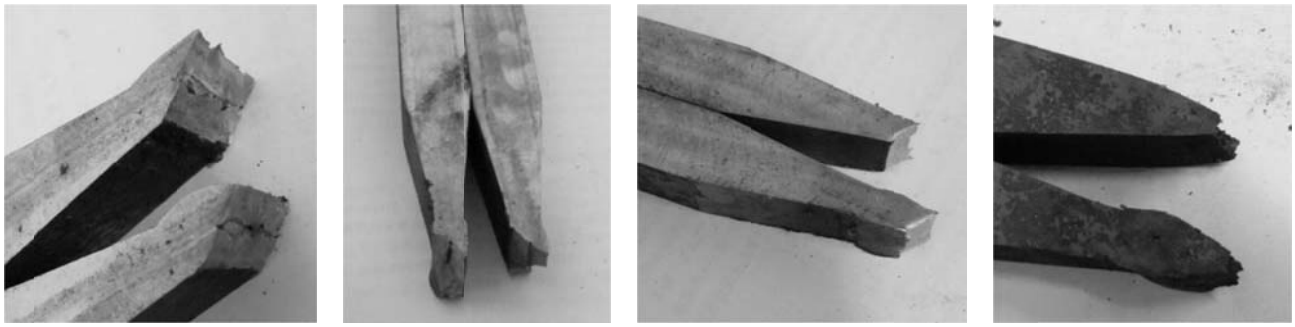

a) shear fracture within the weld

b) irregular fracture within the weld

c) shear fracture at the interface

d) tensile failure at the interface

Fig. 6 The failure modes

Associated with different failure modes, the force-displacement relationships of these specimens show distinct characteristics. When the temperature is from 20ºC to 400ºC, the force increases with the displacement until the peak point and dropped suddenly to zero with a brittle fracture of the specimen. When the temperature is 500ºC and above, the force increases gradually to the peak point and reduces slowly to zero with further increase of the displacement. Therefore, at high temperature, the specimens generally show much better ductility.

3 CONCLUSIONS

This paper reports a set of test results on structural steel welds at elevated temperatures. The purpose of the test was to investigate the ultimate resistance and failure modes of steel welds at various temperatures and provide guidance for the fire safety design of structural steel connections. The test results show that the ultimate resistances of the welds reduce with the increase of temperature after 400ºC. The resistance degradation rate is similar to that of hot-rolled steel. Therefore, no special consideration seems to be necessary for the failure of steel welding. However, when the temperature is from 20ºC to 400ºC, the welds show brittle fracture at small deformations, which could have explained the observation of weld cracks in connection fire tests. At temperatures above that, welded region behaves extremely well in terms of both strength and ductility.

ACKNOWLEDGEMENTS

This work was financially supported by the Fund for Returned Oversea Scholars to Start Research by the Ministry of Education (20091021043).

REFERENCE

Kirby B.R. and Preston R.R., High temperature properties of hot-rolled, structural steels for use in fire engineering design studies, Fire safety journal Vol.13, p. 27-37, 1988.

Cooke G.M.E., An introduction to the mechanical properties of structural steel at elevated temperatures, Fire safety journal, Vol.13, p.45-54, 1988.

Newman G.M., Robinson J.T., Bailey C.G., Fire Safety Design: A New Approach to Multi-Storey Steel-Framed Buildings. The Steel Construction Institute, 2004.

NIST, Final Report on the Collapse of the World Trade Center Building 7- Draft for Public comment. USA, National Institute of Standards and Technology, 2008.

Hu Y., Davison J.B., Burgess I.W. and Plank R.J., Experimental Study on Flexible Endplate Connections in Fire, Proc. 5th European Conf.Steel Structures, Graz, Austria, p.1007-1012, 2008.

Yu H.X., Burgess I.W., Davison J.B. and Plank R.J., Experimental and Numerical Investigations of the Behaviour of Flush Endplate Connections at Elevated Temperatures, J. Struct. Eng., ASCE, V137, No 1, p.80-87, 2011.

CEN (European Committee for Standardization), BS EN 1993-1-2, Eurocode 3: design of steel structures, Part 1.2: General rules- structural fire design. British Standards Institution, UK, 2005.

CECS, DG/TJ08-008-2000 Technical code for fire safety of steel structures in buildings (in Chinese), China Engineering Construction Standard, 2006.

NUMERICAL ANALYSIS OF HSS ENDPLATE CONNECTIONS AT AMBIENT AND ELEVATED TEMPERATURES

Xuhong Qiang[a], Frans Bijlaard[a], Henk Kolstein[a], Leen Twilt[b]

[a] Faculty of Civil Engineering and Geosciences, Delft University of Technology, 2600GA Delft, the Netherlands
[b] Formerly: Center for fire research of Institute TNO for Building and Construction Research, Delft, the Netherlands

INTRODUCTION

In Europe, endplate connections are typical beam-to-column connections for low-rise steel buildings erected using welding at workshops and bolting in situ. The simplicity and economy associated with their fabrication make the connections popular for steel structures.
Rules for the prediction of strength and stiffness of endplate connections at ambient temperature have been included in design codes, such as Eurocode3 Part1-8 (CEN 2005), but they are mainly based on mild steel connections. Girao Coelho and Bijlaard (Girao Coelho and Bijlaard 2007) have found that the high strength steel (HSS) S690 endplate connections satisfy the design provisions for resistance and achieve reasonable rotation demands at ambient temperature. However, no quantitative guidance on HSS endplate connections in fire condition is available.
Recent research on bolted connections has revealed that bolts failure becomes critical at elevated temperatures, although the design for ambient temperature assumes more ductile failure (Burgess 2009, Yu et al. 2008, Yu et al. 2009a, and Yu et al. 2009b). I.e. mild steel bolted connections are relatively brittle at elevated temperatures. So, making bolted connections more ductile at elevated temperatures is a significant mission for structural engineers, in order to improve the robustness of steel connections in fire condition.
In order to enhance fire safety of endplate connections, a numerical research has been conducted, combining HSS endplate with mild steel beam and column. In this paper, the numerical modelling of HSS endplate connections is compared with that of mild steel endplate connections, to gain essential understanding and quantification on how HSS endplate connections behave at ambient and elevated temperatures. The accuracy of this numerical model is validated against the results of tests conducted by Yu et al. on mild steel flush endplate connections (Burgess 2009, Yu et al. 2008, and Yu et al. 2009b). Moreover, a parametric study on the effects of endplate thicknesses is conducted, and an achievement is obtained for improving the ductility of endplate connections at elevated temperatures.

1 TESTS IN UNIVERSITY OF SHEFFIELD

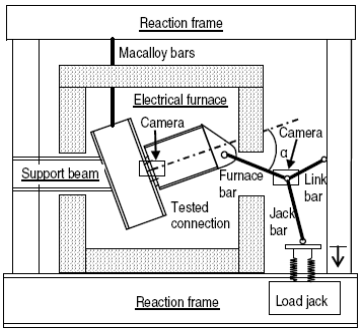

Fig.1 Test setup

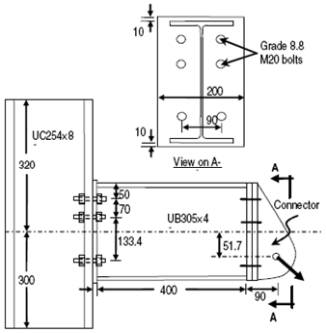

Fig.2 Typical flush endplate connection specimen

From 2005 to 2008, the Universities of Sheffield and Manchester conducted a joint research project with the aim of investigating capacity and ductility of steel connections at elevated temperatures (Yu et

al. 2008, Burgess 2009). A test setup was adopted in which four types of connections were subjected to a combination of tension and shear forces. In order to illustrate the experimental behaviour of mild steel endplate connections at ambient and elevated temperatures, only the tests on flush endplate connections are used herein.

A detailed description of the test setup and test measurements was given by Yu previously (Yu et al. 2008). The tests were performed in an electrical furnace, as shown in Fig.1. Fig.2 shows the details of a typical flush endplate connection in tests. In all cases, a UC254×89 section made of S355 was used for the column, and the beam section was UB305×165×40 made of S275.

2 FINITE ELEMENT ANALYSIS METHOD

The finite element software ABAQUS is used to simulate the behaviour of endplate connections both at ambient and elevated temperatures.

2.1 Geometric Details and Element Type

The details of all connections' components used in FEM are exactly the same with those of the test specimens. Because the geometric details, load, temperature distribution and boundary conditions are symmetric, half of the endplate connection is modelled, to shorten computing time. The FE components are shown in Fig.3, including bolt shank, nut, washer, endplate, beam and column. The bolt holes are modelled 2mm larger than the bolt shank diameter, and the hexagon bolt heads are modelled as cylinders for simplicity. The whole connection is modelled using C3D8I element, because of its excellence in simulating contact interactions, non-linear material properties and stress concentrations.

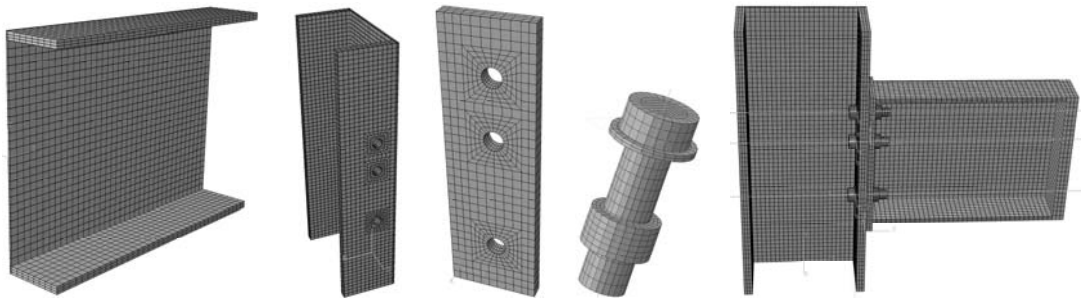

(a) Beam (b) Column (c) Endplate (d) Bolt pair (e) Assembled FE model

Fig.3 FE model and its mesh generation

2.2 Contact Interaction

To handle contact interaction problem, the whole analysis process comprises 6 analysis steps. In the first step, the bolts, the washers and the endplate are restrained of all direction freedoms temporarily, and then a very small pretension is applied to every bolt for restraining the bolt pairs temporarily. The temperature field for all components is 20°C. In the second step, the bolts, washers and the endplate are freed of any temporary restraint. In the third step, the actual magnitude of pretension is applied to every bolt. In the fourth step, the length of every bolt is fixed. In the fifth step, the temperature field for all components is modified to a preselected temperature. (For the analysis at ambient temperature, the temperature field is kept constant.) In the sixth step, an equivalent surface traction converted from the actual inclined force with its preselected initial load angle is applied to the end of the beam. The first four steps help contact interactions to be established smoothly, which is effective to decrease calculation time and eliminate errors.

Surface-to-surface contact, with a small sliding option, is used for all contact surfaces to fully transfer the load. The contact pairs in the endplate connection comprise the washers-to-column flange, column

flange-to-endplate, endplate-to-nuts. And the washer is tied to bolt head in each bolt pair for simplicity and the nuts are tied to the corresponding bolt shanks.

2.3 Material Properties

In this FE modelling, the material properties of mild steels (including S275 and S355) and bolt pairs are the same with those reported by the University of Sheffield (Hu et al. 2008, Renner 2005, and Yu et al. 2009a). The material properties of S690 at elevated temperatures reported by Chen and Young (Chen and Young 2006) are used for HSS.

2.4 Loads and Welds

An additional endplate is modelled at the other end of beam, for applying surface traction, as shown in Fig.3 (e). The initial load angles used in tests are also taken into consideration when applying surface traction. The magnitude of pretension for each bolt is 224kN, to agree with the average reported in the experimental investigation (Yu et al. 2008 and Yu et al. 2009b). The welds between endplate and beam are modelled by tie restraint instead of solid modelling, in order to simplify the model.

3 VALIDATIONS AGAINST EXPERIMENTAL RESULTS

3.1 Ambient Temperature

In Yu et al.'s tests, at ambient temperature experimental results on 10mm S275 endplate with initial load angle of 55 degree (10E55RS275) and 8mm S275 endplate with initial load angle of 35 degree (8E35RS275) are available. So, the corresponding numerical modellings are conducted, using ABAQUS/Standard, based on the above-mentioned FE analysis method.

The force-connection rotation curves for both specimens are shown in Fig.4. It can be seen that the FEM simulations and Yu et al.'s test results are in good agreement. For the two specimens, the maximal discrepancies between numerical simulations and experimental data are both about 10%, and both appear in the converting stage between linear and non-linear performances. It can be concluded that the numerical modelling described here can simulate the response of endplate connections at ambient temperature with reasonable accuracy.

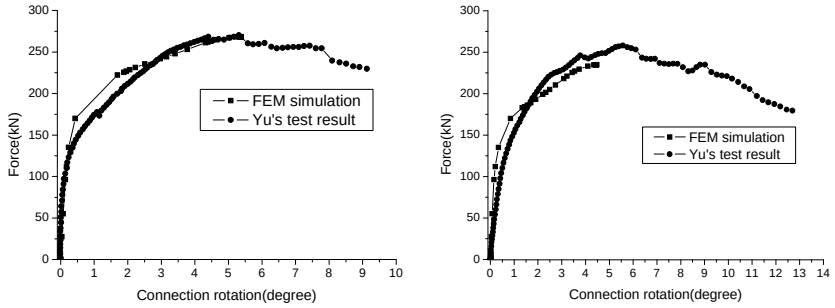

(a) 10E55RS275 (b) 8E35RS275

Fig.4 Force-rotation curves of connections at ambient temperature

3.2 Elevated Temperatures

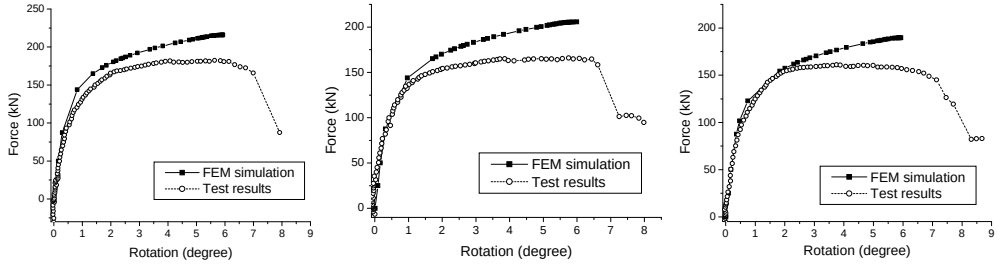

a) 35°initial load angle b) 45°initial load angle c) 55°initial load angle

Fig.5 Force-rotation comparisons of 10mmS275 at 450°C

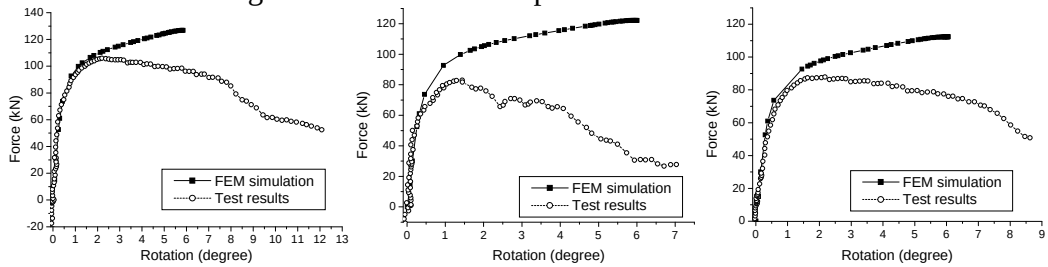

a) 35°initial load angle b) 45°initial load angle c) 55°initial load angle

Fig.6 Force-rotation comparisons of 10mmS275 at 550°C

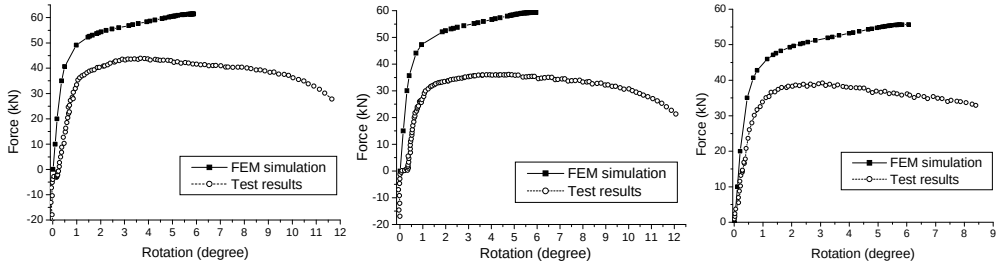

a) 35°initial load angle b) 45°initial load angle c) 55°initial load angle

Fig.7 Force-rotation comparisons of 10mmS275 at 650°C

In Yu et al.'s fire tests, the connection specimens (10mmS275 endplate connections) have been heated to three preselected elevated temperatures (450°C, 550°C and 650°C) and then loaded till failure occurred. For each elevated temperature, the specimens were tested with three initial load angles (35, 45 and 55degree). The corresponding numerical modellings are conducted and shown in Fig.5-7.

For the initial liner stage of the force-rotation curves obtained by FEM simulations, they are in good agreement with Yu et al.'s test results at 450°C and 550°C. But at 650°C the strength of the connections obtained from FEM are much higher than test data. This is because in tests the connections are loaded at a very slow deflection rate (i.e. the specimens are loaded till failure in about 120 min) and at constant temperature, but there are no such material properties of S275 corresponding to so slow steady-state conditions available. So the material property used in FEM can not exactly reflect its actual behaviour in tests, especially at very high temperatures, such as 650°C. Moreover, at very high temperatures, creep effects will have a significant influence, especially when the specimens are heated very slowly. However, in the FE analysis creep has not been taken into account, leading to an overestimation of strength and stiffness of the connections. For these reasons the tests at 650°C will be excluded from the following FE analysis, and the numerical analysis below 650°C is acceptable to simulate or predict the behaviour of endplate connections at corresponding elevated temperatures.

4 NUMERICAL PREDICTION OF HSS ENDPLATE CONNECTIONS

4.1 Same Thick Endplates in Connections

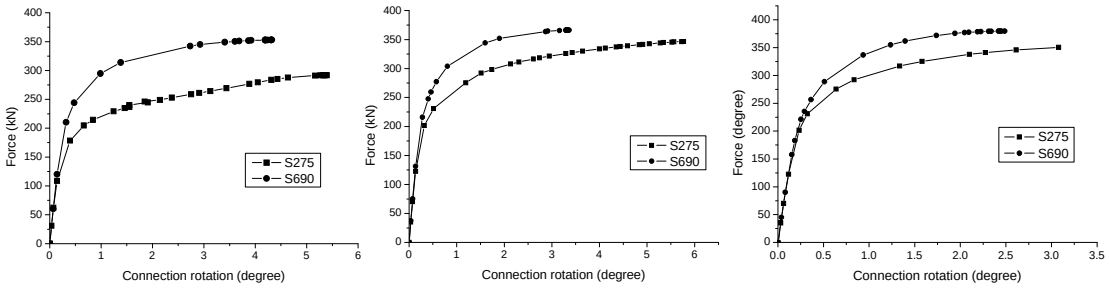

(a) 10mm thickness endplate (b) 12mm thickness endplate (c) 15mm thickness endplate

Fig.8 Force-rotation comparisons of HSS and mild steel endplate at ambient temperature

The force-rotation capacities of HSS endplate connections at ambient temperature and at elevated temperatures are compared with that of mild steel ones, with the same endplate thickness. The results for initial load angle of 45 degree at ambient temperature are illustrated in Fig.8. And the comparison of HSS endplate and mild steel endplate for 10mm thickness with initial load angle of 55 degree at 450°C and 550°C are illustrated in Fig.9.

As we predict, it is found that at ambient temperature the load-bearing capacities of HSS endplate connections are higher than that of mild steel connections using the same thick endplates, but the ductility of the former is worse. So using the same thick HSS endplate in connections to take place of mild steel endplate at ambient temperature is proved not effective to improve ductility.

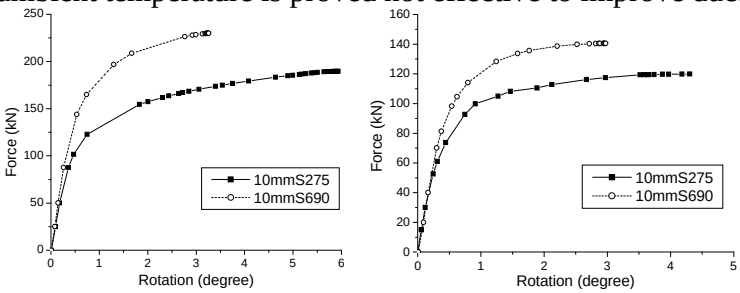

a) 450°C b) 550°C

Fig.9 Comparisons of HSS endplate and mild steel endplate connections at elevated temperatures

Similar to that at ambient temperature, it is found that at elevated temperatures the load-bearing capacities of HSS endplate connections are also stronger than mild steel endplate connections with the same endplate thickness, but the ductility of the former is worse. It is obvious that using the same thick HSS endplate instead of mild steel endplate in connections is not effective to improve the ductility of endplate connections at elevated temperatures.

4.2 Parametric Study on Endplate Thickness

To predict thickness effect of endplate on strength and ductility of connections, a parametric study both at ambient temperature and at elevated temperatures is conducted using the proposed FE model. The parameter concerned, i.e. thickness of endplate, is varied.

4.2.1 Ambient Temperature

The obtained force-rotation capacities of HSS S690 endplate connections with various endplate thicknesses at ambient temperature are compared with that of mild steel S275 endplate connections, as shown in Fig.10 a.

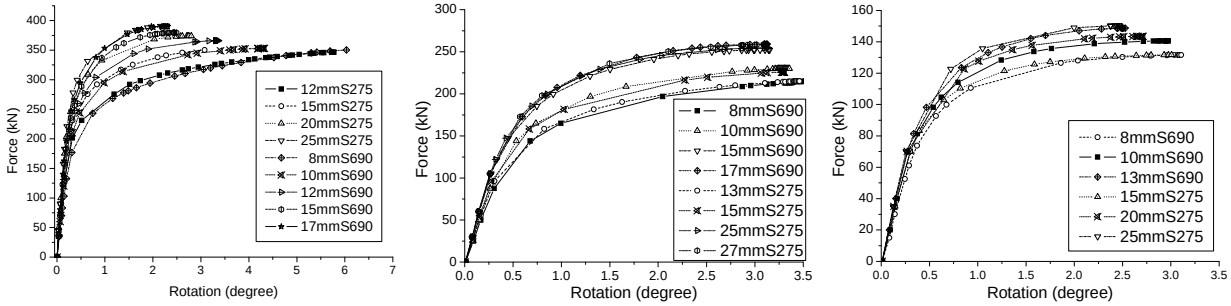

a) ambient temperature b)450°C c) 550°C

Fig.10 Effects of endplate thicknesses at ambient and elevated temperatures

It can be seen that the 8mm thick S690 endplate connection (8mmS690) is as strong as the 12mm thick S275 endplate connection (12mmS275), but the former is more ductile. Similar conclusions can be drawn for the other comparison pairs: 10mmS690-15mmS275, 12mmS690-20mmS275 and 17mmS690-25mmS275.

These conclusions demonstrate that at ambient temperature the connection with a thin HSS endplate enhances its ductility and simultaneously achieves the same resistance as that with a thick mild steel one. This is positive for improving the ductility of endplate connections at ambient temperature, and also indicates a beneficial research idea for enhancing the ductility of endplate connections at elevated temperatures.

4.2.2 Elevated Temperatures

At the same elevated temperature (i.e. 450°C and 550°C), the simulated force-rotation capacities of various thicknesses of HSS endplate connections are compared with that of mild steel endplate connections, as shown in Fig.10 b and c. A similar conclusion can be drawn with that at ambient temperature: at elevated temperatures, a thinner HSS endplate provides the same load-bearing capacity as that of a mild steel endplate connection, and enhances the ductility of the connection by various percentages. This achievement is positive for improving the fire-resistance design of endplate connections at elevated temperatures.

5 CONCLUSION

This paper reports on a numerical analysis method of endplate connections using ABAQUS/Standard, in order to predict the performances of HSS endplate connections at ambient temperature and at elevated temperatures. This analysis may be used as a basis for investigating how HSS endplate connections behave not only in normal condition but also in fire condition.

The challenge of modelling contact interactions is solved successfully by FEM, considering material and geometric non-linear effects. The FE modelling is verified appropriate to simulate mild steel endplate connections at ambient and elevated temperatures with reasonable accuracy. Based on this, the performances of HSS endplate connections at ambient temperature and at elevated temperatures are further analyzed and compared with that of mild steel one.

It is found that a thinner HSS endplate can enhance the ductility of connection both at ambient temperature and at elevated temperatures, and simultaneously achieve almost the same load-bearing capacity with a mild steel endplate connection. This FE model may be used for further investigation of improving the behaviour of HSS endplate connections in fire conditions.

By the present modelling method, the critical locations of endplate connections can be identified, but the occurrence of component failure cannot be predicted. To improve the capability of this numerical simulation, solid modelling of welds taking into account fracture features is necessary in future works.

REFERENCE

Burgess, I.W. (2009), "The Robustness of Steel Connections in Fire", Proceeding of ASCCS 2009, Leeds, 103-114.

Chen, J. and Young, B. (2006), "Behaviour of High Strength Structural Steel at Elevated Temperatures", Journal of Structural Engineering, 1948-1954.

European Committee for Standardization (CEN)(2005), BS EN 1993-1-8, Eurocode3: Design of steel structures, Part 1-8: Design of joints. British Standards Institution.

Girao Coelho, A.M. and Bijlaard, F.S.K. (2007), "Experimental behaviour of high strength steel end-plate connections", Journal of Constructional Steel Research, **63**, 1228–1240.

Hu, Y., Burgess, I.W., Davison, J.B., and Plank, R.J. (2008), "Modelling of flexible endplate connections in fire using cohesive elements", Proceeding of Structures in Fire Workshop, Singapore.

Renner, A. (2005), "The effect of strain-rate on the elevated-temperature behaviour of structural steel", Research dissertation. UK: University of Sheffield.

Yu, H., Burgess, I.W. Davison, J.B., and Plank, R.J. (2008), "Experimental Investigation of the Behaviour of Flush Endplate Connections in Fire", Proceeding of Structures in Fire Workshop, Singapore.

Yu, H., Burgess, I.W. Davison, J.B., and Plank, R.J. (2009 a), "Tying Capacity of Web Cleat Connections in Fire. Part 1: Test and Finite Element Simulation", Engineering Structures, **31** (3), 651-663.

Yu, H., Burgess, I.W., Davison, J.B. and Plank, R.J. (2009 b), "Development of a Yield-Line Model for Endplate Connections in Fire", Journal of Constructional Steel Research, **65** (6), 1279-1289.

FRACTURE SIMULATION IN A STEEL CONNECTION IN FIRE

Simulation of a flush endplate connection at ambient and elevated temperatures including different methods for fracture simulation

Peter Schaumann [a], Thomas Kirsch [a]

[a] Leibniz University Hannover, Institute for Steel Construction, Hannover, Germany

INTRODUCTION

Actual developments in numerical simulations of the structural behaviour in fire situation are focussed on taking into consideration the interaction of all structural members in a global numerical approach. Therefore it is necessary to model the load bearing behaviour of connections in detail.
In this paper a detailed 3D numerical model of a bolted steel endplate connection taking into account nonlinearities, e.g. temperature dependent material, is presented. The simulation is validated by experimental tests conducted at the University of Sheffield in 2008. During some of the experimental tests, large deformations and fractures occurred. These phenomena are simulated with the numerical model as well.

1 STATE OF THE ART

Since the first study of connection behaviour (Wilson et al, 1917), investigations in joints were traditionally based on experiments. The finite element method was used to simulate connection behaviour since 1974, when Krishnamurthy developed a two-dimensional FE-Model to simulate an endplate connection (Krishnamurthy, 1974). While experimental and numerical investigations at ambient temperatures have been conducted in a large number, tests at elevated temperatures are rather seldom. The reason for this might be that studying connection behaviour at elevated temperatures is costly because a number of tests at different temperatures are needed to develop a moment-rotation-temperature curve. However, elevated temperature tests on beam-to-column-connections have been carried out by (Kruppa, 1976), (Wang et al, 2007) and (Schaumann et al, 2008) for example. Further high temperature tests on different connections in fire, taking into account tensional forces caused by catenary action of adjacent beams, have been performed by Yu and will be used for this investigation. Results have been published for different connection types in (Yu et al, 2007), (Yu et al, 2008a), and (Yu et al, 2009), to mention but a few.
In addition, numerical investigations have been conducted for some elevated temperature tests. For example in (Sarraj et al, 2007) a numerical model of fin plate connections has been developed. In (Yu et al, 2008b) a simulation of a steel connection using explicit analysis was presented. The explicit equation solver algorithm was found to be an alternative to the standard algorithm especially if large deformations occur. In (Hu et al, 2008) a flexible endplate connection in fire using an explicit dynamic analysis was presented. To simulate a tensile fracture of the beam web, cohesive elements were included to the analysis.

2 METHODS

In this paper, a numerical simulation of a joint at ambient and elevated temperatures is presented. The numerical calculation has been conducted using the FE-software Abaqus. Both, the implicit (Abaqus/Standard) and the explicit solver algorithm (Abaqus/Explicit) have been applied to the analysis.
A shear fracture in the endplate, which occurred during some of the tests, was simulated using two different methods. The first method was the use of cohesive elements located where shear failure occurred in the test. The second method was a fracture strain criterion for ductile materials. This algorithm is able to reduce the stiffness of elements and delete them during the analysis.

3 PARAMETER OF EXPERIMENTS AND NUMERICAL SIMULATION

3.1 Test Setup and Geometry of the Connection

During 2007 and 2008 the University of Sheffield carried out a wide range of experimental tests within different steel connections, different temperatures and a different load angle α (c.f. Fig. 1). The test setup, geometrical details and material properties of this test have been published in (Yu et al, 2008a) in detail and will be described shortly. The general test assembly is shown in Fig. 1.

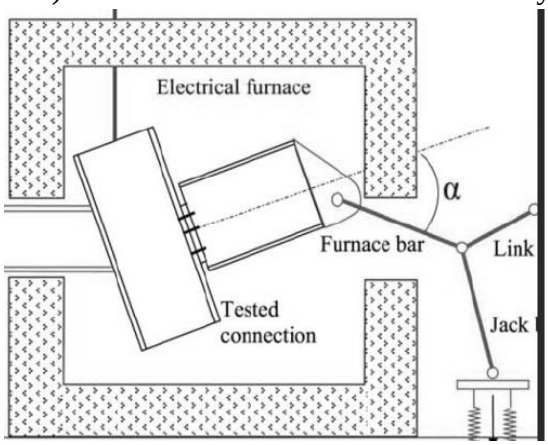

Fig. 1 Scheme of test setup (Yu et al, 2008a)

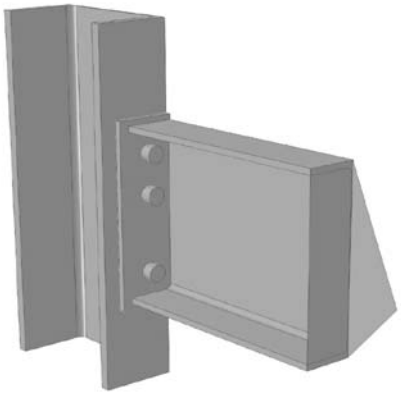

Fig. 2 Numerical model of flush endplate connection (including symmetry)

The distance controlled load is induced by a jack through a construction of three steel struts, which are connected by hinges. Due to this construction, the load angle α (c.f. Fig 1) is variable. For the numerical simulation, tests with an initial load angle of α=55° have been used. It has to be taken into account that the load angle is changing during the test for the reason of the jack movement and the joint rotation.

The investigated connection consists of a flush endplate of dimensions 325x200x10 and is connected to the column by six M20 grade 8.8 bolts. The connection detail can be found in Fig. 2. The beam cross section is UB 305x165x40 and the column cross section is UC 254x89. The numerical model has been created as half-geometry taking into account the connection symmetry to reduce computing time.

3.2 Material Properties

The beam and the endplate are made of S275 grade steel. As described in (Yu et al, 2009) for one of the tests, a standard tensile test specimen has been cut from the beam flange to determine the material properties at ambient temperatures. The Young's Modulus is E=176,350 N/mm², the yield stress is f_y=356 N/mm² and the ultimate tensile stress is f_u=502 N/mm². As there were no tests available for the endplate and the column, the material parameters have been adopted.

There were no tests to gain material properties at elevated temperatures. For this reason investigations of (Renner, 2005), which have been conducted with tensile specimen at different steady-state temperatures and different strain rates, were used to extrapolate the data. Material properties according to the Eurocodes have not been used as those properties are developed for transient temperatures. The material properties used in the numerical model are shown in Fig. 3.

According to bolt behaviour, three bolts have been tested at ambient temperatures. An average tensile force of 224 kN and a Young's Modulus of 206,009 N/mm² were determined (c.f. (Yu et al, 2009)). There is no data available to determine the stress strain relationship for bolts at steady-state elevated temperatures. For this reason the relationship has been determined by equations from (Eurocode 3, 2010). Reduction factors for yield stress according to (Hu et al, 2007) have been used. The stress-strain-relationship used for the bolts is shown in Fig. 4.

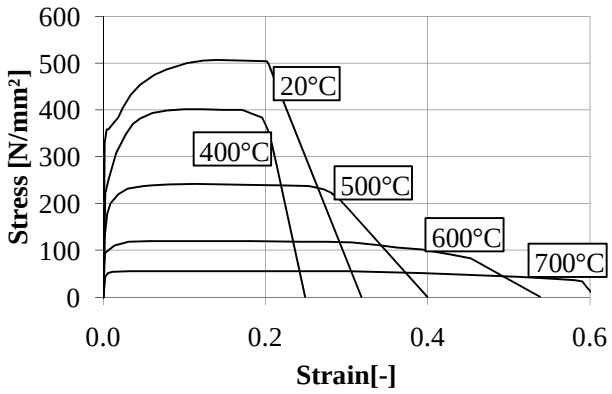

Fig. 3 Stress-strain-relationship for structural steel in numerical model

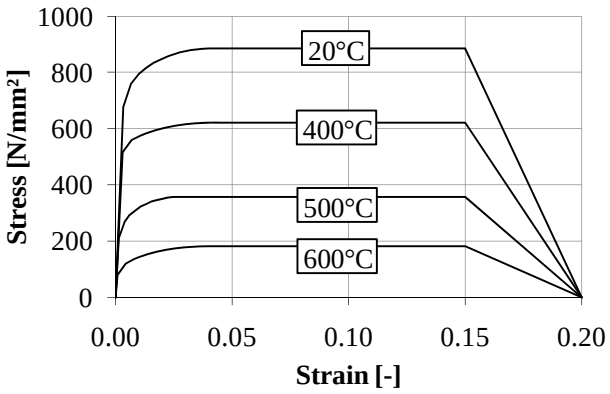

Fig. 4 Stress-strain-relationship for bolts in numerical model

4 RESULTS WITHOUT FRACTURE SIMULATION

The implicit equation solver algorithm (Abaqus/Standard) was used to simulate the connection behaviour first. Up to a rotation of 2°, the calculated behaviour was very close to the test results. The simulation at higher rotations was not possible because of convergence problems due to large deformations.

The load-rotation behaviour of the tested connection, calculated by an explicit equation solver, is shown in Fig. 5 for ambient and elevated temperatures. It can be seen that test results and calculated load-rotation behaviour are correlating very well for rotations up to 5°. At higher rotations, the load capacity of the connection is overestimated by the numerical model. This can be seen at the test at 450°C.

To verify the calculation internal and external energies have been investigated. To avoid singular modes (c.f. hourglass control), artificial energies are added during the simulation. To ensure realistic results, the amount of this energy should be negligible compared to "real" energies. A value of 10% of internal energies was determined to be the maximum allowable fraction. This value has been reached for most calculations at a rotation of about 8°. As the calculation is quasi-static, the kinetic energy fraction should be marginal as well. The kinetic energy was found to be less than 1% of internal energies.

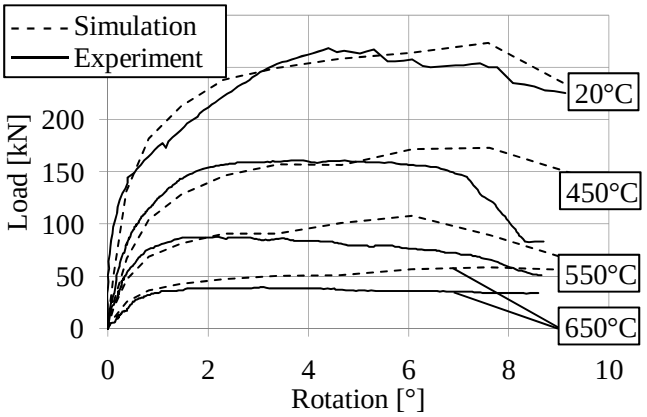

Fig. 5 Load-rotation behaviour at different temperatures (numerical and test results)

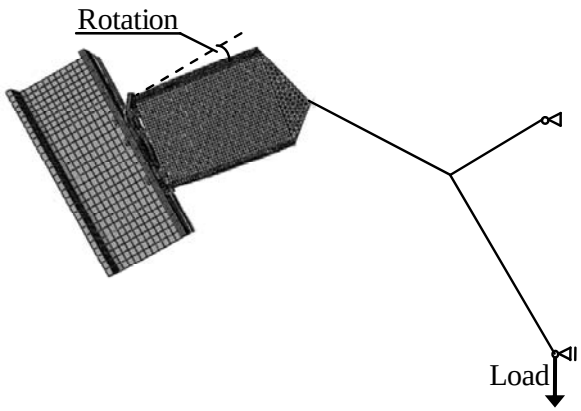

Fig. 6 Definition of load and rotation in Fig. 5, Fig. 8 and Fig. 11

5 COHESIVE ELEMENTS

As described in (Yu et al, 2008a), the test specimen showed two different failure modes. While at higher temperatures of 550°C and 650°C the bolts failed in tension, at 20°C and 450°C a shear fracture occurred very close to the beam web in the endplate.

A thin layer of cohesive elements has been implemented in the endplate next to beam web and flange to simulate this shear fracture. Failure of the cohesive layer has been simulated using material properties based on a fracture strain. As can be seen in Fig. 7, the stress strain relationship of the cohesive elements has been defined as linear elastic until a damage initiation criterion is reached. The damage initiation stress is defined as ultimate stress of the material. The Young's modulus has been defined as ultimate stress divided by the strain at the beginning of failure (c.f. Fig. 3). The failure strain, as defined in Fig. 7, has been determined to $\varepsilon_{fail}=3$. For the reason of a very thin layer of cohesive elements, the influence of failure strain is negligible to the results, while the simulation is more stable using a higher strain.

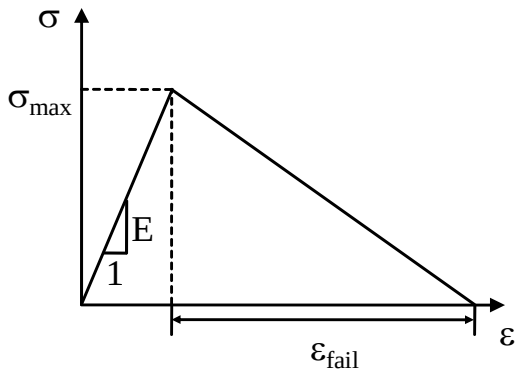

Fig. 7 Scheme of material behaviour of cohesive elements

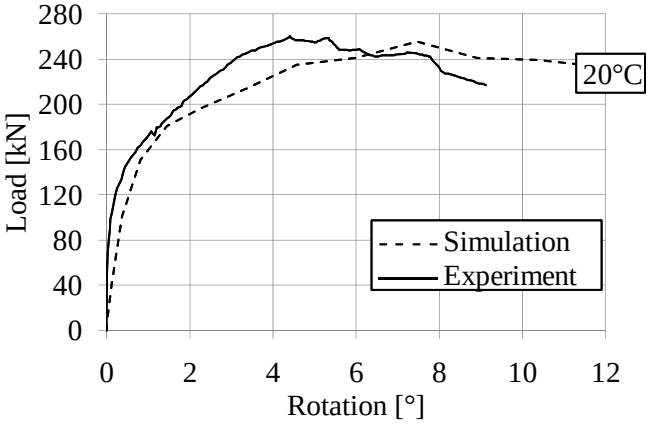

Fig. 8 Load-rotation relationship of connection at 20°C (numerical and test results)

In Fig. 8 the load rotation relationship for the test at ambient temperatures is compared to the calculation including cohesive elements. As can be seen, the curves are correlating very well and the decrease of load capacity can be simulated. The main benefit of the simulation including cohesive elements is the ability to visualise fractures. As can be seen in Fig. 9 and Fig. 10, it is possible to simulate the fracture which occurred in the test at ambient temperature.

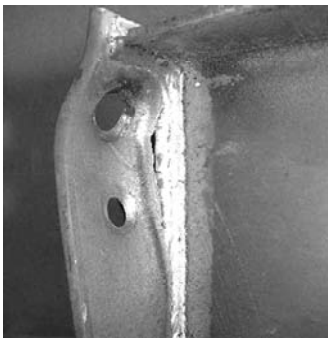

Fig. 9 Fracture of endplate in test specimen after test at 20°C

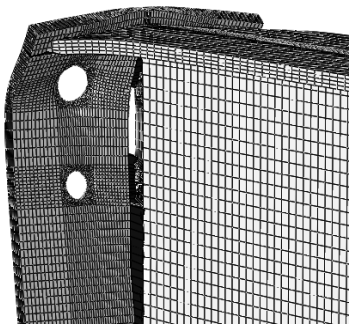

Fig. 10 Fracture of endplate in numerical simulation at rotation of 9°

6 GENERAL IMPLEMENTATION OF DAMAGE

Main problem of the use of cohesive elements in a fracture simulation is the need to know, where a fracture may occur. Otherwise, it is possible to implement a failure criterion to the general material properties.

The failure depends on a damage initiation strain, at which the stress reduction begins and failure strain at which the damage reaches 100%. The damage initiation strain can be described as strain-rate- and shear-stress-ratio-dependent. As there is no available data, the criterion has been set as constant for each temperature. The damage initiation strains have been determined to the strain at the beginning of stress reduction in the stress-strain-relationship (c.f. Fig. 3). Damage initiation strain and failure strain can be found in Tab 1.

Tab. 1 Temperature dependent strains for damage definition

Temperature [°C]	Damage initiation strain $\bar{\varepsilon}_S^{pl}$ [-]	Failure strain $\bar{\varepsilon}_f^{pl}$ [-]
20	0.200	0.5
400	0.200	0.5
500	0.275	0.5
600	0.400	0.5
700	0.575	0.5

The results of the simulation using a damage criterion for structural steel are shown in Fig. 11. It can be seen that the load-rotation-relationship is correlating very well for each temperature. While the results for tests at 550°C and 650°C are comparable to the calculation without a damage criterion, the results at 450°C are much closer to the test results especially at higher rotations and a decreasing load.

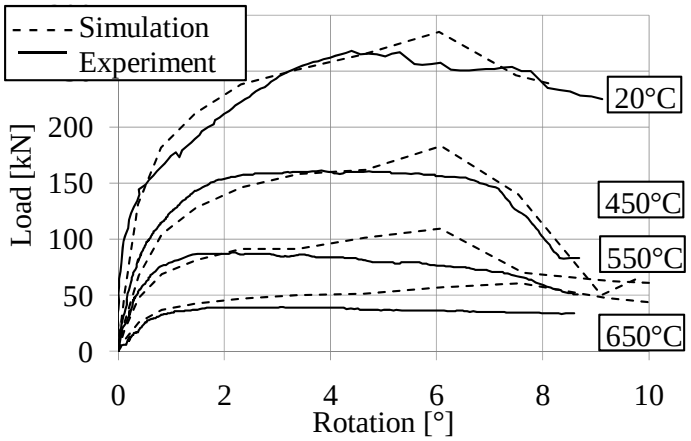

Fig. 11 Load-rotation behaviour of connection for different temperatures including a damage criterion for numerical results (for definition of load and rotation see Fig. 6)

As described in (Yu et al, 2008b), the failure at 20°C and 450°C was due to a shear fracture in the endplate at the beam web, while bolts failed due to tension at higher temperatures. This has been observed in the numerical simulation as well. In Fig. 12 the stress related to the ultimate stress at the specific temperature in the upper left bolt at a rotation of 7.5° is shown for the simulation at 20°C and 550°C. As can be seen by the low stress values in the bolt shaft at 550°C, the bolt has failed. For the reason of this failure, the load inside the endplate is reduced and the fracture at the beam web does not occur. As the bolt at 20°C is still functional, a fracture occurs in the endplate. In contrast to the experiments, the fracture in the simulation occurred as a tensional fracture. The reason for this slightly different behaviour may be found in the weld geometry or in the influence of the welding process in the heat affected zone.

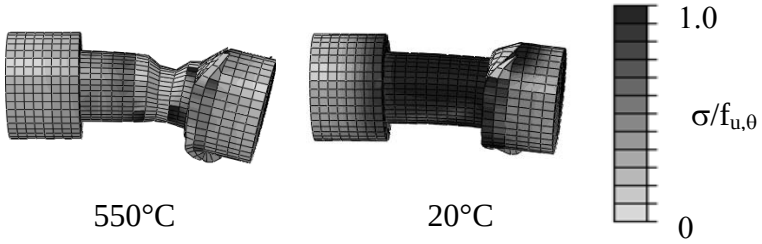

Fig. 12 Upper left bolt at rotation of 7.5° in numerical simulation at different temperatures

7 SUMMARY AND ACKNOWLEDGEMENT

In this paper, an experimental investigation in the load-rotation behaviour of flush endplate connections at ambient and elevated temperatures has been simulated. The simulation was conducted using a 3D finite element model including nonlinear material properties and large

deformations. As in some of the tests a shear fracture occurred in the endplate, different methods to simulate this failure mode were tested.
It was found that an implicit equation solver algorithm was not able to compensate large deformations. Thus an explicit algorithm was preferred and showed good correlations with the test results.
To simulate shear fracture, cohesive elements have been found to be a useful tool. Main disadvantage is the need to know, where the fracture may occur. If this is not known, the implementation of a general failure criterion is possible. This opportunity was investigated and comparisons to the test results showed very good correlation for the load-rotation-relationship. Additionally, the different failure modes at ambient and elevated temperatures were simulated correctly.
The authors would like to thank Ian Burgess and Shan-Shan Huang for providing information and help according to the experimental data. The IGF-Project No. 16586 N from FOSTA is funded by the German "Federal Ministry of Economics and Technology" via AiF.

REFERENCES

Eurocode 3: Design of steel structures - Part 1-2: General Rules – Structural fire design; German version EN 1993-1-2:2005 + AC:2009, Beuth Verlag, Berlin, 2010

Hu Y., Burgess I. W., Davison J. B., Plank R. J., Comparative study of the behaviour of BS 4190 and BS EN ISO 4014 bolts in fire, Proceedings of 3rd international conference on steel and composite structures, 2007.

Hu Y., Burgess I. W., Davison J. B., Plank R. J., Modelling of flexible end plate connections in fire, Proceedings of 5th international conference Structures in Fire, Singapore, 2008.

Krishnamurthy N., Two-dimensional finite element analysis of steel end-plate connections: parametric considerations, Auburn University, Report n. CE-AISC-MBMA-3, Auburn, 1974.

Kruppa, J., Resistance on feu des assemblage par boulous, Centre Technique Industrial de la Construction Metallique, St. Remy Chevzuese, France, 1976, CTICM Report, Document No. 1013-1, English translation available "Fire resistance of Joints with High Strength bolts".

Renner A., The effect of strain-rate on the elevated-temperature behavior of structural steel, Research dissertation, University of Sheffield, 2005.

Sarraj M., Burgess I. W., Davison J. B., Plank R. J., Finite element modeling of steel fin plate connections in fire. Fire Saf J 42 (2007) 408-415, Elsevier, 2007.

Schaumann P., Zhao B., Bahr O., Renaud, C., Fire performance of external semi-rigid composite joints , Proceedings of 6th International Conference Structures in Fire, Singapore, 2010.

Wang W.-Y., Lia G.-Q., Dong Y.-L., Experimental study and spring-component modeling of extended end-plate joints in fire, Journal of Constructional Steel Research 63 (2007) 1127–1137.

Wilson, W. M., Moore, H. F., Tests to Determine the rigidity of Riveted Joints in Steel structures, University of Illinois, Engineering Experimentation Station, Bulletin No. 104, Urbana, 1917.

Yu, H., Burgess I. W., Davison J. B., Experimental investigation of the robustness of fin plate connections in fire, Proceedings of 5th ICASS (Advances in Steel Structures), 2007.

Yu H., Burgess I. W., Davison J. B., Plank R. J., Experimental investigation of the behavior of flush endplate connections in fire, Proceedings of 5th international conference Structures in Fire, Singapore, 2008 (a).

Yu H., Burgess I. W., Davison J. B., Plank R. J., Numerical simulation of bolted steel connections in fire using explicit dynamic analysis, JConstrStRes 64 (2008) 515–525, Elsevier, 2008 (b).

Yu H., Burgess I. W., Davison J. B., Plank R. J., Experimental investigation of the behaviour of fin plate connections in fire, JConstrStRes 65 (2009) 723-736 2009.

THERMOMECHANICAL NONLINEAR ANALYSIS
Finite Element Analysis of Bolted Steel Connections Using Contact Mechanics

Andreas Kalogeropoulos [a], Georgios A. Drosopoulos [a], Georgios E. Stavroulakis [a,b]

[a] Institute of Computational Mechanics and Optimization, Department of Production Engineering and Management
Technical University of Crete, Chania, Greece
[b] Department of Civil Engineering, Technical University of Braunschweig, Braunschweig, Germany

INTRODUCTION

Bolted steel connections have nonlinear mechanical behaviour due to unilateral contact and friction effects arising between the contacting parts as well as the elastoplastic material behaviour. Influence of elevated temperatures, indicating fire conditions, on the overall response of the joints is very important. In this framework, the thermomechanical behaviour of a 3 dimensional extended end-plate steel joint is investigated in the present study.
Simplified models as well as detailed finite element analyses have been used in the literature and compared with experimental measurements up to collapse. A number of experimental studies can be found in (Kruppa, 1976, Lawson, 1990, Al-Jabri et al, 1998, Spyrou et al, 2004, Spyrou et al, 2004, Daryan and Yahyai, 2009).
A lot of computational models for the study of steel connections under fire have also developed in the literature (Hu et al, 2009, Selamet and Garlock, 2010, Yu et al, 2008, Lien et al, 2009, Hozjan et al, 2007).
In the present study a 3 dimensional non linear finite element model has been developed, for the simulation of the thermomechanical behaviour of an extended end-plate steel joint. For the simulation between the end-plate and the column flange, a unilateral contact-friction law has been used. Degradation of the stress-strain non linear law at elevated temperatures together with large displacements, have been considered for the steel parts. Finally, three different load cases have been applied to the developed models. In the first loading scenario, the thermal and the concentrated mechanical load are applied both in the same analysis step, while in the second loading case the thermal loading precedes the point load. According to the third loading case, a small point load is followed by the thermal load; in a final step the total concentrated loading is applied to the connection. In all the aforementioned load cases an initial load step exists, namely the one with the application of the self-weight on the structure.

1 THE EXTENDED END-PLATE CONNECTION

The extended end-plate connection which has been used in this article, was tested to failure at ambient temperatures (Abdalla et al 2007). Eight high strength M20 bolts grade-8.8 with average yield and ultimate stresses F_y=600N/mm^2 and F_u=800N/mm^2 obtained from coupon tests, were used for the connection of the extended end-plate with the column flange. For each test, an IPE-360 beam section was attached to an HEA-220 column section (Fig. 1) through an extended end - plate. Beams, columns, and end-plates were made of steel having average yield and ultimate stresses F_y=314N/mm^2 and F_u=450N/mm^2, respectively, also obtained from three different uniaxial coupon tests. In Fig. 1 and Fig. 2 the geometry of the joint and the position of the point load, are shown.

2 FRAMEWORK OF THE NON-LINEAR MODEL

For the study of the thermomechanical behaviour of the extended end-plate, a three dimensional non linear finite element model has been developed. Unilateral contact law in the normal direction of the interface between the extended end-plate and the column flange, simulates the possible opening of the connected parts. Coulomb friction law is adopted to depict the contribution of the friction to the shear strength of the interface, together with the one obtained by the bolts.
At each point of the interface the basic unilateral contact mechanism can be described by the no-penetration inequality, the no-tension inequality, as well as a complementarity, either-or relation,

indicating that either separation with zero contact force or compressive contact force with zero gap appear.

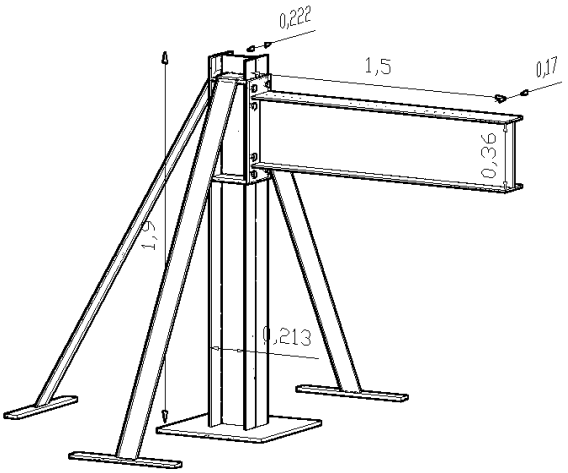

Fig. 1 Geometry of the steel connection

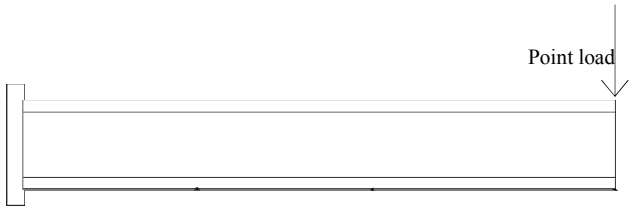

Fig. 2 Concentrated mechanical load

For a discretized structure the previous relations are written for every point of a unilateral boundary or interface by using appropriate vectors. The arising nonsmooth structural analysis problem has the form of a nonlinear complementarity problem. More details can be found, among others, in, (Panagiotopoulos, 1985), (Mistakidis and Stavroulakis, 1998), (Stavroulaki and Stavroulakis, 2002). The behaviour in the tangential direction of the interface is defined by a static version of the Coulomb friction model. Similarly with the contact problem, a complementarity problem arises for friction. The aforementioned scheme has been numerically implemented within commercial finite element packages.

3 THE FINITE ELEMENT MODEL

For the proposed finite element model three-dimensional 8-node brick elements have been used. For the satisfactory convergence of the analysis, a quite small average element size has been applied, resulting in a large number of finite elements (107.326 elements). The mesh which has been applied in the model is denser around the area of the connection while it becomes less dense away from it. In Fig. 3 and Fig. 4 the mesh as well as the structural parts of the joint are shown.
The friction coefficient for the beam–column interface is taken equal to 0.4. For the sake of simplicity, the interface between the bolt shank and the plate has not been considered, while interfaces between the bolts' head and nut and the plate are simulated as tie connections which do not permit neither sliding nor opening. The Young's moduli for the beam, the column and the bolts are approximately equal to 120GPa, as it is obtained from relevant coupon tests. The Poisson's ratio for the whole structure is taken equal to 0.3. Finally, large displacement analysis as well as v. Mises plasticity have been considered for the structure.

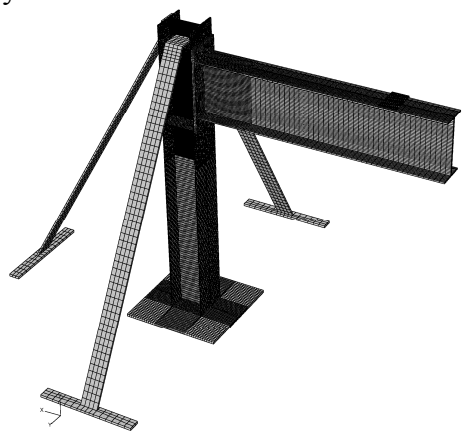

Fig. 3 Mesh of hexahedral 8-node finite elements

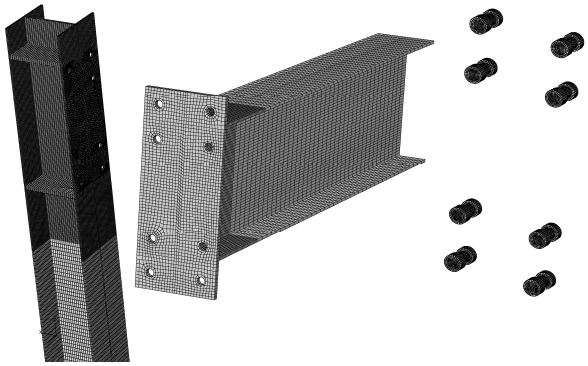

Fig. 4 Structural parts of the connection

4 FRAMEWORK OF THE THERMOMECHANICAL ANALYSIS

Within the aforementioned finite element analysis scheme, heat transfer analysis has been considered. Temperature boundary conditions have been applied as indicated in Fig. 5, Fig. 6 and Fig. 7.

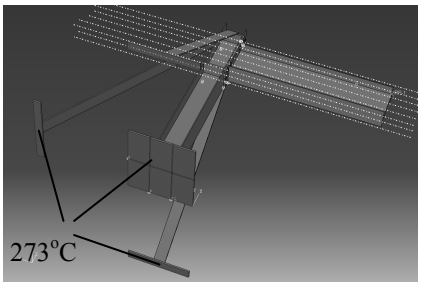

Fig. 5 Temperatures of 273°C

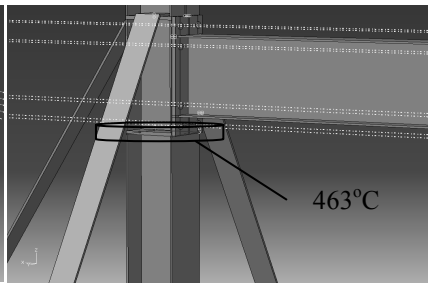

Fig. 6 Temperatures of 463°C

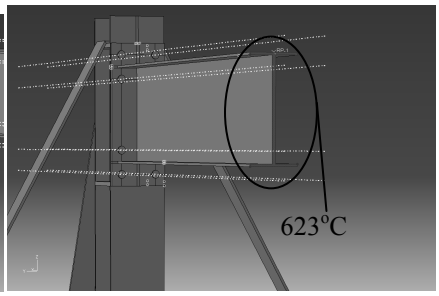

Fig. 7 Temperatures of 623°C

In addition, heat flux equal to 2KW/m^2 has been applied to the beam's web and to the column's web and front flange in the area below the connection, as it is shown in Fig. 8.

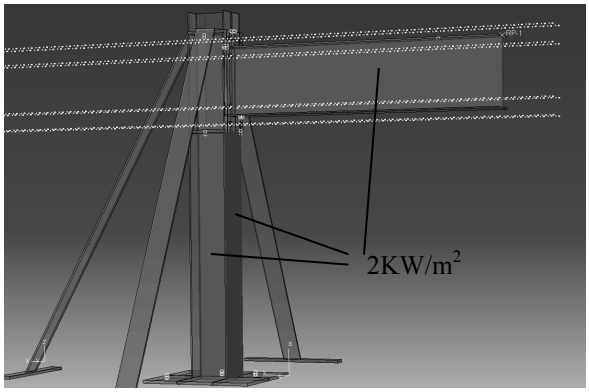

Fig. 8 Heat flux of 2KW/m^2

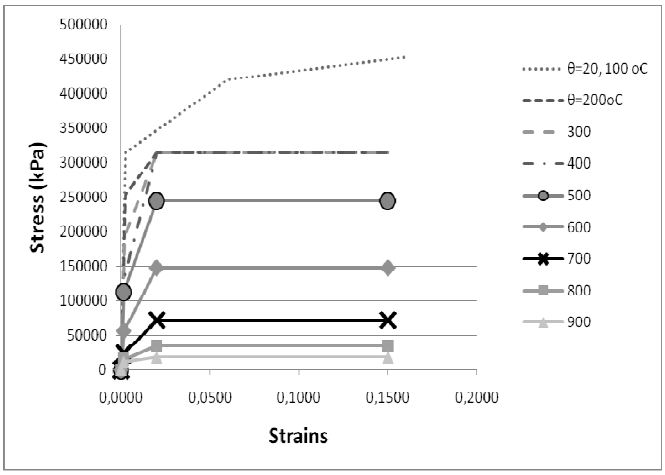

Fig. 9 Degradation of the stress-stain laws

Thermal properties of the materials have been chosen to be as follows: thermal conductivity=45 W/m°C, thermal expansion for the steel parts=12x10^{-6} /°C, thermal expansion for the bolts=13x10^{-6} /°C.

Degradation of the Young's Modulus and the stress-strain materials laws at elevated temperatures have been considered, as it is represented in Fig. 9 (Eurocode 3, 2001).

Three load cases have been considered in the developed models. According to the first one, the thermal and the concentrated mechanical loads are concurrently applied in the same analysis step. Within the second load case the thermal loading precedes the point loading. At the third load case, a small point load (50KN) is followed by the thermal loading; in the final step the total mechanical load is applied to the connection. In all the aforementioned load cases an initial load step exists, in which self-weight of the structure is applied.

5 RESULTS

The sequence of application of the thermal and the mechanical load is proved to be quite significant for the overall behaviour of the connection. In case the thermal and the point load are concurrently applied to the structure, temperatures reach approximately 800°C at the collapse of the joint. Temperatures reach similar values for the third load case, where thermal loading follows a small concentrated load of 50KN. In both cases the connection emits a satisfactory strength to fire although the limit load is significantly reduced in comparison with the structure at ambient temperatures. However, supposing that thermal loading is initially applied to the connection when only the self-weight is present (before the point load, according to second load case), then

maximum temperatures become greater than 2000^{o}C. Consequently, the structure can only support a quite small fragment of the point load which is applied afterwards. In Fig. 10 temperatures distribution at the failure of the connection for the first and the third load cases, are presented. In Fig. 11 and Fig. 12 temperatures distribution for the second load case as well as load-displacement diagrams, are shown. Moreover, if no reduction in the mechanical properties of the steel parts is considered, load-displacement diagram of the thermomechanical analysis is almost the same with the one obtained by the pure mechanical analysis (Fig. 12).

In Fig. 13 the plastic regions of the connection are depicted for the case the thermal and the concentrated load are concurrently applied (first load case). According to this, plastic yielding has been expanded to the whole beam, to the column web near the connection and to small regions of the column flange. In case the thermal load is initially applied with the self-weight and the point load follows in the next step, yielding of the joint is expanded to the whole beam at the end of the thermal loading step, before the application of the point load (Fig. 14). This is occurred due to the particular loading sequence which has been followed. Self-weight and the thermal load cause yielding to the beam, before the application of the concentrated load. As a result, when this is applied only a small part of it can be supported by the structure. For the third load case where the thermal load is applied after a small point load equal to 50KN, failure occurs before the end of the thermal loading step. Consequently, the ultimate load is equal to 50KN, which is smaller in comparison with the case where no fire is present, see diagrams of Fig. 12.

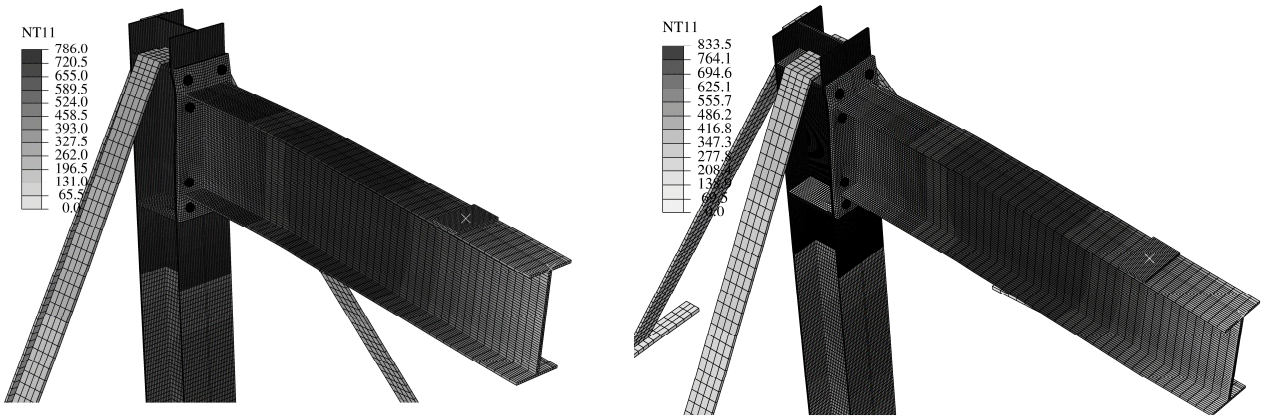

Fig. 10 Temperature distribution at failure for the first and the third load case

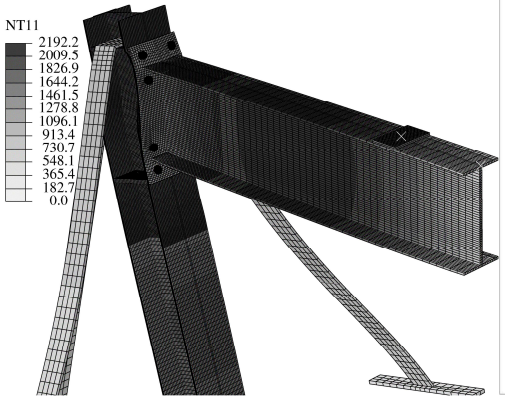

Fig. 11 Temperatures distribution for the second load case

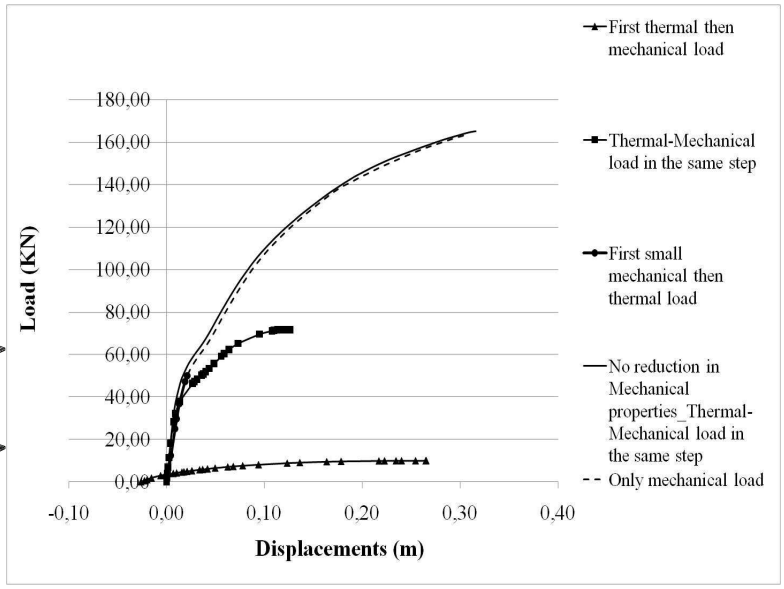

Fig. 12 Force-Displacement diagrams

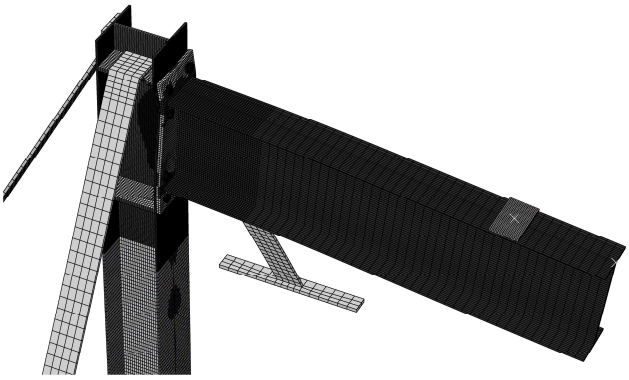

Fig. 13 Plasticity at the first load case

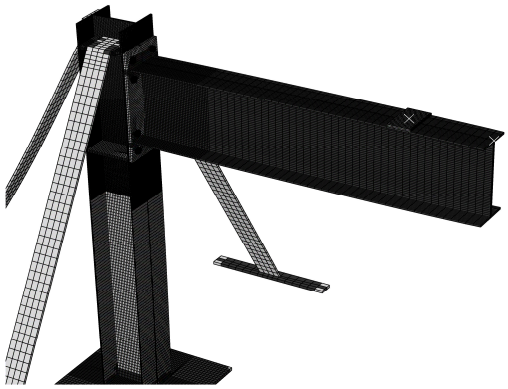

Fig. 14 Plasticity at the second load case

Another interesting aspect of the impact of the fire conditions on the steel connection is related with the opening of the connection. In Fig. 15a opening of the interface at the end of the analysis of the first load case, is shown. According to this, opening reaches a value of 18.7mm. In Fig. 15b opening of the interface at the end of the second load case, is shown. Opening in this case is bigger, thus equal to 38.7mm than the first load case. In addition, in the end of the thermal load step and before the application of the point load, there is a small opening in the interface (Fig. 15c). This is attributed to the total development of fire in the initial step of the analysis, where only the self-weight is present. Finally, in Fig. 16 are shown the opening of the interface for the third load case, where the point load precedes the thermal one. In Fig. 16a opening at the end of the point load of 50KN end before the application of the thermal load is shown. In Fig. 16b opening at the end of the analysis becomes approximately three times bigger than the one before the application of the thermal load (11.8mm instead of 3.5mm). This is due to fire conditions, as in the final step of the analysis the point load is constant and equal to 50KN.

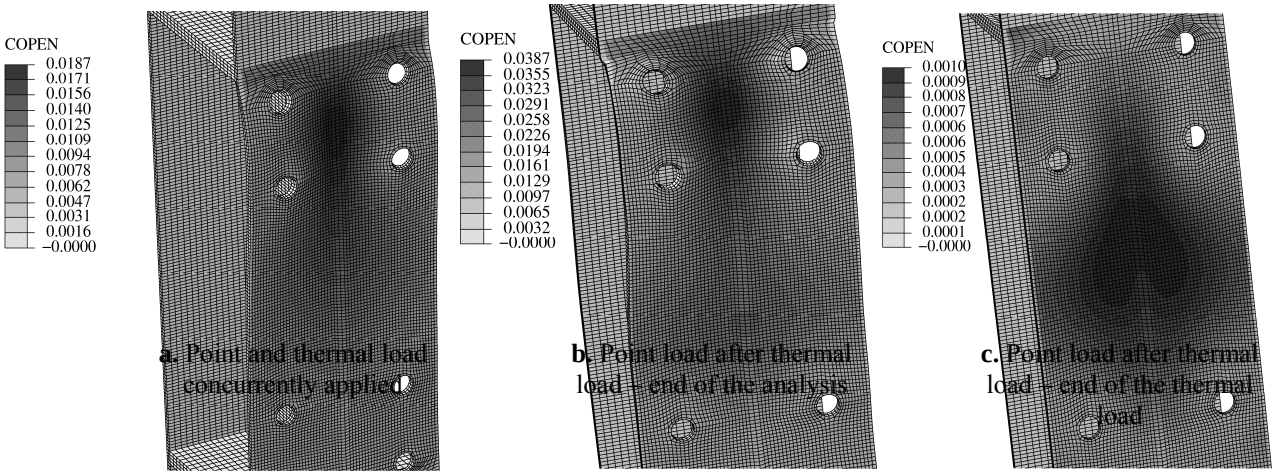

Fig. 15 Opening of the interface for the first (a) and the second (b), (c) load case

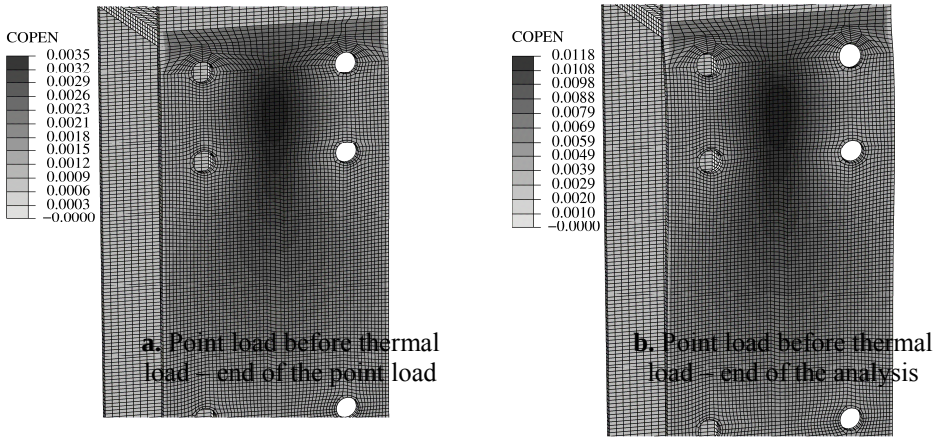

Fig. 16 Opening of the interface for the third load case

6 CONCLUSIONS

A thermomechanical analysis of a bolted steel joint has been performed in the present study, using a three-dimensional nonlinear finite element model. Three loading cases and the influence they have on the behaviour and the opening of the connection, are examined. The analysis has been performed up to collapse of the joint and the different collapse loads have been calculated. The results demonstrate that interaction of thermal and mechanical effects can be very complicated in structural elements. Comparable complexity is expected in the analysis of structures having such structural elements.

REFERENCES

Kruppa J., Re'sistance en feu des assemblages par boulous, CTICM Report, Document No. 1013-1, Centre Technique Industrial de la Construction Metallique, St. Re'my les Chevreuse, France, 1976.

Lawson R. M., Behaviour of steel beam-to-column connections in fire, The Structural Engineer 68, 1990.

Al-Jabri K. S., Lennon T., Burgess I. W., Plank R. J., Behaviour of steel and composite beam–column connections in fire, Journal of Constructional Steel Research 46, 1998.

Spyrou S., Davison J., Burgess I. W., Plank R. J., Experimental and analytical investigation of the ''compression zone'' component within a steel joint at elevated temperatures. Journal of Constructional Steel Research 60, 2004.

Spyrou S, Davison J, Burgess IW, Plank RJ. Experimental and analytical investigation of the "tension zone" component within a steel joint at elevated temperatures. Journal of Constructional Steel Research 60, 2004.

Daryan A. S., Yahyai M., Behavior of bolted top-seat angle connections in fire, Journal of Constructional Steel Research 65, 2009.

Hu Y., Davison B., BurgessI., Plank R., Component Modelling of Flexible End-plate Connections in Fire, Steel Structures 9, 2009.

Selamet S., Garlock M. E., Robust fire design of single plate shear connections, Engineering Structures 32, 2010.

Yu H., Burgess I.W., Davison J.B., Plank R.J., Numerical simulation of bolted steel connections in fire using explicit dynamic analysis, Journal of Constructional Steel Research 64, 2008.

Lien K.H., Chiou Y.J., Wang R.Z., Hsiao P.A., Nonlinear behavior of steel structures considering the cooling phase of a fire, Journal of Constructional Steel Research 65, 2009.

Hozjan T., Turk G., Srpcic S., Fire analysis of steel frames with the use of artificial neural networks, Journal of Constructional Steel Research 63, 2007.

Abdalla K. M., Abu-Farsakh G. A. R., Barakat S. A., Experimental investigation of force-distribution in high-strength bolts in extended end - plate connections, Steel and Composite Structures, An International Journal 7, 2007.

Panagiotopoulos P. D. , Inequality problems in mechanics and applications. Convex and nonconvex energy functions, Birkhaeuser Verlag, Boston, Basel, Stuttgart, 1985.

Mistakidis E.S., Stavroulakis G.E., Nonconvex optimization in mechanics. Algorithms, heuristics and engineering applications by the F.E.M., Springer/Kluwer, Dordrecht, Boston, 1998.

Stavroulaki M. E., Stavroulakis G. E., Unilateral contact applications using FEM software, International Journal of Applied Mathematics and Computer Science 12, 2002.

Eurocode 3: Design of steel structures part 1.2: general rules structural fire design ENV 1993-1-2:2001, Brussels (Belgium): European Committee for Standardization, 2001.

A COMPONENT-BASED MODEL FOR FIN-PLATE CONNECTIONS IN FIRE

Mariati Taib[a], Ian W. Burgess[a]

[a] University of Sheffield, Dept. of Civil and Structural Engineering, UK

INTRODUCTION

Connections can be classified according to their rotational stiffnesses, which are classed as rigid, simple or semi-rigid. Semi-rigid assumptions can be considered to assess the stiffness and capacity of steel framing systems most accurately. The benefits of this treatment are extensively documented, and there is a general acceptance that semi-rigid design results in efficiency, lightness and economical ambient-temperature design[1]. In fire conditions, due to the combinations of thermal expansion and material weakening, beams can be subjected to high normal forces, both in compression (at fairly low temperatures) and tension (at high temperatures), in addition to extremely high rotations, if their ends are fixed horizontally. These beam forces have to be sustained by the connections unless some movement of the beam ends, which relieves the forces, is permitted. Such movements can occur because the connected members move, or because the connections themselves have enough ductility to reduce the forces transmitted. In any case, the vertical shear forces, which the connections are designed to sustain at ambient temperature, are generally largely unaffected by the effects of fire.

Incorporating semi-rigid connections into global thermo-structural analysis requires tools and methods to facilitate the analytical design process, as joint characteristics can clearly have a significant influence on the survival time of the structural assembly during a fire. Advanced finite element models of connections involve high preparation time and computational cost, hence limiting their use for practical design purposes, despite being capable of highly reliable nonlinear joint simulation. Due to the inadequacy of structural databases, full-scale or isolated fire testing is inevitably required to provide the most accurate representation of connection response, although this is unlikely to be an economically appealing solution.

An intermediate approach to incorporating connection behaviour, known as the component-based modelling approach, has now been widely developed for ambient-temperature design. Eurocode 3[4] has implemented this approach to model the strengths and initial stiffnesses of steel joints for semi-rigid design. This approach constructs a connection from extensional zero-length "spring" elements and rigid links, representing the characteristics of its main structural zones realistically. Each active component makes its contribution independently, through its structural properties. This simplified method allows connections and structural system configurations to be varied rapidly, and thus the impact of various parameters on the system's global performance can be analysed.

1 IDENTIFICATION OF ACTIVE COMPONENTS

A very widely used simple connection is the fin-plate connection, classed as a shear connection, which consists of a pre-drilled single plate, welded to the supporting column flange or web, and bolted to the beam web at a number of single- or double-bolted rows (Fig.1a). Simple connections are assumed to develop a moment at the beam end less than or equal to 20% of the fixed-end moment, while the end rotation is greater than or equal to 80% of the end rotation in a simply-supported beam[2]. They are invariably cheaper to fabricate than moment-resisting connections as fabrication is simple, and fin-plates can be standardised. Cost advantages largely influence the choice of this connection, and erection on site is simple. As a simple shear connection, normal design concerns only the strength and ductility needed to transfer the vertical beam end reaction to its support. In fire conditions the connection also needs to provide sufficient rotational ductility to accommodate the rotation of the beam end, as well as a reasonable amount of horizontal movement.

Failure of fin-plate connections at high temperatures involves response to a combination of beam end shear and normal forces, and large rotations[2]. In order to understand the load transfer via bolt shearing, it is convenient to represent a simple shear connection by a lap joint[3] (Fig 1b).

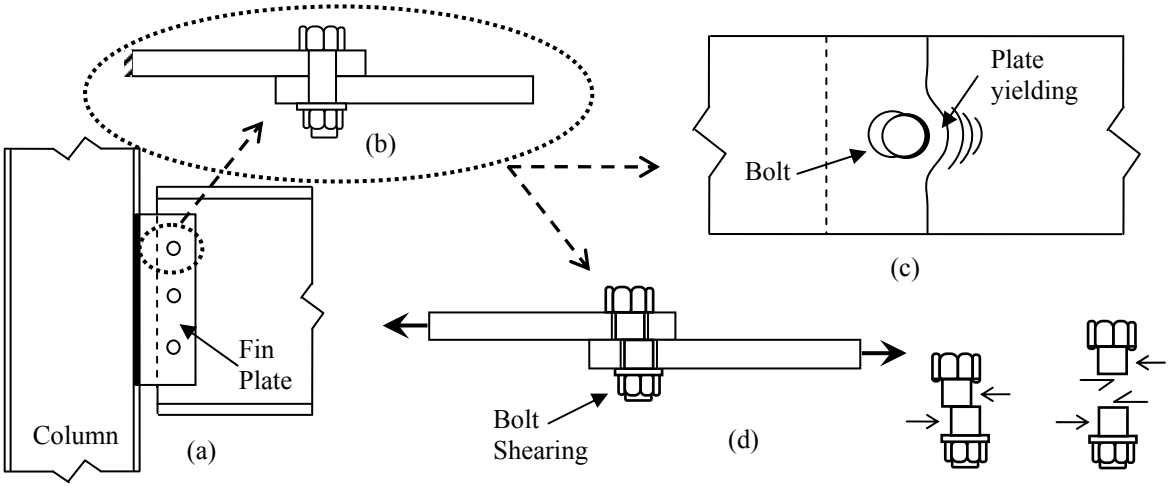

Fig. 1: (a) Fin-plate connection; (b) lap joint; (c) plate bearing; (d) bolt in shear.

1.1 Plate in bearing

Bearing failure of the plates is strongly affected by the lateral constraint to the contact zone by the surrounding material in its vicinity. Yielding of the plates does not cause a substantial loss of load capacity (Fig.1c), and is therefore generally treated as a ductile failure mode. The desired failure mode of a shear connection, as implied by the design guides[4, 5] adopts the conservative design recommendation that plate bearing is the resistance which should govern design. When the bolt is close to the end of the plate, its edge distance controls the tear-out and bearing (which are treated as a single limit state). However, moving away from the end of the plate results in large bearing deformation of the bolt hole without occurrence of tear-out failure. A typical force-displacement relationship with respect to temperature is shown in Fig.2a.

Rex and Easterling[3] concluded that the initial stiffness associated with a plate in bearing depends on three primary stiffness values (bending (K_b), shearing (K_v) and bearing (K_{br})) based on detailed investigation of a single-bolt lap plate connection. Sarraj[6] distinguishes two cases of bearing from a finite element parametric study in order to determine the plate bearing resistance using the most effective curve-fit values; these involve bolts with a small end distance ($e_2 \leq 2d_b$) and with a large end distance ($e_2 \geq 3d_b$). The key difference between these studies was the degree of tightening of the nut on the outer surfaces of the plates. Rex and Easterling's equations are:

Bearing stiffness, $$K_{br} = \Omega t F_y \left(d_d / 25.4\right)^{0.8} \quad (1)$$

Bending stiffness, $$K_b = 32Et\left(e_2 / d_d - 0.5\right)^3 \quad (2)$$

Shearing stiffness, $$K_v = 6.67Gt\left(e_2 / d_b - 0.5\right) \quad (3)$$

Initial stiffness, $$K_i = \frac{1}{\frac{1}{K_{br}} + \frac{1}{K_b} + \frac{1}{K_v}} \quad (4)$$

Where e_2 is the end plate distance (mm),
d_b is the diameter of the bolt (mm),
Ω is a temperature-dependent parameter for curve fitting.

1.2 Bolt in shear

The bolt shear failure mode may significantly affect the integrity of the structural system because it has inadequate ductility to ensure simultaneous plastic distribution of the forces carried by the bolts, and may therefore allow progressive failure. The relationship between the bolt shear deformation

and the force is given in Eq. (5) by a modified Ramberg-Osgood[6] expression for relative bolt deflection:

$$\Delta = \frac{F}{k_{v,b}} + \Omega\left(\frac{F}{F_{v,rd}}\right)^{n} \tag{5}$$

Where F is the level of shear force [N],
$K_{v,b}$ is the temperature-dependent bolt shearing stiffness [N/mm],
$F_{v,Rd}$ is the temperature-dependent bolt shearing strength [N].

In the study by Sarraj[6], bolt shearing failure was assumed to occur immediately after the maximum shear resistance, $F_{v,rd}$ was reached. However, a gradual decrease of shear resistance was observed during tests carried out by Yu[7] at elevated temperatures. It is therefore assumed here that the shear resistance decreases to zero at a displacement equal to the bolt diameter. Example characteristic curves with respect to temperature of a bolt in shear are shown in Fig.2b.

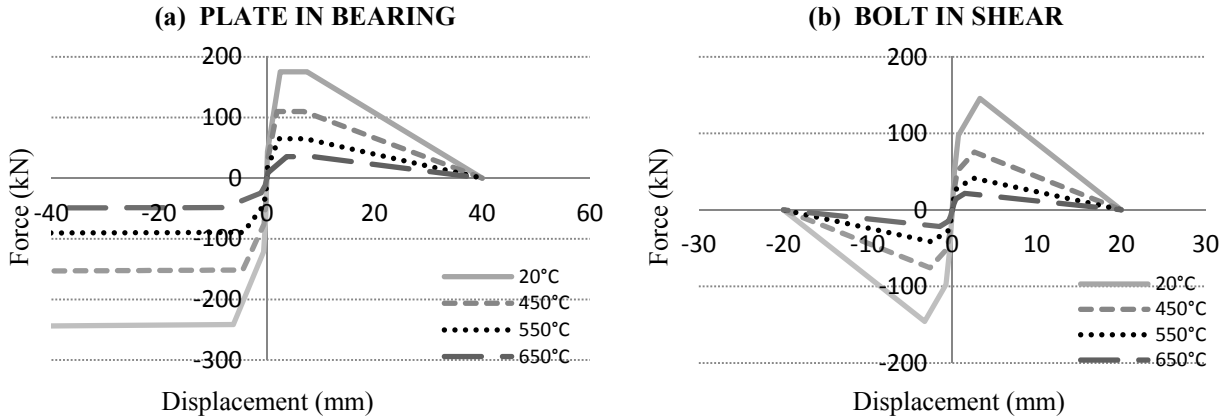

Fig. 2: Properties of components: (a) Plate in bearing; (b) Bolt in shear.

2 JOINT MODELLING

Previously, component-based models of fin-plate connections have been developed by Sarraj[6] and Yu[7] based on two-noded spring elements. The lap-joint zone consists of three fundamental components with no physical length, placed in series, for each bolt row: fin-plate in bearing; bolt in shearing; beam web in bearing. These component models include a friction spring in parallel with this basic spring series. The simplified friction load-deflection characteristic, however, generates low slip resistance, and has little influence on the connection's behaviour.

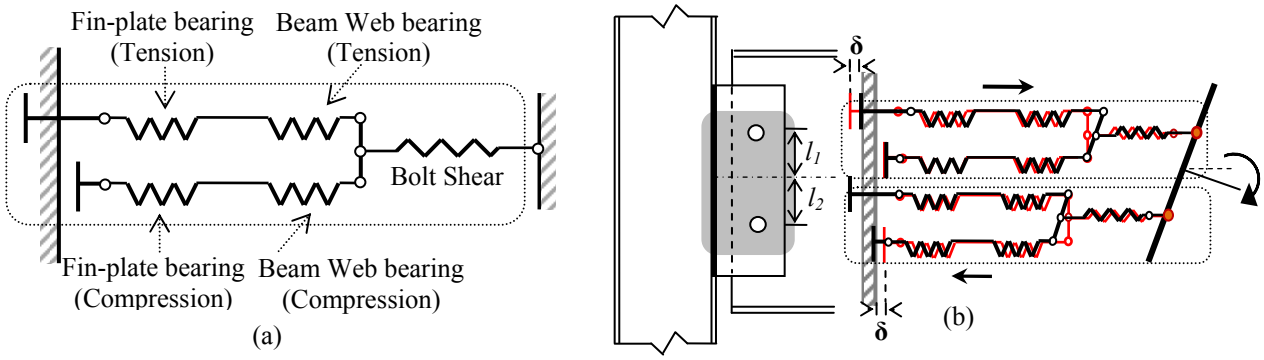

Fig. 3 : (a) Component-based model of a bolt row of a fin-plate connection (b) Component-based model subjected to tension and compression

A component-based model of a single-bolt-row of a fin-plate connection with no physical length is illustrated in Fig. 3a. The minimal effect of the frictional resistance between the two plates has been neglected here. The picture of the component-based model of a whole two-row fin-plate connection shown in Fig. 3b demonstrates that, during a complete analysis, tension and compression do not

follow the same lines of action. The load capacity is predominantly determined by the assembly of springs, from which the weakest individual component spring initiates failure.

2.1 Component-based model in *VULCAN*

The joint element is modelled as an assembly of component springs and rigid links, concentrating on the beam-to-column connection zone. An additional component spring at the lower beam flange level is adopted to account for contact between the lower flange of the beam and the column face at high rotation. A highly simplified version of the model consists of two horizontal rows; a single lap joint, the beam flange/column face contact, and a vertical shear spring, as shown in Fig. 4.

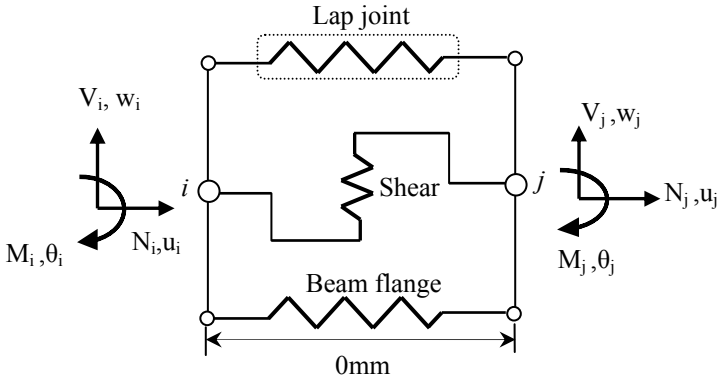

Fig. 4: Forces and displacements of a simplified connection element.

Each degree of freedom of the assembled springs is displaced individually to derive the stiffness matrix of the connection element, which eventually has three degrees of freedom (two translational *u, w* and one rotational θ) at each node. By solving for the global force and moment equilibrium of the whole element, the force-displacement relationships of the degrees of freedom can be calculated. The final tangent stiffnesses of the connection element are shown below.

$$K'_{11} = \sum_{i=1}^{n} k'_{lap,i} + k'_{beamflange,i} \tag{6}$$

$$K'_{15} = K'_{51} = \sum_{i=1}^{n} k'_{lap,i} l_{lap,i} + k'_{beamflange,i} l_{beamflange,i} \tag{7}$$

$$K'_{11} = k'_s \tag{8}$$

$$K'_{15} = K'_{51} = \sum_{i=1}^{n} k'_{lap,i} l_{lap,i} + k'_{beamflange,i} l_{beamflange,i} \tag{9}$$

In these equations, *n* is the number of component bolt rows, and the indices “lap” and “beamflange” indicate the lap joint assembly and beam flange spring respectively. The index *s* indicates the shear spring. Due to the simplicity of this mechanical model, the tangent stiffnesses can be incorporated in *VULCAN* using its existing spring element infrastructure. The component model subroutine subsequently provides the necessary incremental displacement vector for the connection element, and returns the tangent stiffness matrix and force vector to the main routines.

2.2 Loading and unloading of component model

The classic Massing rule[8] is incorporated so that each individual component will respond realistically to load reversals. The hysteresis curve in unloading (Fig. 5a) from the point at which strain reversal occurs, is the loading curve, scaled by a factor of two and rotated 180°. A modification to the Massing rule is applied to account for the initial bolt-slip phase, and only allows force transition into the opposite quadrant when contact is re-established, as shown in Fig. 5b.
During the heating phase, the softening of the material is defined by force-deflection characteristics which are functions of temperature. The permanent plastic deformation, which is recalculated after each temperature change, is considered as unaffected if the temperature changes. Thus, each force-

displacement curve at different temperatures necessarily has to unload completely through the same point. The unloading curve for a new temperature intersects with the previous unloading path at the zero-force axis, and this point is used as the reference point, $\delta_{P,T1}$.

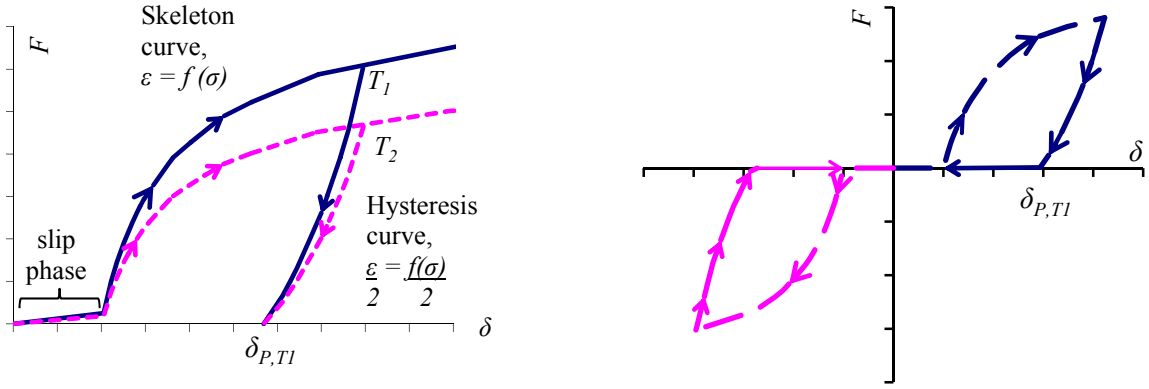

(a) (b)

Fig. 5 Massing Rule for fin-plate connection at varying temperature.

3 EXPERIMENTAL VALIDATION AT ELEVATED TEMPERATURE

Yu *et al.*[7] carried out an experimental investigation of the robustness of steel connections at elevated temperatures for flush endplates, flexible endplates, fin-plates and web cleats. The design setup for fin-plates used 200mm deep × 8mm thick fin-plates with three rows of bolts, designed in accordance with UK design recommendations[5]. Inclined tying forces were applied to represent the catenary action phase of a beam in fire. The results shown in Fig. 6 are for applied force inclinations of α=35° at ambient temperature and at 450°C, to represent a temperature range in which the properties of both structural and bolt steels have started to degrade rapidly.

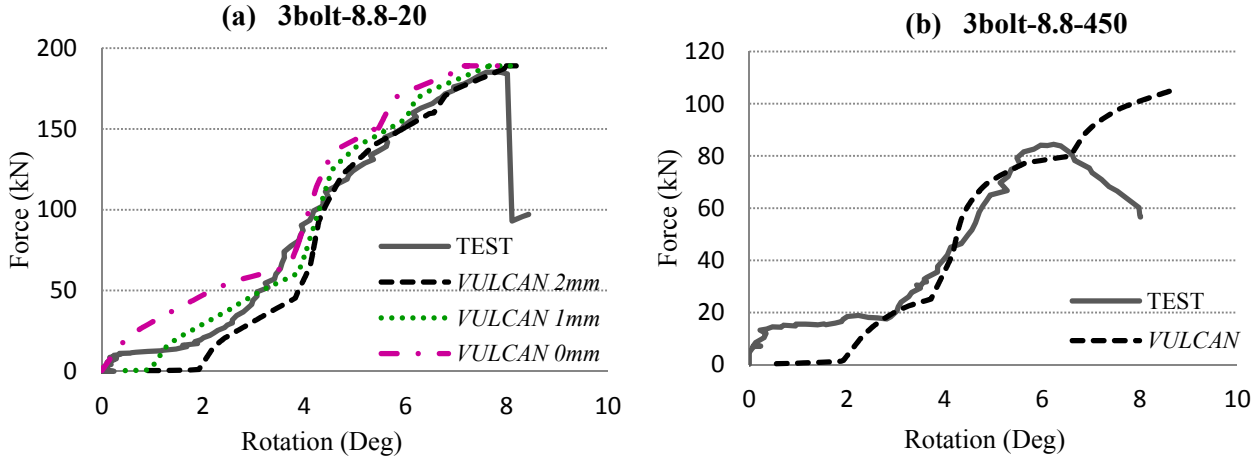

Fig. 6: Comparisons of test results to the component model (load angle 35°) at steady-state temperatures; (a) ambient temperature, (b) elevated temperature.

The responses of the component model and the test results are generally in close agreement for similar loading arrangements. Comparisons of the force-rotation relationship assume M20 bolts, initially installed centrally in clearance holes of 22mm diameter, producing 2mm initial slip between the plates. This initial slip ends with the first positive contact of the bolt against the bolt hole, which considerably influences the rotational response, as shown in Fig.6a. As the model is loaded, geometry changes cause the relationship between the force and rotational displacement to be non-linear. Subsequently, the second-order geometric effects, which create increased moments, are taken into account in the finite element analysis.

The resistance gradually increases after positive contact has been made by the bolt with the plate, until the maximum resistance of the top bolt is exceeded. The bottom flange subsequently comes into contact with the column face, resulting in a stiffer deformation response. The connection

strength is then controlled by consecutive bolt failures until the lowest bolt reaches its ultimate load. The component model was able to produce relatively close predictions of the maximum resistance and the rotational ductility of a connection, at both ambient and elevated temperatures.

4 CONCLUSION

A component-based connection model allows the behaviour of connections to be included in practical global thermo-structural analysis, provided that knowledge about the characteristics of key components is available from test data, numerical simulations or analytical models. At this stage, a basic component model for fin-plate connections has been developed and successfully incorporated in *VULCAN*. The stiffness matrix of the model has been derived to generate the connection's response to combinations of forces and displacements, and has subsequently been validated both at ambient and elevated temperatures. This component model, when embedded in *VULCAN*, allows direct analysis of whole structures or large substructures, including consideration of the interaction between realistic connection behaviour and that of the adjacent structural members.
A major modification to the model, which helps it to consider the real situation in fire, allows the lower beam flange to come into contact with the column face when the connection has undergone large rotation. It has been found that the complex nature of load reversal during a fire can be represented by adapting the Massing Rule, but with modification of the initial slip phase to account for the usual case where bolt holes are larger than the bolts. As part of the global structural assembly of beam-column, slab and connection elements, the component-based model will guarantee that the connection deformations are accounted for within the equilibrium of the whole assembly. This can be beneficial not only in design but also in assisting in the interpretation of experimental and analytical responses of connections within structures in fire.

5 ACKNOWLEDGMENT

The authors gratefully acknowledged sponsorship and support of the first author by the Malaysian Government for this research.

REFERENCES

A. Astaneh (1989). "Demand and Supply of Ductility in Steel Shear Connections." Journal of Constructional Steel Research 14:1-19.

E.Bayo, J.M. Cabrero, B.Gil (2006) "Component-Based Method to Model Semi-Rigid Connections for the Global Analysis of Steel and Composite Structures." Journal of Engineering Structures 28:97-108.

Sarraj, M. "The behaviour of steel fin-plate connections in fire" .Ph.D. Thesis. University of Sheffield; 2006

European Committee for Standardisation (CEN), BS EN 1993-1-8, Eurocode 3; Design of Steel Structures, Part 1.8: Design on Joints, UK :British Standard Institutions; 2005

Yu, H., I. W. Burgess, et al. (2009). "Experimental investigation of the behaviour of fin-plate connections in fire." Journal of Constructional Steel Research 65(3): 723-736.

Rex, C.O., Easterling, S.W. (2003)."Behaviour and modelling of a bolt bearing on a single plate." Journal of Structural Engineering, ASCE 129(6):792-800.

BCSA, The British Constructional Steelwork Association, "Joints in Steel Construction : Simple Connection", The Steel Construction Institute (2002)

Block, F.M. Development of a component-based finite element for steel beam-to-column connections at elevated temperature.Ph.D. Thesis. University of Sheffield; 2006

European Committee for Standardisation (CEN), BS EN 1993-1-2, Eurocode 3; Design of Steel Structures, Part 1.2: General rules-Structural Fire Design, UK: British Standard Institutions; 2005

BEHAVIOUR OF HEATED COMPOSITE JOINTS
Preliminary numerical studies

Cécile Haremza [a], Aldina Santiago [a] and Luís Simões da Silva [a]

[a] Department of Civil Engineering, University of Coimbra, Portugal

INTRODUCTION

The work presented in this paper is part of the European RFCS ROBUSTFIRE project, in which the behaviour of steel and composite structures subject to an exceptional event is investigated. The study of the structural individual response of the affected structural elements is actually on progress and three approaches (experimental, numerical and theoretical) will be combined with the aim to derive behavioural models for elements. Some experimental tests on a composite steel-concrete beam-to-column frame are currently under development at the University of Coimbra. In order to define theses tests and to justify some preliminary results, numerical models were performed with the non-linear finite element package ABAQUS, v6.10. This paper presents these numerical studies.

1 THE EXPERIMENTAL PROGRAMME

The main objective of the experimental tests is to observe the combined bending moment and axial loads in the heated joint when catenary action develops in the frame after the loss of the column. The composite joint zone is subjected to high temperatures in order to simulate the effect of the localised fire that leads to the column loss. Fig. 1 presents the seven beam-to-column frames being tested in Coimbra. According to previous experimental works performed in real composite steel-concrete open car park structures subjected to fire, a majority of the temperatures measured in the beam bottom flanges were lower than 500ºC; however temperatures of 700ºC were observed in recent tests performed in France (Simões et al., 2009). Based on these previous observations, five sub-structures are heated up to 500ºC or 700ºC; one sub-structure is tested at ambient temperature (test 1) and finally, a sub-structure is planned to be subjected to a demonstration test, for which the frame will be subjected to an increase of the temperature up to the failure of the column (test 7), see Fig. 1. The effect of the axial restraint to beam coming from the unaffected part of the building is also studied: tests 2 and 3 - no axial restraint to the beam; tests 4 and 5 - total axial restraint to the beam; and tests 1, 6 and 7 - realistic axial restraint to the beam. At this moment, three tests at elevated temperatures have been performed: tests 2, 3 and 4.

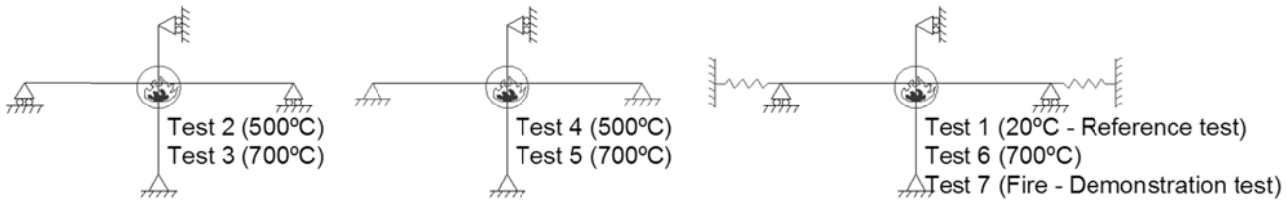

Fig. 1. Seven experimental tests

The two dimension sub-structure tested in Coimbra was selected from the actual composite building specially designed for the European ROBUSTFIRE project (Demonceau, 2010; Gens, 2011). This building was chosen to be the most general possible in order to obtain, at the end of the project, general rules on the design of such structures that ensure sufficient robustness under fire conditions. The selected structure is a braced open car park structure with eight floors of 3 m height, composite slabs, composite beams and steel columns. The sub-structure is defined by two unprotected composite beams with IPE550 steel cross-sections, grade S355, and one unprotected HEB300 cross-section steel column, grade S460 (Fig. 2). The steel beams are fully connected to the 130 mm thickness composite slab by 22 shear studs, and to the column by a flush end-plate with eight steel

bolts M30 cl. 10.9 (Fig. 3). In order to ensure the composite behaviour of the beam-to-column connections, ten steel rebars of diameter 12 mm are placed in the composite slab at each side of the column. Steel temperatures are increased using Flexible Ceramic Pad (FCP) heating elements. The heated zone consists of a length of 0.6 m of beam at each side of the joint, of the bolts and of 1 m of column. Servosis hydraulic jack ($F_{max.}$ = 1000 kN; $\Delta_{max.}$ = 280 mm) is used to apply the mechanical loading at the column top.

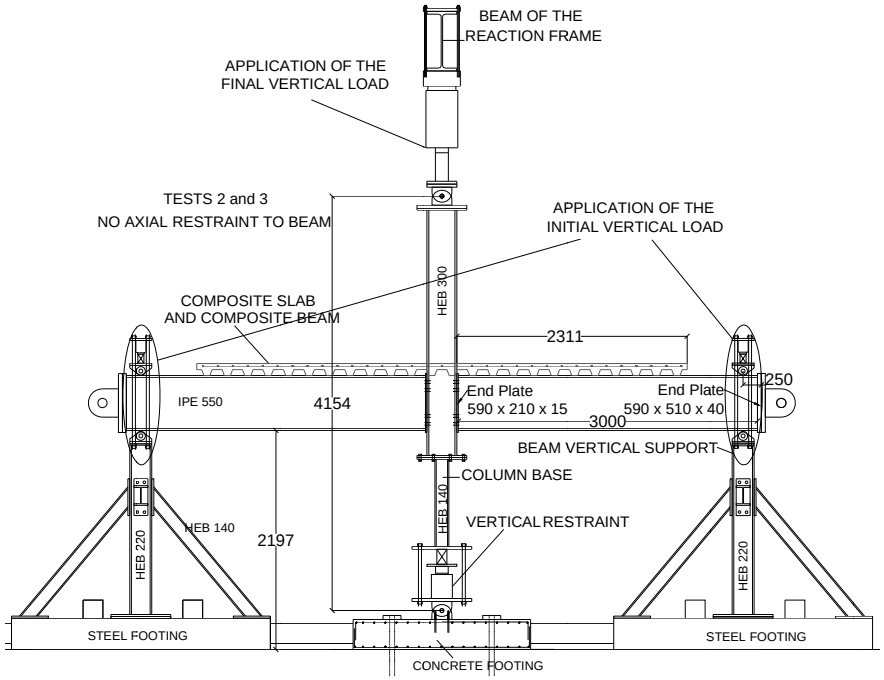

Fig. 2. General layout, longitudinal view of Tests 2 and 3

Fig. 3. Composite beam-to-column joint

2 NUMERICAL MODELS TO PREPARE THE EXPERIMENTAL TESTS

In order to define and to prepare the experimental tests, two simple preliminary models simulating the tests were performed in ABAQUS, v6.10. The first numerical model was used to define the initial loading: the initial load step reproduced the internal loads in the beam-to-column connections as in the actual car park. The applied hogging bending moment was predicted in this simple 2D model, using the loads at the service limit state (SLS) defined during the design of the car park structure (Fig. 4).

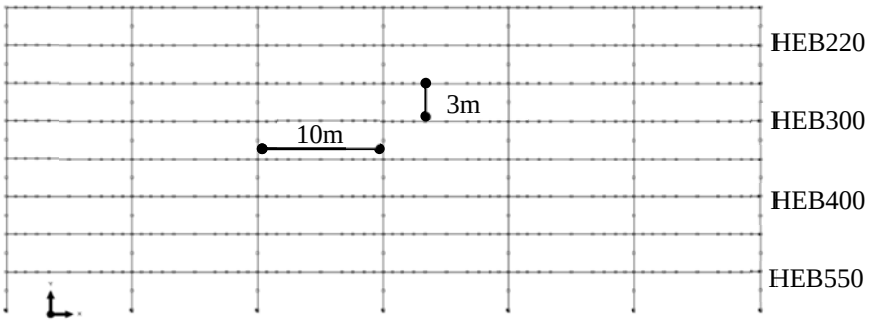

Fig. 4. Steel composite open car park modelled in ABAQUS

For the beam-to-column connections between the composite beams and the HEB 300 column, a hogging bending moment equal to -450 kNm was given in ABAQUS. According to EC1 part 1.2, effects of actions under fire may be deduced from those determined at ambient temperature, by

calculating a reduction factor η_{fi} (53% in this case), resulting in a target hogging bending moment of -236 kNm.

The second numerical model (sub-structure to be tested in the laboratory) was performed to define the required capacities of the load cells, displacement transducers, hydraulic jack and the axial restraints at the ends of the beams. Because the increase of the temperature with the FCP elements was not yet known before the tests, the temperatures into the cross-sections were obtained by a heat transfer analysis (ISO 834 fire curve was adopted). This heat-transfer problem involves conduction, and boundary radiation and convection (0.5 and 25 W/m^2K respectively). The two heat transfer models (composite steel-concrete beam and steel column) were developed using 2D deformable elements DC2D4. The analyses were stopped once the beam bottom flange temperature reached 500ºC or 700ºC. After the heat-transfer analysis, a static analysis was performed. Materials temperature dependent properties were defined according to EC3 part 1.2 for steel and EC2 part 1.2 for concrete. The thermal expansion coefficient was defined constant equal to 1.4 x 10^{-5} /ºC and 1.8 x 10^{-5} /ºC for steel and concrete respectively. The true stress-logarithmic strain measures $(\sigma - \varepsilon)$ calculated by the equation (1) were used in ABAQUS (Malvern, 1969):

$$\sigma = \sigma_{nom}(1 + \varepsilon_{nom}) \text{ and } \varepsilon = \ln(1 + \varepsilon_{nom}) \quad (1)$$

where σ_{nom} and ε_{nom} are respectively the nominal stress and nominal strain.

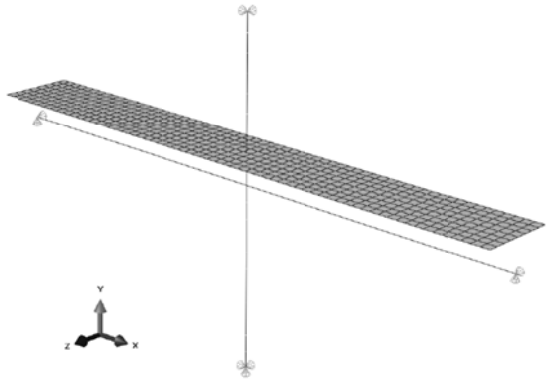

Fig. 5. Sub-frame modelled in ABAQUS (test 2)

Beams and columns were modelled by 3D beam elements B31, and the composite slab was simplified by a reinforced concrete slab using shell elements S4R (Fig. 5). Steel rebars were specified in the later by adding layers of reinforcement within the shell element virtual thickness at specified depth and angle of orientation. For the three tests with realistic axial restraint (tests 1, 6 and 7), connector elements were used to model the elastic linear behaviour of the "spring" restraint to beam (50 kN/mm). The full interaction between steel and concrete was modelled using a Tie constraint, and in this simple model, a Coupling constraint was used between beams and column simulating a rigid beam-to-column connection. No initial imperfections were applied. Each loading step was applied as to be performed in the laboratory (Haremza et al., 2011): step 1 – mechanical loading up to reach the target hogging bending moment in the joint (previously calculated); step 2 – heating of the joint zone with the temperatures obtained from the heat transfer analyses (applied as predefined fields); and step 3 – simulation of the loss of the column and increase of the sagging bending moment up to the failure of the joint, with the temperatures maintained constant. Thermal loading was defined at specific points through the beam/shell sections (ABAQUS Manual, 2010). From these analyses, the following conclusions were obtained: i) the maximum vertical load at the column top, leading to the failure of the joint under sagging bending moment (900 kN in the numerical model of test 1), was lower than the Servosis hydraulic jack capacity; ii) pins to link the axial restraint to the beam were designed according to the results of tests 4 and 5 (total axial restraint), for which the horizontal reaction load was the biggest (about 2200 kN in the numerical model); iii) load cells and displacement transducers were selected from the reaction loads and displacements numerical results.

3 NUMERICAL MODEL OF THE END-PLATE DEFORMATION

In the three experimental tests performed up to now, a localised deformation was observed at the steel end-plate centre (Fig. 10). A detailed three-dimensional model was developed in ABAQUS to reproduce and to study this end-plate local deformation. Steel temperature dependent properties are defined according to EC3 part 1.2, with steel S355 for the end-plate and S460 for the column. Bolts strain behaviour is estimated from previous experimental tests performed on M20 bolts grade 10.9 at ambient temperature, see Fig. 6 (Santiago, 2008). This curve is modified at elevated temperatures according to the reduction factors defined in EC 3 part 1.2 for the steel elastic modulus and for bolt tension and shear. The thermal steel expansion coefficient is defined constant (1.4×10^{-5} /ºC).

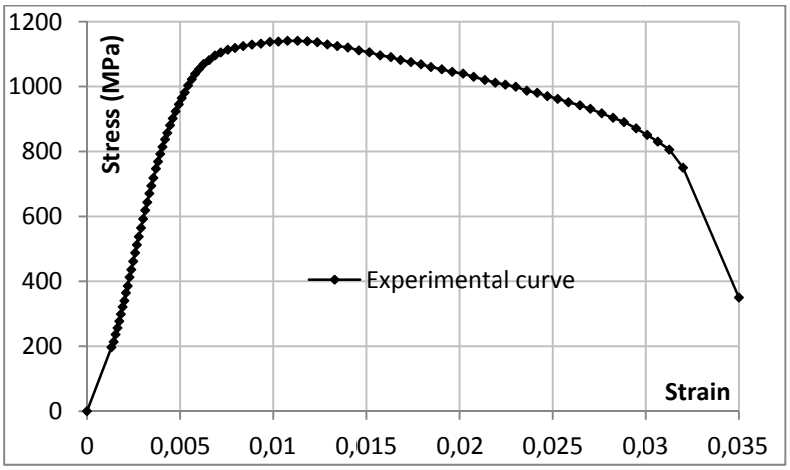

Fig. 6. Experimental and approximated bolt strain behaviour for grade 10.9 bolt (Santiago, 2008)

The symmetry of the joint is taken into account and half of the column, the end-plate and eight bolts are modelled combining C3D8R solid elements (Fig. 7). The axial displacement in the Y-direction is restrained, and at the bottom of the column, the displacements in the directions Y and Z are restrained. An initial deformation of the end-plate centre (0.6 mm) is measured before the experimental test 3 and is reproduced in ABAQUS.

Fig. 7. Numerical model in ABAQUS

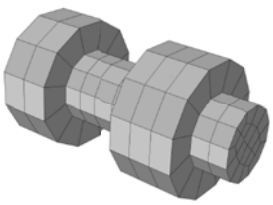

Fig. 8. Bolt mesh

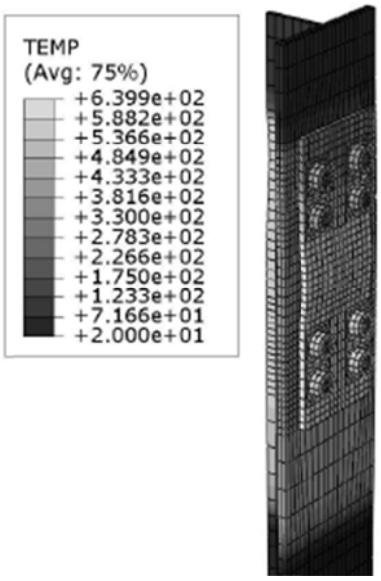

Fig. 9. Temperature results

Contact interactions are defined between the plate and the column flange, and between each bolt and the column flange and the end-plate: nut – column flange; bolt head – end-plate; bolt shank –

column flange hole; bolt shank – end-plate hole. Contacts are defined as surface-to-surface contact with a small sliding option. Normal contact is defined as "hard contact" with default constraint enforcement method, and separation is allowed after contact. The friction coefficient 0,25 is used in the tangential behaviour with penalty friction formulation. Bolts are meshed with the coarser mesh and their surfaces are defined as the master surfaces (Fig. 8). The static analysis algorithm is really difficult to solve once contact pairs are defined (33 in this model), and an easy way to pass through this is to pre-load the bolts at the beginning of the analysis, using the "Bolt load" option. A force is applied in each bolt equal to the pre-loading effectuated in the laboratory (120 kN). Bolt head and the nut are modelled circular as two washers are used.

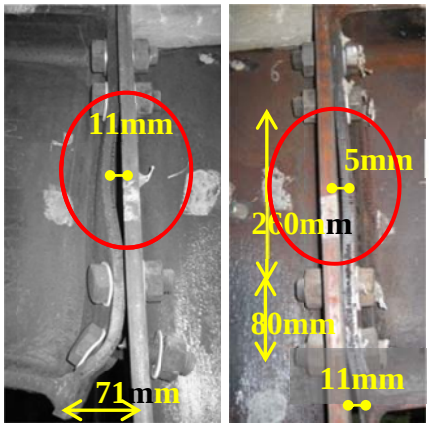

Fig. 10. Joint deformation in test 3

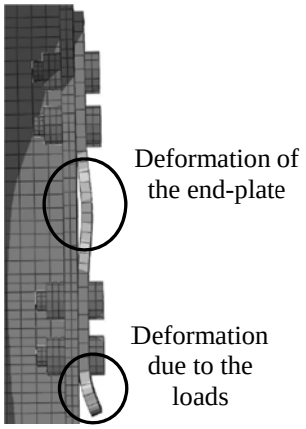

Fig. 11. End-plate deformation modelled in ABAQUS (Scale 2:1)

In this model, three load steps are defined: 1 – pre-loading of bolts, 2 – increase of temperatures, and 3 – increase of the horizontal displacement of the end-plate bottom part in order to approximate the real deformation under sagging bending moment (Fig. 11). Temperatures measured during test 3 are directly applied in the elements using the predefined temperatures. The temperature gradient measured in the end-plate and the column is applied, with four different temperatures in the plate and two different temperatures in the column web and in the column flange (Fig. 9). The comparison between the test and the numerical model is showed in Fig. 10 and Fig. 11. The end-plate deformation obtained by the numerical model is similar to the deformation obtained by the experimental test, and this local deformation happens during the increase of temperatures (step 2).
Currently, the numerical model of the entire sub-frame tested in the laboratory is in development (Fig. 12). The composite slab is modelled with the steel rebars, concrete damaged plasticity material model, and ribs are modelled with a rectangular section in order to simplify the mesh of this part.

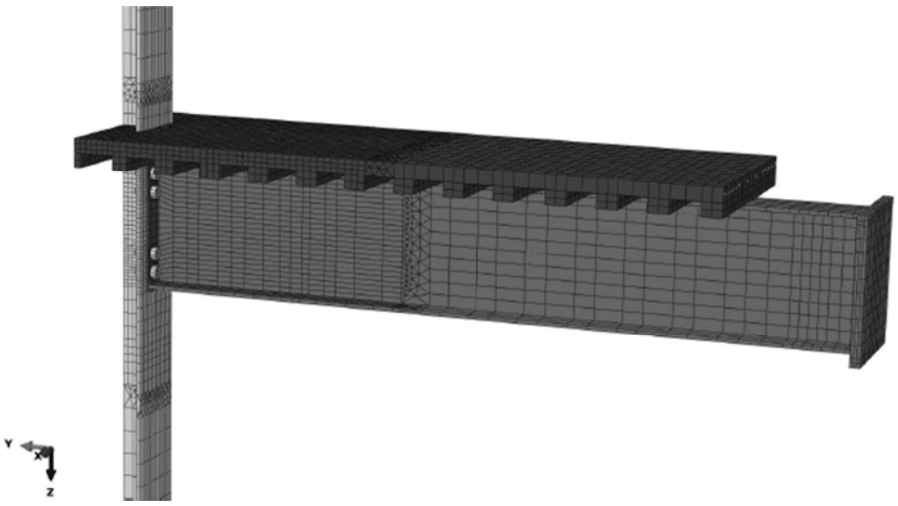

Fig. 12. Detailed 3D model in ABAQUS

A Tie constraint is used between concrete slab and the steel beam to model the total interaction. Because of the symmetry, only half of the frame is modelled. In this numerical model, the loading steps performed as in the experimental test are reproduced. Calibrations of the 3D finite element (FE) model against the test results are in development.

4 FINAL REMARKS

In this paper, preliminary numerical models, performed in order to prepare the experimental tests, and a more sophisticated 3D model of the localised joint deformation observed after some tests, were presented and described. As part of the ROBUSTFIRE project, the next step will be to experimentally study the influence of the axial restraint to beam and to observe the combined bending moment and axial loads in the heated joint when catenary action develops in the frame, and continue the calibration of the 3D FE models with the experimental tests results.

ACKNOWLEDGEMENTS

Financial support from the European Union (Research Fund for Coal and Steel) under contract grant RFSR-CT-2008-00036 and material support provided by PECOL, FELIZ and MARTIFER are gratefully acknowledged.

REFERENCES

ABAQUS Theory Manual & Users Manuals, v. 6.10, Hibbitt, Karlsson and Sorensen, Inc. USA, 2010.

Demonceau, JF, “ROBUSTFIRE Project - Design of the joints - notes”, Internal document, University of Liège, 2009.

EN 1992-1-2:2004, “Eurocode 2: Design of concrete structures – Part 1-2: General rules – Structural fire design”, European committee for standardization, 2004.

EN 1993-1-2:2005, “Eurocode 3: Design of steel structures – Part 1-2: General rules – Structural fire design”, European committee for standardization, 2005.

Gens, F, “ROBUSTFIRE Project - Pre-dimensionning of the reference’s car park”, Internal document, Greisch, 2010.

Haremza, C, Santiago, A, Simões da Silva, L, “ROBUSTFIRE Project, Document 6 – Experimental Tests – v2”, Internal document, University of Coimbra, 2011.

Malvern L.E., “Introduction to the mechanics of a continuous medium”, Englewood Cliffs, NJ: Prentice-Hall, 1969.

Santiago A., “Behaviour of beam-to-column steel joints under natural fire”, Ph.D. Thesis, Department of Civil Engineering, University of Coimbra, 2008.

Simões da Silva, L, Santiago, A, Haremza, C, “ROBUSTFIRE Project, Document 1 – Car Parks – v1(11)”, Internal document, University of Coimbra, 2009.